A geophysical investigation of the Eyjafjallajökull glaciovolcanic system, South Iceland, using radio echo sounding

Sara M. Strachan

Doctor of Philosophy

University of Edinburgh

November 2001

Declaration

I declare that this thesis was composed by myself and is my own work.

Sara M. Strachan
Department of Geography
University of Edinburgh
November 2001

Abstract

This thesis investigates the behavioral dynamics of Eyjafjallajökull, a glaciovolcanic system in South Iceland. The past and present eruptive environment of the volcano and its ice cap are determined by a combination of geophysical and geomorphological methods. The properties and subglacial topography of the ice cap are surveyed by radio echo sounding. Previously identified volcanic landforms on the deglaciated sections of the volcano, integrated with knowledge of subglacial volcanic processes, are used to infer the evolutionary dynamics of the system. Results indicate that Eyjafjallajökull is a special type of system which is highly susceptible to volcanigenic ice disruption. The repeated catastrophic disruption of the ice cap in the past and likely disruption in the future indicates that the marginal fluctuations of the ice cap cannot be solely attributed to climate change. Radio echo sounding experiments conducted at representative sites on the ice cap (crater, flank, toe of Gigjökull) determined the electromagnetic wave propagation velocity in ice at each site: $v_{crater} = 187 \pm 23$ m μs^{-1}, $v_{flank} = 140 \pm 8$ m μs^{-1}, $v_{Gigjökull} = 138 \pm 10$ m μs^{-1}. Electromagnetic wave velocity is based on the dielectric properties of the materials through which it propagates. Therefore, the ice in the crater has significantly different dielectric properties than the ice outside the crater. The derived velocities indicate that there are two discrete spatial zones of ice at Eyjafjallajökull: thin, dense ice on the volcano flanks and at the foot of Gigjökull, and thicker ice with a lower bulk density contained within the crater. A well-documented difficulty with the radio echo sounding method is the subjective identification of the ground wave. This obstacle is surmounted by establishing a quantifiable level of uncertainty in waveform interpretation by repeating measurements at each point. Picking uncertainty equals approximately 3 m in ice depth. Ice depths are validated by the experiments, which establish that similar depths can be produced by multiple frequencies. Point data from low frequency radio echo soundings are interpolated to produce maps of the surface and subglacial topography of Eyjafjallajökull. These maps reveal a number of features underlying the ice cap: a deep (>200 m ice thickness) N-S striking trough in the crater which constitutes the main flow line of ice towards the northern rim breach, an elongate hump in the center of the crater which could be a remnant vent cone, possible parasitic craters on the east flank, and an overdeepening at the base of Gigjökull's icefall. In the past, Eyjafjallajökull has been a relatively thin, temperate glacier, occupying the summit region of the volcano and has suffered repeated catastrophic disruption. Eyjafjallajökull is spatially split into two glaciological systems based on ice thickness and structure. The area containing the summit crater and its outlet glacier, Gigjökull, is less sensitive to the influence of climate in its current topographical confines. In the event of a summit eruption, the thick, impermeable ice in the crater may confine meltwater, then suddenly release it as a jökulhlaup. Thermal and mechanical erosion from flooding meltwater could severely disrupt the ice of Gigjökull. The area outside the summit crater contains thin (<150 m) ice and a probable well-developed subglacial drainage system. This section is more sensitive glaciologically to climate change and, in the event of an eruption, will allow meltwater to drain continuously, lessening the hazard of flooding. The maximum flood volume at Gigjökull could reach 0.63 km^3. The fluctuations of Gigjökull, compared to the rest of the ice cap, are anomalous. Gigjökull and the rest of Eyjafjallajökull are separate glaciological systems during periods of deglaciation, resulting from differences in their catchment hypsometry. Consequently, it is concluded that the fluctuations of Gigjökull alone are not representative of the oscillations of the ice cap as a whole and should not be used exclusively to make inferences about the past regional climate. This last finding can be applied to glaciovolcanic systems in general. By combining evidence of topographical features from the ice-free areas of the volcano with indications of features inferred from a subglacial surface interpolated from discrete radio echo soundings, a greater understanding of the overall characteristics and dynamics of the Eyjafjallajökull glaciovolcanic system is achieved.

Acknowledgements

I would like to thank the following people for their help and support during the production of my thesis:

- Dr. Nick Hulton, supervisor and 'Big Picture' guy. Thanks for keeping an eye on the wider implications of my research and for being a friend as well.
- Dr. Iain Woodhouse, supervisor and 'Details' man. Thanks for making sure all the equations are in order and for patient discussions about resolution.
- Dr. Ross Purves, shadow supervisor. Thanks for suggesting the field experiments and multiple frequency data collection method, without which this thesis would not be complete, and thank you for always being available, interested, and expecting the best.
- Dr. Andy Dugmore. Thanks for your enthusiasm about Iceland and sharing your knowledge of Eyjafjallajökull.
- Dr. Anthony Newton. Thanks for all your software tips and Coreldraw tutorials.
- Dr. Malcolm Murray. Thanks for sharing your statistical and interpolation knowledge.
- Dr. Trina Dinnis. Thanks for making some sense of the radar instrument and its mysterious ways.
- Dr. Sue Loughlin. Thanks for lending me your thesis and providing a geological basis for my research.
- Mom and Dad. Thanks for the cash. Oh, and thanks for all your love and support over the years and for always being enthusiastic about what I do. You guys are great!
- Tom Bradwell. Thanks for being a great friend, a co-worker in the field, and an interested colleague in the office. And for falling off a glacier.
- Keith Turner and Kieran Allen. Thanks for your hard work and good-humored field assistance.
- Steve Roberts. Thanks for the great road trip in Iceland and sharing your vast body of knowledge, from scanning to baked goods.

- Javier Corripio. Thanks for taking me to Argentina and showing me what real dedication is, and for being the only other glaciologist in the department.
- Hannah Avis. Thanks for sharing your lovely home and always knowing what to do in the middle of the night.
- The rest of my friends and colleagues in the Geography Department. Thanks for making my time in Scotland so productive and enjoyable.
- Nick Hardy. Thanks for everything.
- Field support for the 1999 season was provided by the North Atlantic Bio-Cultural Organization (NABO) and the National Science Foundation's (NSF) Office of Polar Programs.

Table of Contents

CHAPTER 3: THEORETICAL METHODS

List of Figures

Chapter 1: Introduction

Chapter 2: Physical principles of radio echo sounding

Chapter 3: Theoretical Methods

Chapter 4: Field Experiments

Chapter 5: Practical Methods

Chapter 6: Results

Chapter 7: Discussion

List of Tables

Chapter 2: Physical principles of radio echo sounding

Chapter 3: Theoretical Methods

Chapter 4: Field Experiments

Chapter 5: Practical Methods

Chapter 7: Discussion

List of Equations

Chapter 2: Physical principles of radio echo sounding

Chapter 4: Field Experiments

Chapter 5: Practical Methods

Chapter 7: Discussion

Chapter 1: Introduction

1.1 Introduction

Eyjafjöll, an ice-capped central volcano on the southern coast of Iceland, is a prominent landmark in a region dominated by extensive ice caps, volcanic edifices, and sandur plains. It is often referred to as the "Quiet One" (Guðmundsson, 1996), in reference to its relative inactivity compared to neighbors Katla and Hekla. At 100 km^2, the ice cap is considerably smaller in extent than Mýrdalsjökull, but its strikingly uniform massif, extending on a long E-W axis and culminating in an ice-filled summit crater, is a classic example of stratovolcanic form ***(Figure 1.1)***.

Named Eyjafjallajökull ("island mountain glacier") for its proximity to Vestmannæyjar (the Westmann Islands), which lie directly offshore to the south, the glacier system presents a particularly interesting site at which to study glaciovolcanic interaction. The massif's location on the south coast of Iceland makes the ice cap susceptible to the vagaries of the North Atlantic Oscillation, an oceanic circulatory system believed to be one of the most important controlling factors in northern hemisphere climate (***Figure 1.2***). Seismically and volcanically, Eyjafjöll lies within the South Iceland Seismic Zone (SISZ) and the Eastern Volcanic Zone (EVZ), systems which are linked seismically and volcanically to the Mid-Atlantic Ridge. Eyjafjöll is more locally adjacent to, and may share a volcanic plumbing system with, Katla, a prolific central volcano. Recent intimations of a volcanic re-awakening make Eyjafjöll a timely study (Iceland Review, 1999).

1.2 Aims

This research aims to develop a greater understanding of a specific glaciovolcanic system by a) exploring the evolutionary dynamics of the past eruptive environment, b) characterizing the current eruptive environment, and c) determining potential hazards which may occur in the event of a subglacial eruption. In addition,

this study aims to examine the validity of using glaciovolcanic systems as climate change proxies.

This thesis seeks to achieve these objectives by mapping the subglacial topography of Eyjafjallajökull by radio echo sounding. The radar survey will serve to increase understanding of the past evolution of the glaciovolcanic regime and reveal the present glaciovolcanic environment into which future eruptions will proceed.

The research seeks to answer two questions in particular:

How have ice and lava interacted to create the eruptive environment which exists today and how can this give us insight into what the ice was like in the past?

What can the present glaciovolcanic environment tell us about possible future lava-ice interaction and the hazards which may arise as a consequence?

This thesis aims to answer these questions in the following way:

- Examine landform evidence from the deglaciated sections of the volcano, historical observations, and reconstructions of past glacial fluctuations to determine the past eruptive environment of Eyjafjallajökull.
- Map the subglacial topography of Eyjafjallajökull using radio echo sounding in order to quantify the glacial and topographical properties which constitute its current eruptive environment.
- Combine quantities derived from the radar survey with knowledge of historically observed subglacial eruption processes to assess the location and impact of potential hazards through the determination of possible jökulhlaup routes and volumes.
- Integrate the evidence of historical glacier fluctuations at Eyjafjallajökull with knowledge of volcanigenic ice disruption processes to explore the causes for the anomalous fluctuations of Gigjökull, compared to the rest of the ice cap.
- Use the knowledge of glacier dynamics gained by this study to assess the suitability of using glaciovolcanic systems as climate change proxies.

Since Eyjafjallajökull is still considered an active volcano, having last erupted in 1823 and recently making noises again (Iceland Review, 1999), this survey is especially topical. The following quotation describes the present importance to the local Icelandic community of gathering geometric and topographic information about Eyjafjallajökull.

> "The Civil Defense Committee of the district of Rangárvallasýsla, south Iceland, will evaluate the dangers and set up a plan of action for the communities around Eyjafjallajökull glacier, south Iceland, should an eruption occur. The threat of subsequent glacial floods is what has the locals most worried, as farms on the nearby lowlands could be in great danger." (Iceland Review, 1999)

1.3 Approach

This thesis aims to achieve the objectives of the research by taking an interdisciplinary approach, combining geophysics with geomorphology to investigate the intersection between endogenic and exogenic processes at Eyjafjallajökull.

The quantitative geophysical method is the utilization of ice radar to survey the glacier, and the qualitative geomorphological method is the interpretation of evidence from the radar survey, historical observations and reconstructions, and case studies. By combining these two disciplines, the strengths can be extracted from each method: the ability of geophysics to quantify and the ability of geomorphology to produce educated interpretations from synthesized data.

1.4 Wider implications

This study has a number of important implications.

Studies of the causes of glacier fluctuations assist in the identification of those glaciers best used as climate proxies. Glacier behavior results from a combination of internal and external processes (Menzies, 1995b). The dynamics of some are driven more by endogenic than exogenic sources. By investigating these

systems, glaciers dominated by topographic processes may be delineated from glaciers whose main behavioral influence is climate. Active ice-capped volcanoes where these themes may be addressed exist in North and South America, Asia, Africa, and Antarctica.

Studies of environmental processes inform paleo-climatic reconstructions. Ice caps covering volcanoes are a special case; their interaction creates specific landforms that when deglaciated can be used to estimate past ice limits, proxies of paleo-climates. By understanding these processes, insight is added to paleo-environmental reconstructions, both on Earth and Mars (Zimbelman, 2000). The reconstruction of past climates helps scientists to understand how the Earth's climate has changed in the past and may again in the future. This knowledge is applied to planetary studies, where remotely-sensed landforms are the only data available at present from which to extract information about the natural processes that create, for example, Martian landforms. Terrestrial analogs form the basis for planetary geomorphology.

Radar surveys of temperate glaciers refine radio echo sounding techniques and improve understanding of temperate glaciers, important water reservoirs. Temperate glaciers are inherently more difficult to survey than cold-based or polythermal glaciers because the large quantities of liquid water contained within them directly interfere with radar signals. The majority of glaciers located in the more populated regions on Earth are temperate and constitute sources of water for consumption and irrigation, are places of recreation, and, in the present case, are origins of possible flooding hazards. Any incremental improvement in the method of ice radar data collection and processing will allow more accurate assessment of, among other things, ice volume and density, which would enhance estimation of liquid water equivalency and prediction of flood potential.

1.5 The study site

The glaciovolcanic system of Eyjafjöll reaches a height of 1666 m above sea level and comprises an area of approximately 400 km^2. The south, west, and north sides of the volcano rise steeply from a flat sandur plain. The east side shares a high

(~1000 m) plateau with Mýrdalsjökull. About seven miles to the south is the North Atlantic coast; the Markarfljót River drains the valley to the north. A long east-west axis, concurrent with the local tectonic regime, is evident, with high plateaus on these flanks containing subaerial and subglacial volcanic products. The north and south flanks of the massif are steep and deeply incised by valley glaciers and runoff streams. The crater rim is clearly delineated at the summit by a ring of nunataks, broken by a northern breach, through which the main outlet glacier, Gigjökull, drains.

The following sections introduce the study site and its known volcanic and glacial history. This history is put in a regional context by examining the geology and glacial history of Iceland. The processes of glaciovolcanic interaction are then described, providing a background from which to proceed to a description of two main causes of glacial fluctuations: climate change and volcanism. It is important to understand these processes so that their influences can be identified at the current study site.

1.5.1 Geology of Iceland

Iceland is one of the most tectonically and volcanically active places on Earth. Centered over a mantle plume, the island uniquely forms the only subaerial section of the Mid-Atlantic Ridge. The divergent plate boundary is separating the Eurasian and North American plates at a rate of about 1 cm per year (Sæmundsson, 1979). The rift zone strikes NE-SW across Iceland, extending offshore to the south as the Reykjanes Ridge and to the north as the Kolbeinsey Ridge (***Figure 1.3***). The mantle plume (or 'hot spot') and the ridge combine to form a number of volcanic and seismic zones (Sigurðsson, 2000). The rift propagation relative to the hot spot causes 'ridge jumps' which are expressed as transform zones linking the active volcanic zones in the north and south to the offshore ridges (Einarsson, 1994; Sæmundsson, 1979). The seismic and volcanic zones relevant to the evolution of the Eyjafjöll volcano can be identified in ***Figure 1.3***. The Eastern Volcanic Zone (EVZ) is linked by the transform South Iceland Seismic Zone (SISZ) to the Western Volcanic Zone

(WVZ), which extends directly into the Reykjanes Ridge. Current (postglacial) volcanic activity is confined to the Neovolcanic Zones which are composed of separate volcanic systems (Walker, 2000). Each volcanic system comprises a central volcano and a fissure swarm. Eyjafjöll is a central volcano in the NE/SW striking EVZ and may be influenced by the E-W trending SISZ (Jakobsson, 1979a).

The bedrock of Iceland is represented by four basic units, the spatial distribution of which mirror the tectonic fabric of the island (Jakobsson, 1979a; Sæmundsson, 1979) (***Figure 1.4***). Iceland is almost wholly composed of lavas and hyaloclastites, interbedded with sediments. The main formations are the Plateau Basalts, formed in the Upper Tertiary, the Grey Basalts, erupted during the Upper Pliocene and Lower Pleistocene, the Möberg Formation, also known as the Palagonite Formation, formed in the Upper Pleistocene, and the Postglacial Formation, composed of lavas, tills, and soils (Einarsson, 1994).

The ***Tertiary Formation*** is found on the outermost margins of the island, the farthest distance away from the spreading zone. Older than 3.1 M years, the rock is chiefly basaltic lava (83%) with smaller components of rhyolitic (8%) and andesitic (3%) lava. Most of the basalt flows erupted subaerially from fissures, while some of the rhyolitic and andesitic products erupted from central or shield volcanoes (Einarsson, 1994).

The ***Plio-Pleistocene Formation*** occupies an intermediate zone between the Tertiary Basalts and the current Neo-Volcanic Zone. These lavas, aged 3-0.7 M years, are gray-colored, long distance flows, erupted subaerially during the Quaternary interglacials. Like the Tertiary Basalts, the Grey Basalts originate chiefly from fissures or shield volcanoes, but are also intercalated with fluvial or lacustrine sediments (Einarsson, 1994).

The ***Upper Pleistocene Formation*** (0.7 M-10,000 years) fills the present boundaries of the Neo-Volcanic Zone. This unit is the product of lavas erupted subglacially during Quaternary glaciations (intercalated with glacial tills) and is of most interest to the present work. Subglacially-erupted lava (whether basaltic, intermediate, or acid) interacts with water to create a specific volcanic product. The Icelandic term Möberg refers to a collective unit called the Palagonite Formation,

composed of altered pillow lavas and hyaloclastites (Einarsson, 1994). A discussion of subglacially-erupted volcanic products follows in *Section 1.6*.

The ***Postglacial Formation*** (less than 10,000 years) is spatially limited to the present-day fissure swarms and volcanic systems. The lavas erupted from local fissure swarms and central volcanoes (Guðmundsson, 1996). Glacial tills and fluvial sediment have been deposited during and since deglaciation. Soils have formed on deglaciated landscapes.

1.5.1.1 Central volcanoes

Central volcanoes are composite, polygenetic complexes, produced by both shield and fissure eruptions. Shield eruptions center at a single vent while fissure eruptions emerge from adjacent elongate fissures. This results in the typical structure of a central vent around which fissure eruptions form radial ridges, or in some cases, ridges which follow the regional seismic trend (Walker, 2000).

A contributing factor in the general morphology of a central volcano is the lava composition. The central volcanoes of southern Iceland tend to produce explosive acid and intermediate lavas (Guðmundsson, 1996). These eruptive types form steep-sided stratovolcanoes. Most shield eruptions emanate from the central vent, but parasitic shield eruptions may occur on the flanks as well (Walker, 2000).

1.5.1.2 Eyjafjöll

Eyjafjöll is a central volcano with a form that fits the diagnostic description. The summit crater comprises the central vent. Fissure ridges radiate out from the vent, following the magmatic stress regime. Eyjafjöll has a general stratovolcanic form, but does not exhibit radial symmetry; the east-west extent of the massif is more than twice that of the north-south extent. This indicates that some of the fissures follow an anomalous E-W local tectonic trend (Jakobsson, 1979b). Since the main strike of the EVZ is SW/NE, it has been suggested that Eyjafjöll's strong E-W orientation reflects the tectonic fabric of the SISZ (Loughlin, 1995).

Eyjafjöll is approximately 0.78 million years old, built up over the course of six glacial and six interglacial periods (one period being approximately 70,000-120,000 years) (Loughlin, 1995). The volcanic activity has shown a westward progression over time. Two historic eruptions were recorded during 1612-1613 (questionable) (Jakobsson, 1979b) and 1821-1823 (Simkin and Siebert, 2000).

The most recent eruption from the main vent (1823) produced tephra, which indicates that the eruption broke through the ice surface, melting a large amount of ice in the process. The meltwater was released as a jökulhlaup, which flowed through a breach in the northern rim, down the Gigjökull icefall, and out onto the sandur plain in the Markarfljót valley (Dugmore, 1987).

More recent activity occurred in 1999 and 2000, when seismic activity increased and the southern flank below the summit was observed to inflate by 5 cm, signifying an accumulation of liquid magma below the surface (Iceland Review, 1999). The volcano has quieted since.

1.5.2 Glacial history of Iceland

Throughout its history, Iceland has experienced alternating periods of glacials and interglacials (Geirsdóttir and Eiríksson, 1994). Only the glacial history since the last glacial maximum (LGM) (~ 20,000 BP) will be described here. During the LGM, most of Iceland was covered by an icesheet. At about 18,000 BP, in response to a warming climate, the ice retreated. Periods of general glacial readvance during Postglacial time took place during the Older Dryas (12,000 BP), the Younger Dryas (11,000-10,000 BP) (Ingolfsson and Norðdahl, 1994; Kaldal and Víkingsson, 1990; Norðdahl, 1990), and the Neoglaciation (500 BC-1000AD) (Björnsson, 1979).

At the time of Settlement ('Landnám') in Iceland (~1000 AD), the historical record of glacial fluctuations began. These observations were not systematic before 1930, but were made in reference to areas of settlement. For example, in 1772 an observation of the growth of a glacier in the northwest cirque of Skarðsheiði at Drangjökull noted that the "glacier covers ground which was green and fertile 20 years ago" (Þórarinsson, 1943). For the time previous to this, glacial oscillations have been reconstructed and inferred from proxy evidence (Björnsson, 1979). From

about 1000-1300 AD, a general retreat of the glaciers was observed. It is unclear what occurred during the period from 1300 until 1600, after which the Little Ice Age (LIA) set in. During the LIA, which lasted until the 1920s, most glaciers reached their maximum extension since Settlement (Þórarinsson, 1943). Many were at their maxima as late as the 1880s. There has been a gradual recession of outlet glaciers and thinning of ice masses since the start of the twentieth century. The years between 1930 and 1960 saw a general rapid retreat. Since 1960, the pace of retreat has decreased (Rist, 1967; Sigurðsson, 1989; Sigurðsson, 1999).

1.5.2.1 Eyjafjallajökull

During the LGM, Eyjafjallajökull formed a separate icecap from the Markarfljót valley glacier. Striae evidence of this large glacier is present on the northern and western flanks of the volcano (Jóhannesson, 1985). At the time, Eyjafjallajökull joined Mýrdalsjökull at Fimmvörðuháls, a 1000 m pass shared by both ***(Figure 1.5)***. Subsequent evidence of the fluctuations of Eyjafjallajökull is derived from geomorphological studies and historical observation of the marginal fluctuations of the icecap's outlet glaciers (Dugmore, 1987; Rist, 1967; Sigurðsson, 1989; Sigurðsson, 1999; Þórarinsson, 1943).

Gigjökull, Eyjafjallajökull's main outlet glacier, reached its maximum LIA extent during 1750-1790 (Þórarinsson, 1943). The outlet glacier retreated slowly until about 1907, when it advanced again. Around 1930, the foot of Gigjökull reached the proximal slopes of the large terminal moraine (Dugmore, 1987). During the years 1930-1958, Gigjökull experienced severe backwasting, retreating 675 m. Then the toe advanced, moving forward 231 m from 1958 to 1990 (Sigurðsson, 1999). Since 1990, Gigjökull has once again retreated.

Two other of Eyjafjallajökull's glacial outlets have been monitored during the last century: Seljavellajökull, on the steep southern flank, and Steinholtsjökull, a neighbor of Gigjökull's on the north side. Both of these glaciers have been retreating since their maxima during the LIA. Seljavellajökull has wasted much more rapidly than Gigjökull (Dugmore, 1989). Most modern maps do not even name Seljavellajökull individually (Iceland Geodetic Survey, 1990; Jóhannesson *et al.*,

1990). Steinholtsjökull was severely disrupted during 1967 when a catastrophic non-volcanigenic landslide fell onto the lower reaches of the glacier and pulverized it, causing a massive flood (Kjartansson, 1967). The healing process has complicated the evaluation of its fluctuations.

1.6 Glaciovolcanic interaction

The processes of glaciovolcanic interaction which create specific landforms have been studied and observed in Iceland for some time (Smellie, 2000). The morphology of volcanic products is strongly dependent on eruptive type and deposition environment. The form indicates from which type of vent (shield or fissure) the deposits issued and into which environment (subaerial, subglacial, or subaqueous) they were emplaced. Thus, the volcanic landforms of Iceland provide evidence of past eruption processes and the climate required to create the necessary environment.

The two main volcanic eruptive types are ***shield*** and ***fissure*** eruptions (Einarsson, 1994). Shield eruptions are mainly monogenetic, erupting from a single vent, but can also occur parasitically on volcano flanks (Walker, 2000). Fissure eruptions originate from elongate vents aligned with local or regional magmatic trends (Walker, 2000).

The form of shield and fissure eruptions depends on the deposition environment, lava composition, and the length of the eruption (Smellie, 2000). An important determining factor in deposition environment is whether an eruption occurs subglacially or subaerially. Subaerial shield eruptions form domes with shallow slopes; subaerial fissure eruptions form ridges capped with cinder and spatter cones (Smellie, 2000). Subglacial eruptions introduce confining ice and liquid water into the process of landform creation. The interaction of magma with ice and liquid water creates ***tuyas*** from subglacial shield eruptions and ***tindars*** from subglacial fissure eruptions (Jones, 1969; Smellie, 2000).

When a volcano erupts beneath ice, magmatic heat melts ice, producing meltwater. If an eruption occurs under relatively thick ice (>200 m), the ice confines the meltwater, causing it to accumulate above the vent. The extrusion of magma into

ponded meltwater produces pillow lavas (Batiza and White, 2000). The cooling, or quenching, of magma by water forms hyaloclastite (Batiza and White, 2000). If an eruption continues long enough to melt all of the overlying ice, explosive, phreato-magmatic activity sets in, producing hyalotuff. If magma extrusion continues and the volcanic pile breaks through the water surface, the entire subglacial unit may be capped by a lava flow. This generalized process produces a tuya (table mountain) when erupted from a shield source, or a tindar (möberg or hyaloclastite ridge), when erupted from a fissure source (Jones, 1969; Smellie and Skilling, 1994).

The form of subglacial volcanic products specifies the quantity of meltwater present in the eruptive environment during formation. The height of ponded water confined by thick ice above an eruptive vent is indicated on a tuya or tindar unit at the transitional contact between the hyalotuff and the capping lava flow (Sigurðsson, 2000). The ice thickness at the time of eruption is assumed to be co-eval with the contact with the capping flow and therefore the height of ponded water (Smellie and Skilling, 1994). Subglacially erupted volcanic units which have not developed the full suite of stacked pillow lava, hyaloclastite, hyalotuff and capping lava, but do indicate interaction with meltwater by containing hydrothermally-altered material like hyaloclastite, testify that the ice under which the eruption took place was relatively thin (<200 m) (Smellie and Skilling, 1994). Thin ice provides a smaller quantity of meltwater than thick ice and allows it to drain continuously, rather than accumulate.

Volcanic landforms erupted from both shield and fissure sources into subaerial and subglacial environments are present on Eyjafjöll. Many of these volcanic products can be identified on the deglaciated sections of Eyjafjöll ***(Figure 1.5)*** and studied to determine its volcanic and glacial history. However, the landforms which occupy the glaciated part of the volcano are more difficult to study, requiring remote sensing methods, like radar, to detect and quantify their characteristics.

Once volcanic products are emplaced, the erosional force of a glacier further alters their form. Hyaloclastite lithologies are relatively soft, allowing rapid erosion of units during glacial periods (Batiza and White, 2000). As a result, steep, incised gorges develop on the sides of the central volcanoes. Björnsson (1979) estimates the

rates of denudation in the Mýrdalsjökull region to be about 4.5 mm yr^{-1}. Lawler (1991) produced a slightly higher erosion rate of 5.4 mm yr^{-1} for the Jökulsá Á Sóheimasandi basin. However, Bentley and Dugmore (1998) estimate an erosion rate of about 40 m per glacial cycle (approximately 0.4 mm yr^{-1}). The north and south slopes of Eyjafjöll are evidence of continued erosion. The topographical lows are continually excavated by ice and meltwater and provide ideal pathways for lava flows and jökulhlaups during eruptions.

Future lava and ice interaction may be predicted if the present eruptive environment is known. The subglacial topography determines the topographical lows down which lava and meltwater will flow during an eruption. The thickness and density of overlying ice can be used to calculate potential volumes of meltwater. Both the subglacial topography and the quantity of ice can be used to identify areas where meltwater may dam and accumulate, eventually bursting forth as a flood of predictable volume.

1.7 Causes of glacial fluctuations

The margins of glaciers advance and recede. The causes of these fluctuations have been attributed historically to climate change, in the form of temperature or precipitation changes, or internal mechanisms, such as those that cause glaciers to periodically surge (Menzies, 1995a; Benn and Evans, 1998). It is a basic tenet of glacial geomorphology that the fluctuations of glacier margins are good proxies for paleo-climates (Lowe and Walker, 1997). The marginal fluctuations of glaciers on volcanoes can be caused by volcanic eruptions as well. The extent to which each of these causes dominates a glacial system varies from site to site. Some glaciers are extremely sensitive to a changing climate and its margins respond rapidly (Menzies, 1995b; Benn and Evans, 1998). Other glaciers are not as sensitive to climate change and show a considerable lag in response.

1.7.1 Climate change (exogenic)

The ebb and flow of glaciers are usually attributed to the effect climate has on mass balance (Menzies, 1995b). As the average temperature rises, melting outpaces accumulation, causing a glacier to recede. If the average temperature drops, ice accumulates quicker than it can melt, causing a glacier to advance (Menzies, 1995b). In addition, changes in precipitation input can alter the mass balance of a glacier, causing advance or retreat. Although overly simplistic, this explanation is sufficient to illustrate the commonly made connection between glacier fluctuation and climate change. The especially rapid recessions of glaciers around the world, including Iceland, during the last century, have been attributed to a rising average temperature (Benn and Evans, 1998).

1.7.2 Volcanism (endogenic)

Glacial fluctuations are strongly influenced by climate, but cannot be attributed exclusively to this cause. The interaction between ice and volcano affect both the volcanic products that emerge from an eruption phase as well as the extent of ice cover. Sveinn Pálsson originally recognized that the origin of glacier fluctuations can be volcanic as well as climatic, noting that climatically-influenced oscillations are periodic, volcanic are not (Þórarinsson, 1943). A subglacial eruption will typically melt a great deal of ice, after which a glacier must heal itself, a process which interrupts climatically-driven waxings and wanings. In addition, subglacial eruptions can quickly change the dynamic of a glacier, by emplacing new topographical features in the catchment area which disturb the organization of accumulation and drainage.

1.8 Past work at site

The geology of Eyjafjöll, describing the evolution of the volcanic system and the deglaciated landforms, was studied by Jónsson (1988) and Loughlin (1995). The geomorphology of the outlet glaciers Gigjökull, Steinholtsjökull, and Seljavellajökull was researched by Dugmore (1987), who also carried out an extensive investigation of the tephrastratigraphy in the Markarfljót valley. Glaciological work at the foot of Gigjökull has taken place since 1988, during annual field trips by the University of Edinburgh Geography Department. However, the subglacial topography of the crater region and ice-covered flanks is unknown.

1.9 Structure of thesis

Chapter 2 introduces the physical principles of radio echo sounding for the medium of temperate ice and describes the equipment utilized in the survey. ***Chapter 3*** describes the theory of data collection and post-processing techniques for radio echo sounding on ice, critically discusses ice radar surveys from the literature, and explains the methodological approach taken for the current survey. ***Chapter 4*** summarizes experiments performed at the study site in order to characterize the radar equipment and collect empirical data about the dielectric properties of the ice at Eyjafjallajökull. This chapter also introduces the development of waveform interpretation and depth validation techniques, and discusses calculations used to derive electromagnetic wave velocities in ice. ***Chapter 5*** describes how the data were collected, processed and interpreted. The methods of map preparation and interpolation are also discussed. ***Chapter 6*** presents the results of the survey. ***Chapter 7*** describes processes of lava/ice interaction which occur during subglacial eruptions and properties of glaciers which affect these processes. Hazards which result from subglacial eruptions and an explanation of the eruptive history of Eyjafjöll are presented. The current eruptive environment of Eyjafjallajökull determined by the survey is discussed and potential hazards quantified. Finally,

thoughts on the past fluctuations of the ice cap and its outlet glaciers are presented within the theoretical framework introduced in *Chapter 1*. ***Chapter 8*** summarizes the main findings of the research, reflects on their significance, points to further work that could be done to improve and extend the results, and concludes the thesis.

1.10 Summary

This thesis aims to develop a greater understanding of Eyjafjallajökull, a temperate ice cap located on Eyjafjöll, an active central volcano in southern Iceland. The research is based on the rationale that, in order to qualify assumptions that glaciers fluctuate according to changes in climate, it is important to investigate the internal processes of glacial dynamics. Specifically, glaciers which form on volcanoes may reveal different fluctuation mechanisms which result from ice interaction with lava and meltwater during eruptions. Furthermore, by characterizing subglacial topography and ice quantities, future ice/volcano interaction processes, such as flooding, may be predicted.

Figure 1.1 The volcano Eyjafjöll and its ice cap Eyjafjallajökull (photo by author).

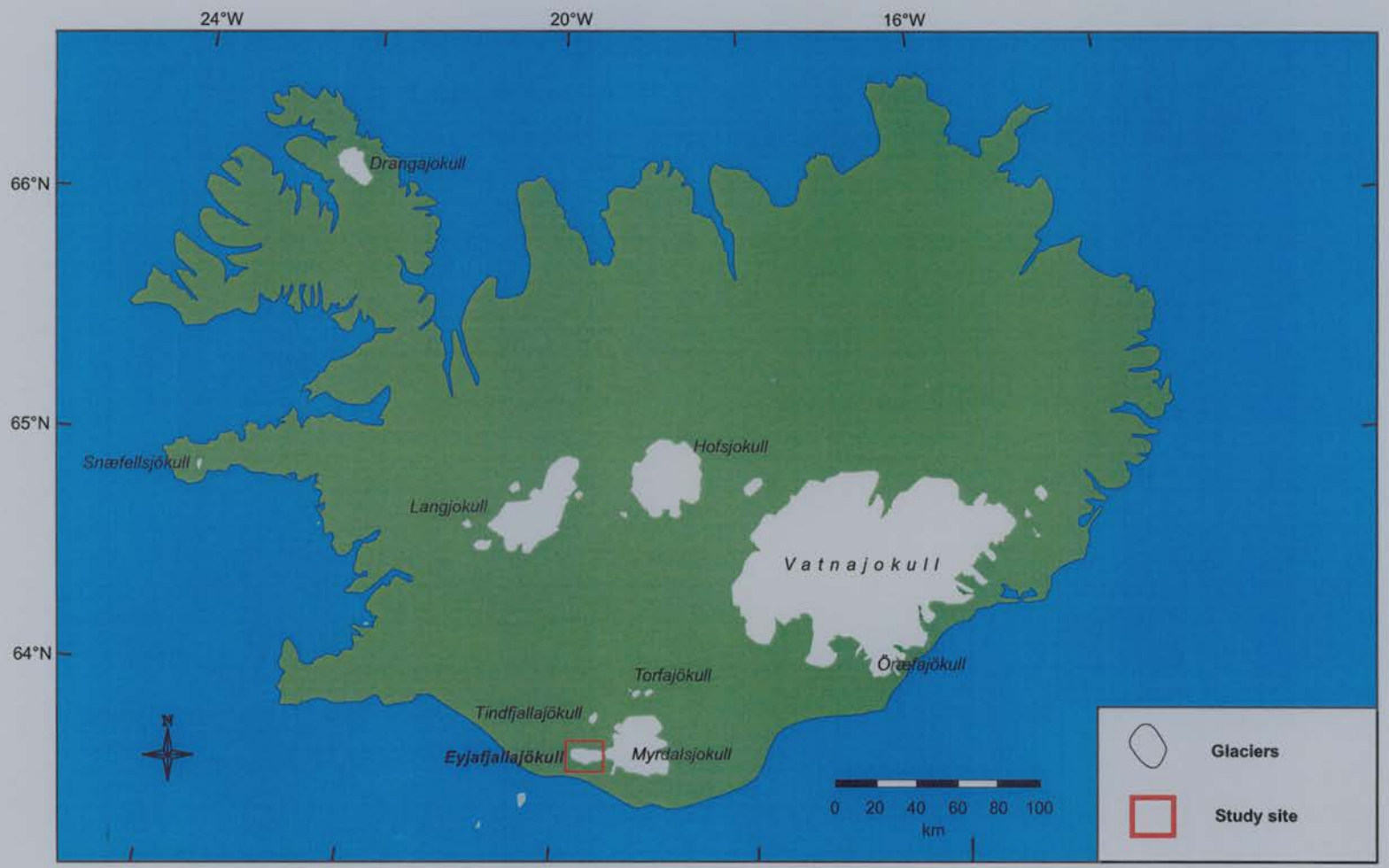

Figure 1.2 Location of study site in south Iceland. Eyjafjallajökull lies directly to the west of the larger and more volcanically active Mýrdalsjökull.

Figure 1.3 Tectonic and volcanic structure of Iceland (Larsen *et al.*, 1998; Jóhannesson and Sæmundsson, 1998), from Newton (1999). The Eyjafjöll central volcano and fissure swarm resides in the Eastern Volcanic Zone (EVZ), south west of the South Iceland Seismic Zone (SISZ).

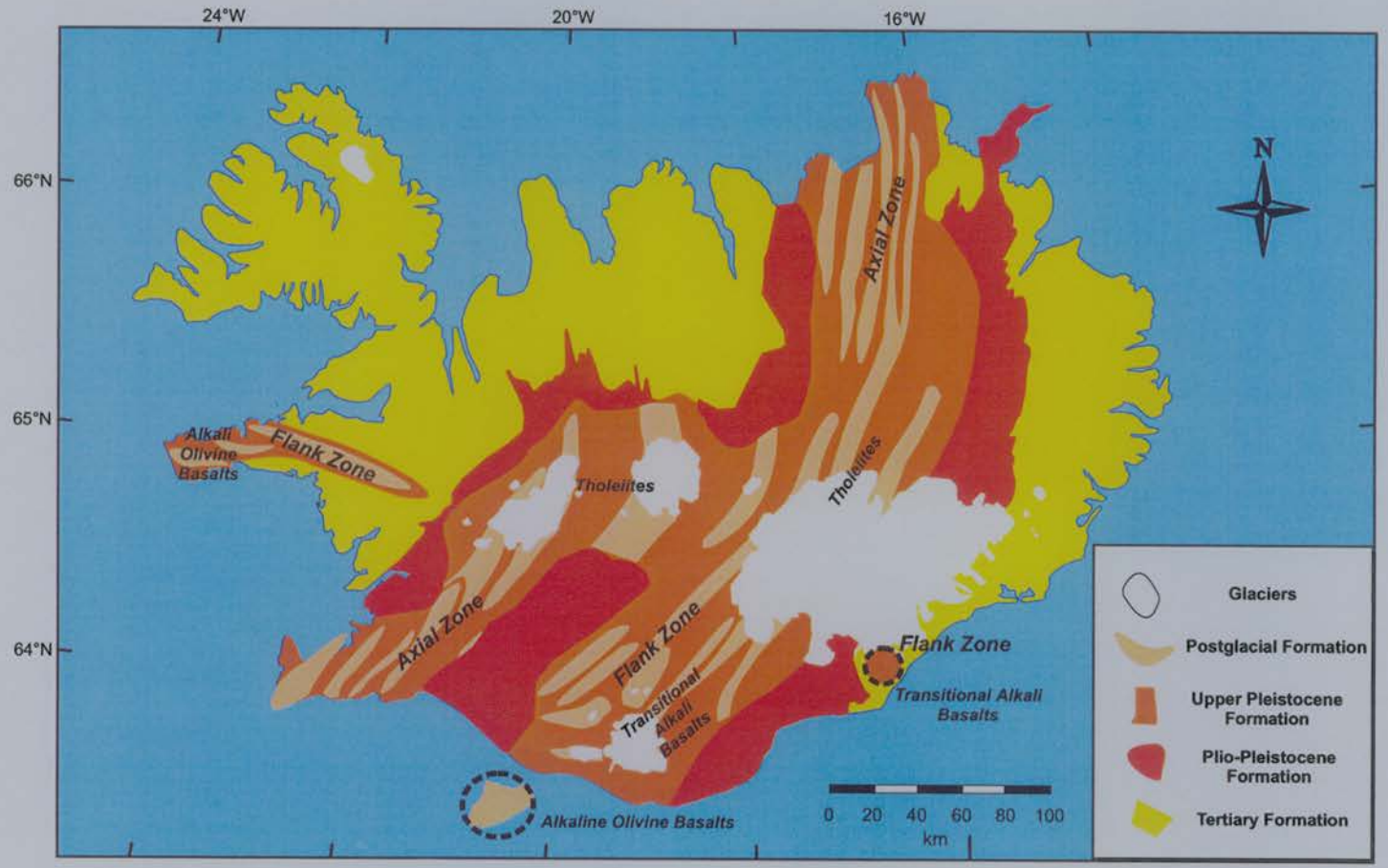

Figure 1.4 Gross geologic and petrologic structure of Iceland (Sæmundsson, 1979). The Eyjafjöll volcano is in a flank zone dominated by transitional alkali basalts.

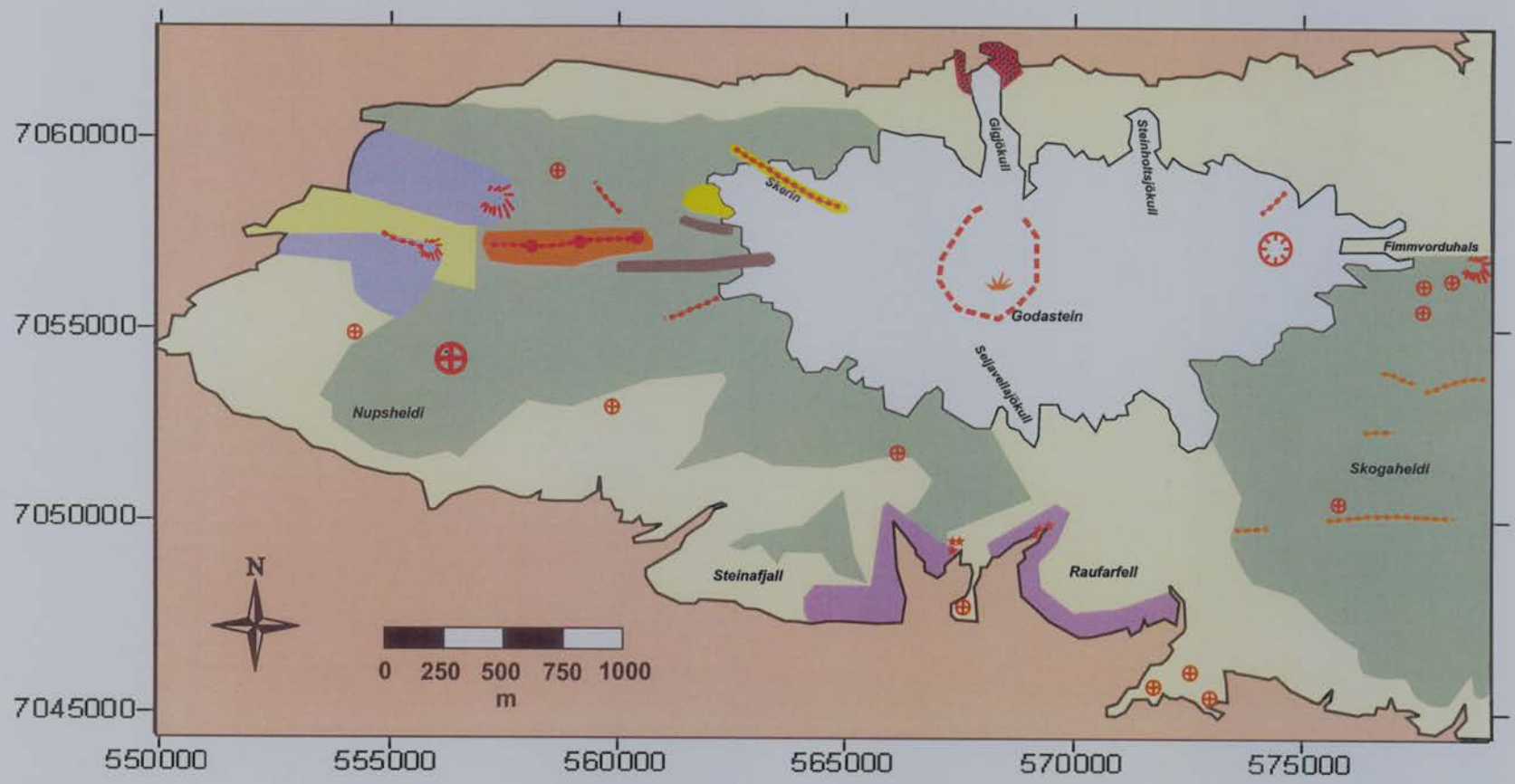

Figure 1.5a Geologic structure and volcanic landforms of Eyjafjöll (Jakobsson, 1979b; Jóhannesson *et al.*, 1990; Jónsson, 1988; Loughlin, 1995). The landforms apparent on the deglaciated sections of the volcano provide information about the glacial and volcanic history of the system.

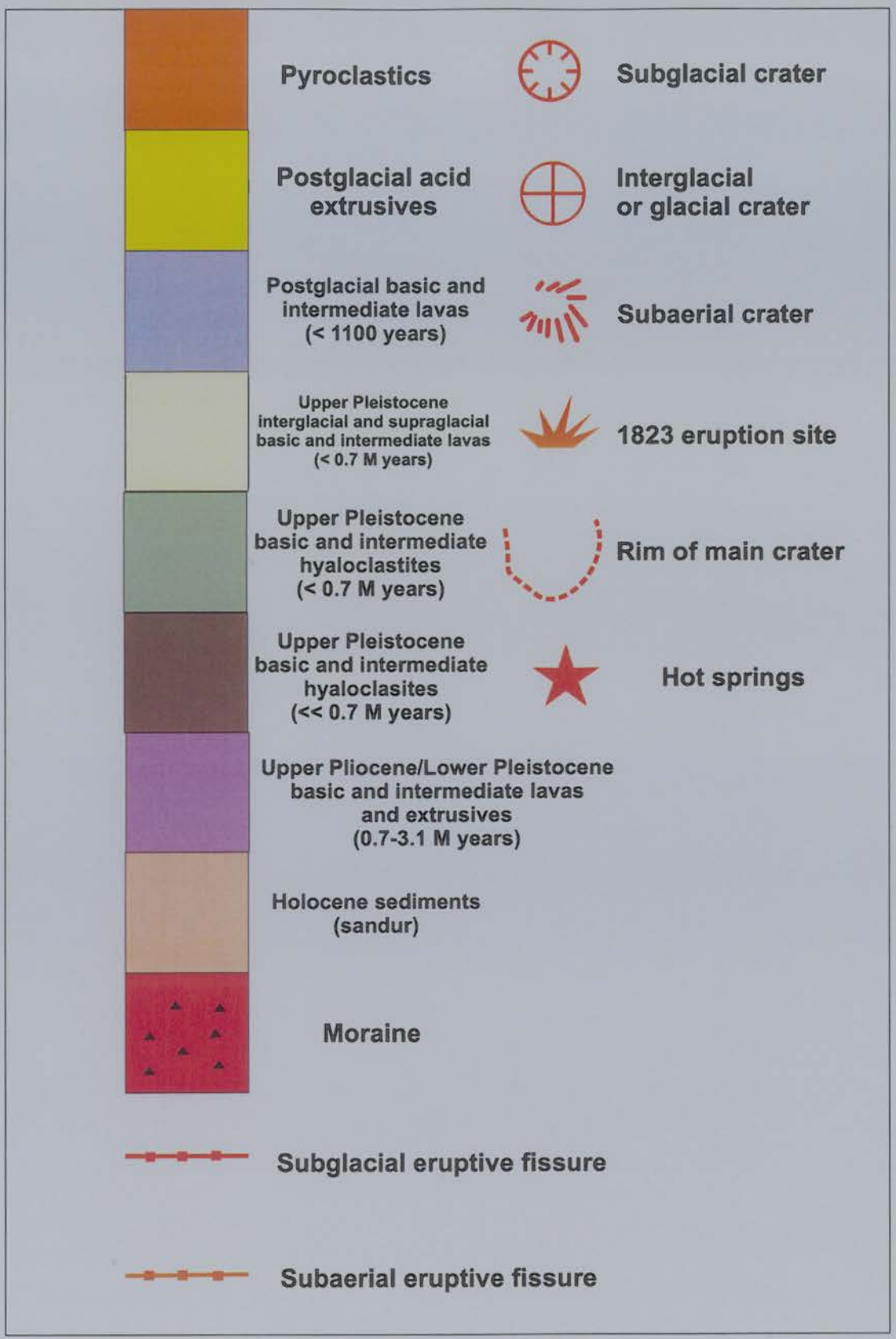

Figure 1.5b Key to geology and volcanic landforms of Eyjafjöll.

1.11 References

Batiza, R., and White, J.D.L., 2000. Submarine Lavas and Hyaloclastite. In: Sigurðsson, H., Houghton, B.F., McNutt, S.R., Rymer, H., and Stix, J. (Editors), *Encyclopedia of Volcanoes*. Academic Press, New York, pp. 361-381.

Benn, D.I., and Evans, D.J.A., 1998. *Glaciers and Glaciation*. John Wiley and Sons, London, 734 pp.

Bentley, M.J., and Dugmore, A.J., 1998. Landslides and rate of glacial trough formation in Iceland. In: L.A. Owen (Editor), *Mountain Glaciation*. Quaternary Research Proceedings No. 6, John Wiley and Sons, Ltd., Chichester, pp. 11-15.

Björnsson, H., 1979. Glaciers in Iceland. Jökull, 29: 74-80.

Dugmore, A.J., 1987. Holocene glacier fluctuations around Eyjafjallajökull, South Iceland: A tephrochronological study. Unpublished PhD Thesis, University of Aberdeen.

Dugmore, A.J., 1989. Tephrochronological studies of Holocene glacier fluctuations in South Iceland. In: J.E. Oerlemans (Editor), *Glacier Fluctuations and Climatic Change*. Kluwer Academic Publishers, pp. 37-55.

Einarsson, Þ., 1994. *Geology of Iceland: Rocks and Landscape*. Mál og menning, Reykjavík, 309 pp.

Geirsdóttir, Á., and Eiríksson, J., 1994. Growth of an intermittent ice sheet in Iceland during the Late Pliocene and Early Pleistocene. Quaternary Research, 42: 115-130.

Guðmundsson, A.T., 1996. *Volcanoes in Iceland: 10,000 years of volcanic history*. Vaka-Helgafell, Reykjavík, 136 pp.

Iceland Geodetic Survey, 1990. Mýrdalsjökull 1:50,000. Defense Mapping Agency Hydrographic/Topographic Center, Washington D.C.

Iceland Review, 1999. Heightened alert in the vicinity of Eyjafjallajökull Ice Cap. Daily News, http://www.icenews.is/08der99.html.

Ingolfsson, O., and Norðdahl, H., 1994. A review of the environmental history of Iceland 13,000-9000 yr BP. Journal of Quaternary Science, 9(2): 147-150.

Jakobsson, S.P., 1979a. Outline of the petrology of Iceland. Jökull, 29: 57-73.

Jakobsson, S.P., 1979b. Petrology of Recent basalts of the Eastern Volcanic Zone, Iceland. Acta Naturalia Islandica, 2(26): 103.

Jóhannesson, H., 1985. On the ages of the two recent lava flows in Eyjafjöll and the late glacial terminal moraines in South Iceland. Jökull, 35: 95.

Jóhannesson, H., Jakobsson, S.P., and Sæmundsson, K., 1990. Geological map of Iceland, Sheet 6, South Iceland. Icelandic Museum of Natural History and Icelandic Geodetic Survey, Reykjavík.

Jóhannesson, H., and Sæmundsson, K., 1998. Geological Map of Iceland: Tectonics. Icelandic Institute of Natural History, Reykjavík.

Jones, J.G., 1969. Intraglacial volcanoes of the Laugarvatn region, south-west Iceland - I. Quaternary Journal of the Geological Society of London, 124: 197-211.

Jónsson, J., 1988. Geological Map of the Eyjafjöll Area. Research Institute Neðri Ás, Hvéragerði.

Kaldal, I., and Víkingsson, S., 1990. Early Holocene deglaciation in Iceland. Jökull, 40: 51-66.

Kjartansson, G., 1967. The Steinholtshlaup, Central-South Iceland on January 15th, 1967. Jökull, 17: 249-262.

Larsen, G., Guðmundsson, M.T., and Björnsson, H., 1998. Eight centuries of periodic volcanism at the center of the Iceland hot spot revealed by glacier tephrastratigraphy. Geology, 26(10): 943-946.

Lawler, D.M., 1991. Sediment and solute yield from the Jökulsá Á Sólheimasandi glacierized river basin, southern Iceland. In: Maizels, J.K. and Caseldine, C. (Editors), *Environmental Change in Iceland: Past and Present.* Kluwer, Dordrecht, pp. 303-332.

Loughlin, S.C., 1995. The evolution of the Eyjafjöll Volcanic System, Southern Iceland. Unpublished PhD Thesis, University of Durham, 319 pp.

Lowe, J.J., and Walker, M.J.C., 1997. *Reconstructing Quaternary Environments.* Addison Wesley Longman Ltd., Harlow, UK, 446 pp.

Menzies, J., 1995a. Dynamics of Ice Flow. In: J. Menzies (Editor), *Modern Glacial Environments: Processes, Dynamics, and Sediments*. Butterworth-Heinemann, Oxford, pp. 621.

Menzies, J., 1995b. Glaciers and Ice Sheets. In: J. Menzies (Editor), *Modern Glacial Environments: Processes, Dynamics, and Sediments*. Butterworth-Heinemann, Oxford, pp. 621.

Newton, A., 1999. Ocean-transported pumice in the North Atlantic. Unpublished PhD thesis Thesis, University of Edinburgh.

Norðdahl, H., 1990. Late Weichselian and early Holocene deglaciation history of Iceland. Jökull, 40: 27-50.

Rist, S., 1967. Glacier variations in meters 1964/65, 1965/66, and 1966/67. Jökull, 17: 321-325.

Sæmundsson, K., 1979. Outline of the geology of Iceland. Jökull, 29: 7-28.

Sigurðsson, H., 2000. Introduction. In: Sigurðsson, H., Houghton, B.F., McNutt, S.R., Rymer, H., and Stix, J. (Editors), *Encyclopedia of Volcanoes*. Academic Press, New York, pp. 1-13.

Sigurðsson, O., 1989. Glacier Variations (1930-1960, 1960-1980, 1980-1987, and 1987-1988). Jökull, 39.

Sigurðsson, O., 1999. Glacier variations: 1930-1960, 1960-1990, and 1995-1996. Jökull, 47: 101-107.

Simkin, T., and Siebert, L., 2000. Appendix 2: Catalog of Historically Active Volcanoes on Earth. In: Sigurðsson, H., Houghton, B.F., McNutt, S.R., Rymer, H., and Stix, J. (Editors), *Encyclopedia of Volcanoes*. Academic Press, New York, pp. 1365-1367.

Smellie, J.L., 2000. Subglacial Eruptions. In: Sigurðsson, H., Houghton, B.F., McNutt, S.R., Rymer, H., and Stix, J. (Editors), *Encyclopedia of Volcanoes*. Academic Press, New York, pp. 403-418.

Smellie, J.P., and Skilling, I.P., 1994. Products of subglacial eruptions under different ice thicknesses: two examples from Antarctica. Sedimentary Geology, 91: 115-129.

Þórarinsson, S., 1943. Oscillations of the Iceland glaciers in the last 250 years. Geografiska Annaler, 25: 1-54.

Walker, G.P.L., 2000. Basaltic Volcanoes and Volcanic Systems. In: Sigurðsson, H., Houghton, B.F., McNutt, S.R., Rymer, H., and Stix, J. (Editors), *Encyclopedia of Volcanoes*. Academic Press, New York, pp. 283-289.

Zimbelman, J.R., 2000. Volcanism on Mars. In: Sigurðsson, H., Houghton, B.F., McNutt, S.R., Rymer, H., and Stix, J. (Editors), *Encyclopedia of Volcanoes*. Academic Press, New York, pp. 771-783.

Chapter 2: Physical principles of radio echo sounding

2.1 Introduction

In order to undertake a survey using ice radar (or radio echo sounding), it is first necessary to understand the physical principles of electromagnetic waves and their transmission and propagation through the medium of ice. The propagation velocity of electromagnetic waves is highly dependent on the dielectric properties of the material through which they pass and are a function of the frequency and wavelength at which they are transmitted. Electromagnetic waves are typically transmitted by pulse radar for glaciological applications like the current study. As electromagnetic waves pass through temperate ice, the energy is absorbed, refracted, reflected, and scattered by liquid water and englacial debris. When electromagnetic waves encounter a boundary between two dielectrically-different materials (like ice and bedrock), a large amount of the energy is reflected and travels back through the ice to be sampled by a receiver at the surface. The radar receiver records echoes which have propagated across different travel paths, creating a waveform from which ice depth and other information can be extracted.

This chapter describes the ice radar equipment utilized in the survey and introduces the principles of radio echo sounding as a foundation from which the research methodology develops.

2.2 Ice radar equipment

The instrument used for the survey is a Mark II impulse radar, designed by Frank Jacobsen (Jacobsen, 1996), based on the principles set forth by Watts and England (1976). It is an instrument created for use on temperate glaciers and designed for portability. The system components include an impulse transmitter, oscilloscope receiver, 12 half-lengths of antennae, and a receiver connector box with a coaxial cable (***Figure 2.1***).

2.2.1 Transmitter

The transmitter is a monopulse sounder with a center frequency range, depending on the antenna dimensions used, of about 2-10 MHz. Pulses with a rise time of less than 0.1 μs are generated by an avalanche transistor. A short pulse width between 0.11 and 0.66 μs and a radiated power of 8 kW allow the signal to be strong in comparison to radio-frequency noise (Watts and England, 1976). It is possible to transmit approximately one cycle at a center frequency determined by the antennae length (Jacobsen, 1996).

2.2.2 Antennas

The antennas are broad-band half-wave dipoles, resistively-loaded, similar to those described by Wu and King (1965). The evenly-spaced resistors reduce the amount of noise introduced by antenna ringing (Watts *et al.*, 1975). Ringing occurs when the signal reflects from the antenna ends (Jacobel *et al.*, 1988). There are three sets of antennas: one is 20 m in half-length and the other two are 10 m in half-length; of these two, one set has twice the resistance.

2.2.3 Receiver

The receiver is a Fluke 99B Series II digital oscilloscope which samples, displays, and saves incoming signals. The scope provides a time-step resolution of 0.04 μs and a sampling rate of 5 giga-samples per second (GS s^{-1}). The oscilloscope has the ability to stack (or average) a total of 512 individual waveforms to create a final waveform with a high signal-to-noise ratio.

The transmitter attaches to two half-lengths of antennae laid on the ice surface a set distance away from the receiver connector box to which are attached matching antennas. The receiver box connects to the oscilloscope by coaxial cable.

With this radar arrangement, the minimum vertical range (the smallest depth that may be sounded) is about 30 m. The range resolution, which describes to within

what accuracy a received signal can be resolved, is 8 m (Jacobsen, 1996). The range resolution is based exclusively on the system components, and does not include the vertical resolution based on transmission frequency.

2.3 Frequency and wavelength of electromagnetic waves

Electromagnetic waves are periodic disturbances transmitted through media as energy. Each wave is comprised of a magnetic and an electrical component, represented by the magnetic flux density, B, and the electrical field strength, E, respectively (***Figure 2.2***). These two components are at right angles to each other but maintain the same phase and frequency (Allaby and Allaby, 1990). The periodic wave pattern repeats itself in both time and space as harmonic repetition. Electromagnetic wave motion is usually described by a sine function:

$$u = A\sin\left(2\pi\left[\frac{x}{\lambda} - \frac{t}{T}\right]\right),$$

Equation 2.1

where

u = the harmonic displacement of a wave from its mean position

A = amplitude

x = displacement along the x-axis (or direction of travel)

λ = wavelength

t = time

T = period (Lowrie, 1997).

The components of the electromagnetic wave most relevant to the current research are the frequency and the wavelength. Since the objective of the survey is to measure ice depth at Eyjafjallajökull in order to determine the morphology of the subglacial surface and quantify ice volume, ice depth values must be extracted from the received waveforms. In order to do this, the frequency and wavelength of the transmitted energy must be known so that the velocity can be calculated and depth determined from travel times.

The wavelength, λ, is the regular distance at which the maximum disturbance (represented by the amplitude) is repeated along the direction of travel (Lowrie, 1997). The frequency, υ, describes how rapidly the wavelength is repeated in time and is measured in Hertz (s^{-1}), the number of cycles per second. The electromagnetic spectrum specifies the range of frequencies (Hz) or wavelengths (m) of electromagnetic radiation (***Figure 2.3***). Ice radar frequencies lie in the HF (High Frequency) to VHF (Very High Frequency) range, approximately 1 MHz to 1 GHz, with corresponding wavelengths of 100 m to 1 m.

In radio echo sounding, electromagnetic energy is transmitted in pulses. The systems are typically impulse radar, sometimes called ground-penetrating radar (GPR). Gogineni *et al.* (1998) provide a summary of various impulse radar systems used for ice radar surveys. Pulses of electromagnetic energy are transmitted at equal time intervals and are sampled (or read) by a receiver (the sampling interval). A single pulse of electromagnetic energy contains a collection of frequencies, the range of which is called 'bandwidth'. The pulse width, or duration of the transmitted pulse, is the inverse of the center frequency, the frequency around which most of the pulse energy is concentrated (Parasnis, 1997). The 'frequency of an electromagnetic wave', refers to the center frequency. The center frequency is a function of the speed of light, the antenna dimensions, and the dielectric composition of the material through which the electromagnetic pulse is transmitted, such that

$$\upsilon_c = \frac{c}{\left(4h\sqrt{\varepsilon_r}\right)},$$

Equation 2.2

where

υ_c = center frequency (MHz)

c = velocity of electromagnetic energy in free space (300 m μs^{-1})

h = half-length of antenna (m)

ε_r = relative permittivity (Parasnis, 1997).

If the permittivity of free space, ε_0, is assumed to equal one, then the frequency of an electromagnetic wave transmitted through free space is between 2

and 8 MHz. ***Table 2.1*** gives the center frequency values for the Mark II impulse radar, using the available antenna dimensions in various combinations.

The wavelength of electromagnetic waves in free space is related to the transmission frequency, such that

$$\lambda_0 = \frac{c}{\upsilon}.$$

Equation 2.3

Therefore, the corresponding wavelengths of electromagnetic energy transmitted at 2-8 MHz in free space are between 40 and 160 m (***Table 2.1***).

Since the frequency and wavelength of electromagnetic waves in free space are shown to depend on the free space velocity, then the wavelength in ice is calculable if the ice velocity is known. The velocity in ice is a function of its dielectric properties.

2.3.1 Dielectrics

Ice is a dielectric material, a substance defined by the varying proportions of water it contains, its density, and electrical and magnetic behavior. The ease with which a dielectric material conducts electromagnetic energy (its permittivity) is measured relative to that of free space and is referred to as the relative permittivity (or the dielectric constant), such that

$$\varepsilon = \varepsilon_r \varepsilon_0,$$

Equation 2.4

where

ε = permittivity

ε_r = relative permittivity (or dielectric constant)

ε_0 = free space permittivity (8.854×10^{-12} (Clarke *et al.*, 1989)).

Table 2.2 provides examples of the relative permittivity of a variety of materials (Reynolds, 1997).

The variation in relative permittivity between materials makes electromagnetic waves useful in detecting changes in media. If a wave propagating through a medium encounters a dielectric material with a different relative permittivity, the velocity of the propagating wave will change, because the velocity is determined by the relative permittivity, such that

$$v = \frac{c}{\sqrt{\varepsilon_r}}.$$

Equation 2.5

Radio wave velocities will decrease, for example, as waves move between ice layers of increasing density (Robin, 1975). ***Table 2.2*** gives the electromagnetic wave velocities associated with the differing relative permittivities of various materials.

Now the wavelength of electromagnetic waves in ice can be calculated. Just as the velocity in ice is computed relative to the velocity in free space (***Equation 2.5***), the wavelength in ice is determined relative to the wavelength in free space (Welch *et al.*, 1998). Dividing by the square root of the relative permittivity of ice gives

$$\lambda_{ice} = \frac{\lambda_0}{\sqrt{\varepsilon_r}}$$ (Davis and Annan, 1989).

Equation 2.6

Table 2.1 provides the wavelength values calculated for a theoretical relative permittivity in ice of 3.2 (Watts and England, 1976). It is clear that wavelengths are reduced when electromagnetic energy enters ice.

2.4 Electromagnetic wave propagation in ice

The concepts of electromagnetic wave propagation are derived from seismic reflection principles and adapted for the specific medium of ice (Welch *et al.*, 1998). The principles of ray path geometry and reflection are an essential part of

understanding how electromagnetic radiation travels through ice. The received waveform records the travel paths of electromagnetic waves through, and interaction with, the material of ice.

If an electromagnetic pulse is transmitted in a homogeneous medium, such as free space, the energy propagates equally in all directions. However, if a pulse is transmitted across a boundary between two media, such as air and ice, the transmitted energy no longer propagates with radial symmetry. The energy is bent by the boundary where the interface focuses the pulse by refraction.

A ray is the instantaneous direction of electromagnetic wave propagation at any point within a medium (Parasnis, 1997). Snell's Law calculates the constant angle of the cone into which all rays are refracted when they encounter a boundary between two media. It states that the angle of a ray incident to an interface, divided by its velocity, will be equivalent to the angle of a ray refracted by an interface, divided by its velocity, such that

$$\frac{\sin\theta_i}{v_i} = \frac{\sin\theta_r}{v_r},$$

Equation 2.7

where

θ_i = angle of incidence

θ_r = angle of refraction

$v_{i,r}$ = velocity.

Consequently, an incident ray, travelling at the speed of light, c, is proportional to a refracted ray travelling at the speed of electromagnetic waves in ice. Assuming a theoretical velocity of 169 m μs^{-1} (Watts and England, 1976), θ_r = 34°. The maximum angle of propagation of a refracted ray is therefore 34°. Any ray which propagates at a greater angle of incidence is refracted inward upon transmission across the boundary, focusing all the energy into a cone (***Figure 2.4***).

When the electromagnetic energy contained within this cone intercepts a boundary between two media with different relative permittivities (for example, the boundary between ice and bedrock), the base of the cone, or 'footprint', defines a surface area within which all the energy is concentrated. All the reflected energy in the area of the footprint contributes to a single ground signal that is recorded by the

receiver. The first 'Fresnel zone' describes the circular area at the base of the cone (***Figure 2.5***). The size of the first 'Fresnel zone' is a function of the frequency and travel time of the electromagnetic wave from source to reflector (t). The radius of the first Fresnel zone (r) is

$$r = \frac{v}{2}\sqrt{\frac{t}{v}}.$$

Equation 2.8

Thus, an electromagnetic pulse transmitted at a frequency of 5 MHz, propagating at a velocity of 169 m μs^{-1} for 1 μs, will intercept an area of the boundary surface with a radius of about 38 m. A circle with a diameter of about 76 m will represent the 'footprint' area at an ice depth of just over 150 m.

2.4.1 Waveforms

All of the energy which intercepts the bedrock surface within the first 'Fresnel zone' may be reflected back to the ice surface and recorded by the receiver as an echo. When the receiver samples the transmitted pulse, the signal received is called the ***waveform***, and is comprised of multiple echoes which correspond to the transmitted pulse following different path lengths. A waveform is displayed graphically with travel time on the x-axis and amplitude on the y-axis. At least two and sometimes three or more separate waves can be identified in each waveform. The most important are the air wave (or direct wave), the lateral wave, and the ground wave (***Figure 2.6***).

The ***airwave (or direct wave)*** travels directly across the ice surface through the air from transmitter to receiver. The airwave is commonly used to trigger the oscilloscope sweep; it makes the receiver start timing the arrival of the reflected wave. The velocity of electromagnetic waves in air is faster than the velocity in ice, so the air wave will always arrive first in the waveform. The travel time of the air wave is calculated from the separation distance (m) between transmitter and receiver, divided by the speed of electromagnetic waves in air, c.

The ***lateral wave*** travels from transmitter to receiver through the near surface ice. It is not always detectable in the received waveform and its existence has been debated (Jezek *et al.*, 1978). The behavior of the lateral wave is not well known for the medium of ice; it may cause interference with the airwave, delaying its arrival at the receiver (Dinnis, 2000).

The ***ground wave*** travels from the transmitter to the receiver through the ice, reflecting off the bed surface. The wave propagates at the velocity of electromagnetic waves in ice, which, at a theoretical velocity of 169 m μs^{-1} (Evans, 1965), is slower than c. In addition, the path length of the ground wave will always be longer than that of the air wave. Thus it arrives after the air wave in the received waveform. The two-way travel time of the ground wave is measured on the waveform as the difference between the arrival of the air wave and the arrival of the ground wave, plus the travel time of the air wave.

The Law of Reflection, which states that the angle of incidence equals the angle of reflection, describes the process by which the ground wave is reflected (Lowrie, 1997). Based on this principle, a simple geometric relation can be constructed to calculate the depth of ice through which the ground wave has travelled (***Figure 2.7***).

If one considers a right-angled triangle, where d_2 is the hypotenuse, Pythagorean geometry states that

$$(d_1)^2 + (H_i)^2 = (d_2)^2,$$

Equation 2.9

from which

$$H_i = \sqrt{(d_2)^2 - (d_1)^2}.$$

Equation 2.10

By substituting time and velocity parameters for distance, depth is determined as

$$H_i = \sqrt{\frac{(t_2 v)^2}{4} - \frac{(t_1 c)^2}{4}}.$$

Equation 2.11

The travel time of the ground wave, converted to a depth, represents the ice depth over the whole area of the footprint. The implication of this for the current study is that the depth value extracted from a single waveform represents the shallowest depth over what can be quite a large area.

2.4.2 Temperate ice

The specific medium through which electromagnetic waves propagate in this study is temperate ice. The properties of temperate ice have profound implications for the propagation and reflection of electromagnetic energy and the application of radio echo sounding techniques.

The presence of liquid water in temperate ice makes interpreting received waveforms difficult. Temperate ice is, by definition, at the pressure melting point, and contains liquid water within the ice mass, in lenses, pockets, channels, and inter-crystalline gaps (Paterson, 1994). Temperate ice is not only warmer than cold ice, but the ice itself is less homogeneous as a whole. Many layers of varying density are present, resulting from the melting, re-freezing, flow, and metamorphosis processes which have occurred (Benn and Evans, 1998). Importantly, the difference between the relative permittivities of water and ice is greater than that of ice and bedrock. Electromagnetic energy reflected from liquid water contained within the ice creates a stronger echo in a received waveform than energy reflected from the bed surface. This makes it difficult to identify the ground wave in the received waveform.

The presence of water in temperate ice can also act to attenuate a radar signal by scattering or absorbing the energy. This weakening of the signal can likewise interfere with the interpretation of the received waveform.

In addition to water, temperate ice contains debris. Rock is accumulated at the ice surface from valley walls and incorporated within the ice. Tephra, ash from volcanic explosions, is deposited on the surface and remains layered within the glacier after successive years of snow accumulation. This englacial debris reflects and scatters radio waves.

One way to surmount these difficulties is to transmit electromagnetic waves at a wavelength that is much larger than the diameter of englacial debris and liquid

water bodies, so that the amount of scattering from the englacial obstacles will not obscure the ground wave. This is accomplished by reducing the transmitted frequency. If the diameter of an obstacle is much greater than the wavelength, all the energy will be reflected by the obstacle. If an englacial obstacle is smaller than the wavelength, some of the energy will pass by, while only a small amount will be reflected, scattered, or absorbed by the material. The scattering that occurs is called Mie scattering, where objects with dimensions of the same order as the wavelength of the transmitted pulse cause scattering of energy in a highly complex manner (Reynolds, 1997).

Watts and England's (1976) seminal paper on equipment requirements for sounding temperate glaciers established the ideal frequency range needed to limit the amount of scattering. They stress that it is not the attenuation of the signal that is most affected by internal scatterers, but rather the "masking of the bottom [echo] by the diffuse return from a multitude of scatterers." The most desirable operating frequency is below 10 MHz, ideally 5 MHz. Other researchers have tried a variety of frequencies, usually in the 1-32 MHz range (Björnsson *et al.*, 1977; Strangway *et al.*, 1974; Sverrisson *et al.*, 1980; Watts and Wright, 1981). The frequencies used in the Eyjafjallajökull study range from 2-10 MHz.

Electromagnetic energy is reduced as it travels from the transmitter to receiver through ice. The physical properties of the material through which the radiation propagates determine the amount of energy loss. The received energy is always less than that which was originally transmitted, diminished by reflection, refraction, absorption, geometrical spreading, and scattering (Davis and Annan, 1989) (***Figure 2.8***). The reduction in amplitude of the radar signal is referred to as attenuation.

The physical properties of the target material will likewise contribute to energy loss. These include bulk conductivity and other electrical behavior, the thickness of the layer, the composition of the material, and the relative abundance of each constituent (Annan and Davis, 1977; Reynolds, 1997). For example, if a bed material, such as deforming till, contains a highly conductive saturating fluid like liquid water, then the proportion of energy reflected will be higher than that of bedrock (the relative permittivity between ice and water being greater than that

between ice and rock). The roughness of the boundary, relative to the wavelength of the transmitted wave, will also affect the amount of energy reflected. A smooth surface reflects more energy than a rough surface, returning a sharper echo. A rough surface scatters more of the energy and shows very few, if any, distinct reflection events (Reynolds, 1997).

2.5 Resolution

An important part of any radar survey is defining the resolution. Resolution is the "action or process of separating or reducing something into its constituent parts" (Mifflin, 1982). The determination of the size of individual components which can be distinguished from one another influences the choice of application for the dataset. The ability to resolve small-scale bed features on the order of ~ $1m^3$, as opposed to 10 m^3 or even 100 m^3, will obviously have a major impact on how the subglacial features can be interpreted. In the present case, it is important to define the horizontal resolution so that the limit of separability between individual volcanic landforms such as tuyas and tindars across the bed surface can be identified. The vertical resolution will define the accuracy of the ice depth estimation.

The ability to accurately resolve a reflector horizontally and vertically depends on the transmitted wavelength and the depth to the reflector.

2.5.1 Vertical

In a radio echo sounding survey, vertical resolution is the "ability to differentiate between two signals adjacent to each other in time" (Reynolds, 1997). The equivalent length in meters defines the size of reflector which can be resolved. Vertical resolution is a function of transmitted wavelength. The Rayleigh criterion states that a reflecting feature less than one-quarter of the transmitted wavelength cannot be resolved (Skolnik, 1969). For a transmission frequency of 5 MHz, the wavelength is 60 m; the smallest vertical feature that can be resolved is therefore 15 m. By increasing the frequency, the wavelength is reduced and the vertical resolution is consequently improved. The trade-off, however, is that scattering

increases. ***Table 2.1*** gives the vertical resolution in meters for the Eyjafjallajökull dataset, using the instrument frequencies available.

2.5.2 Horizontal

Horizontal resolution is the minimum surface area of a feature on a reflecting bed surface which can be disinguished from an adjacent feature. It is a function of both the area of the first Fresnel zone and the spatial sampling. Theoretically, the larger the first Fresnel zone (or the deeper the ice), the poorer will be the horizontal resolution in discriminating between adjacent bed features (Reynolds, 1997). If the sampling grid is fine enough so that each footprint borders or overlaps another footprint, then the area of the footprint will define the horizontal resolution. However, if the sampling density is much coarser, there will be gaps between the individual footprints and the horizontal resolution will be lower than the area defined by the first Fresnel zone. The horizontal resolution for the Eyjafjallajökull dataset is calculated in *Appendix B*, after the spatial sampling distance has been introduced.

2.6 Summary

The physical principles of radio echo sounding provide a foundation from which to develop a survey methodology. The components of the Mark II impulse radar described transmit electromagnetic energy at a frequency range of 2-10 MHz in free space. The wavelengths produced by this range of frequencies are sufficiently long enough to bypass internal scatterers which may otherwise obscure the ground reflection. The ice depth can be determined from the ground wave travel times measured by the received waveform. The vertical resolution of the Eyjafjallajökull radar survey is between 5 and 25 m, allowing adjacent features greater than this scale to be distinguished from one another. The horizontal resolution of the dataset is definable only when the spatial sampling density is known.

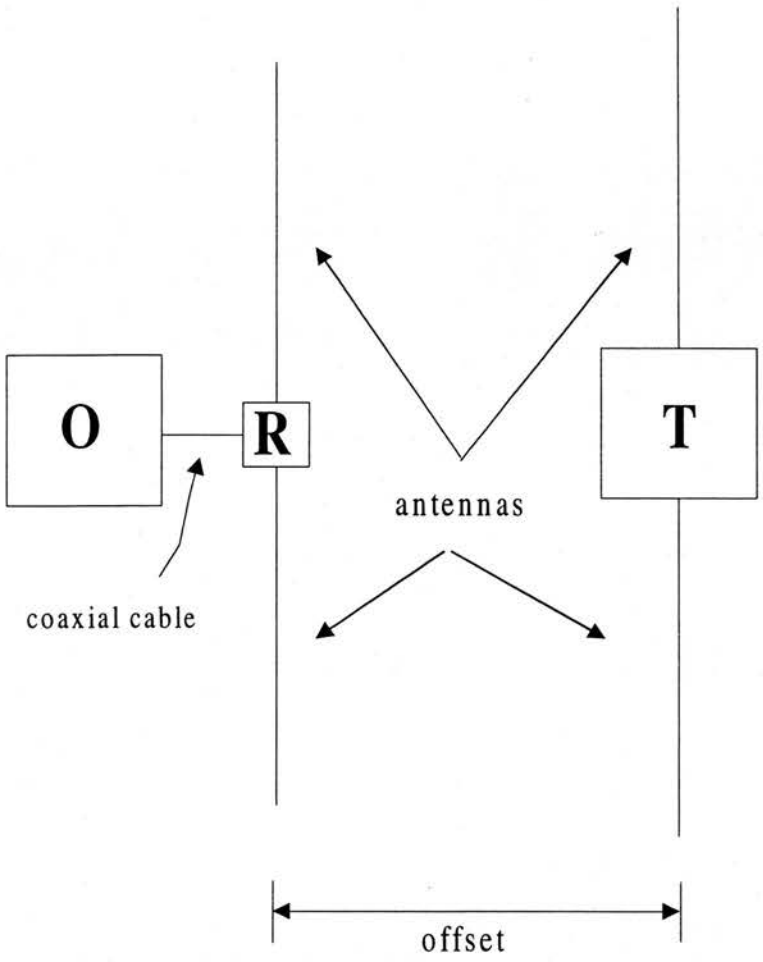

Figure 2.1 Radar instrument components and setup (T = transmitter, R = receiver, O = oscilloscope). Two antenna half-lengths attach to both the transmitter and receiver, components which are placed on the ice surface a set distance apart. The oscilloscope connects to the receiver by coaxial cable.

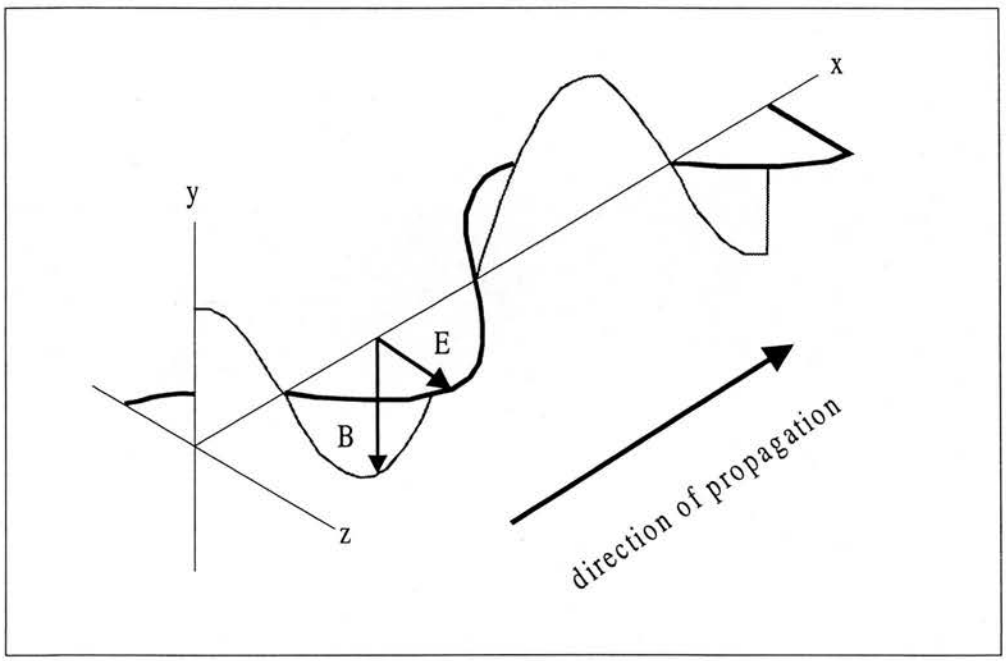

Figure 2.2 Structure of an electromagnetic wave (redrawn from Reynolds, 1997). Two components, magnetic and electric, compose an electromagnetic wave. The magnetic flux density, *B*, is perpendicular to the electrical field strength, *E*. The two wave components maintain the same phase and frequency.

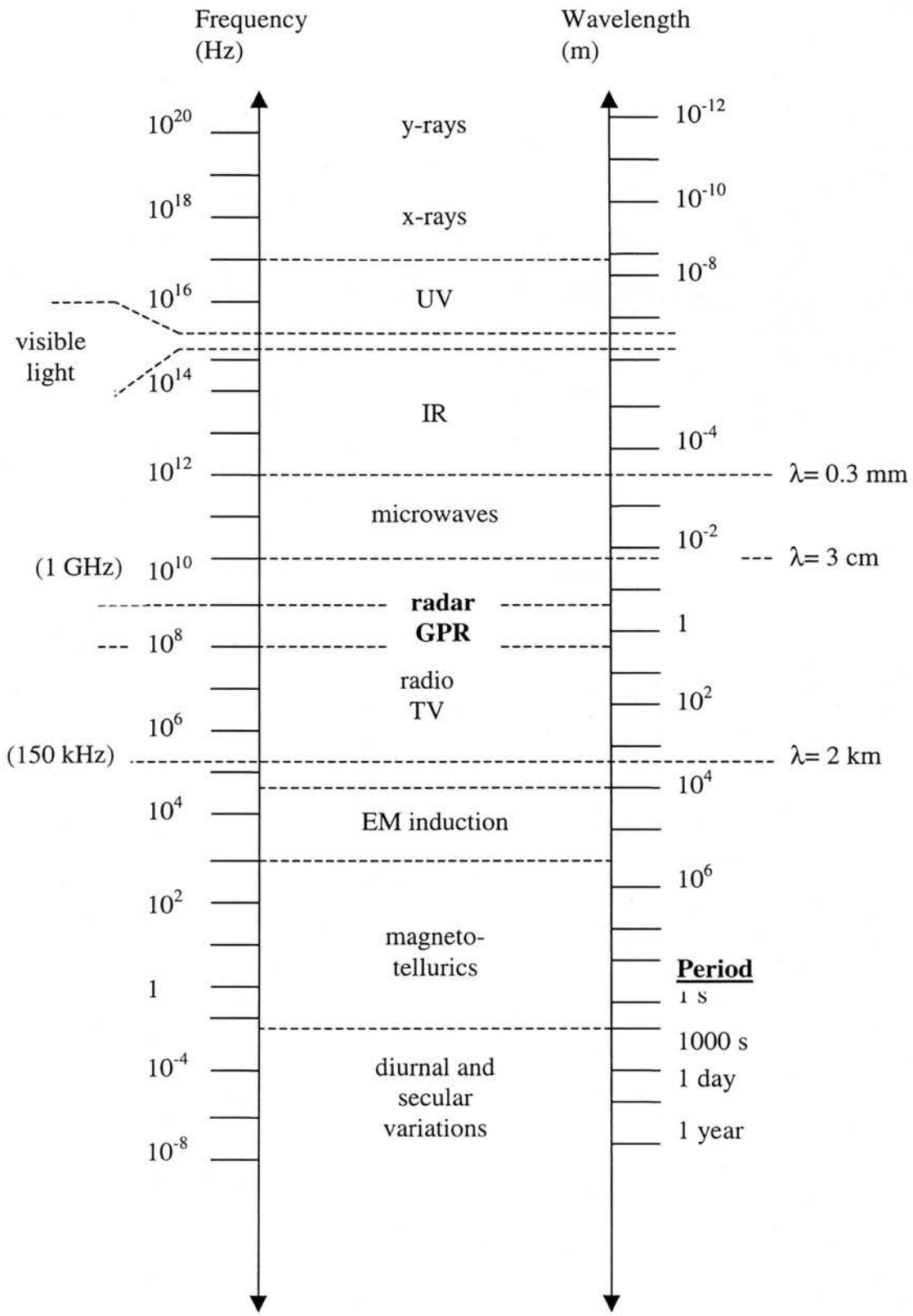

Figure 2.3 The electromagnetic spectrum. Radar frequencies are typically between 1 MHz and 1 GHz, with corresponding wavelengths of 100 - 1 m.

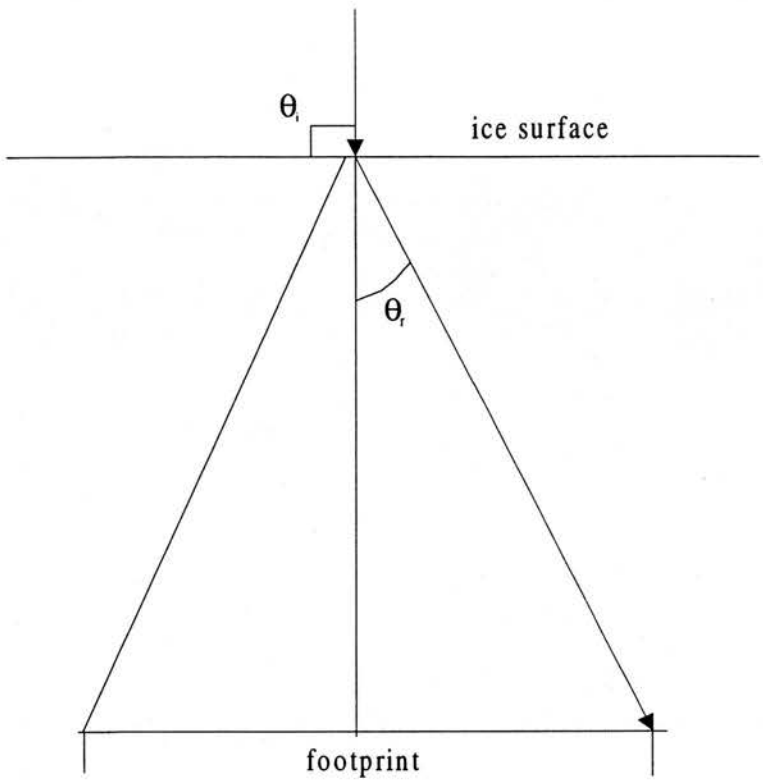

Figure 2.4 Cone of refracted electromagnetic energy derived from Snell's Law. An incident ray ($\theta_i = 90°$), travelling at the speed of light, *c*, is proportional to a refracted ray ($\theta_r = 34°$), travelling at electromagnetic wave velocity in ice (169 m μs^{-1}) (Reynolds, 1997).

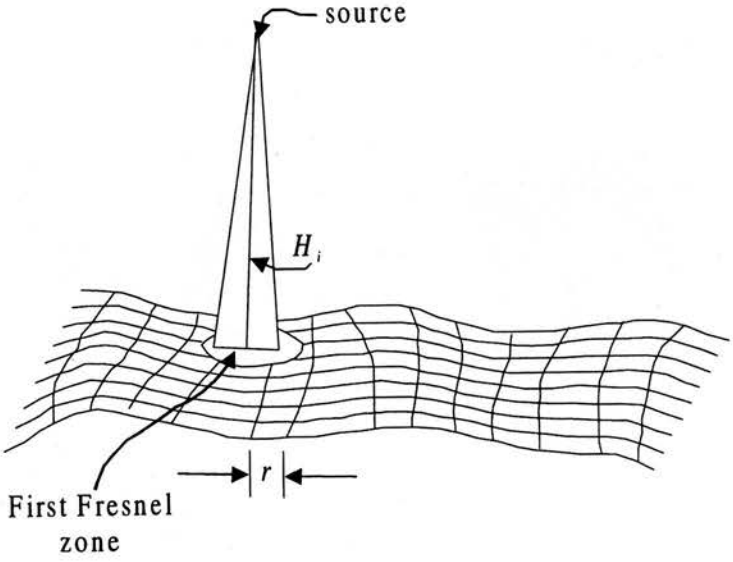

Figure 2.5 The first Fresnel zone defines the size of the area within which all propagating electromagnetic energy intercepts a dielectric interface. The radius, *r*, is a function of the frequency and ice depth, H_i (redrawn from Reynolds, 1997).

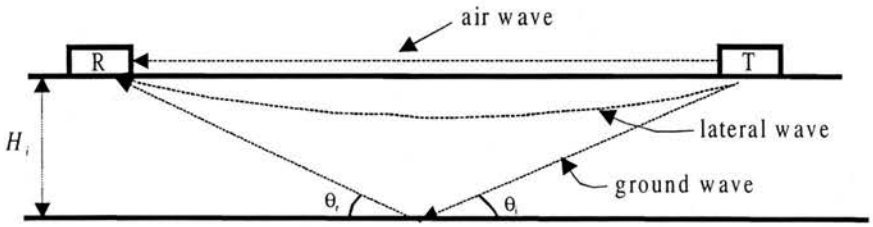

A

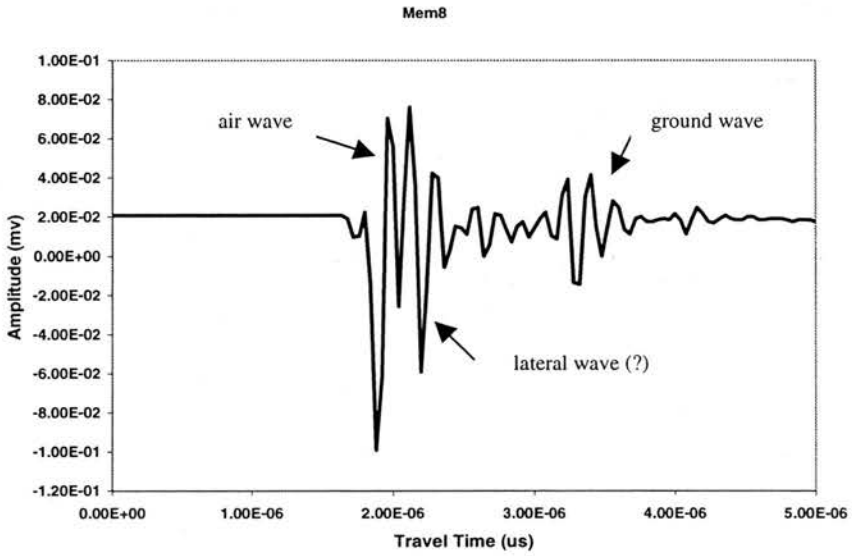

B

Figure 2.6 Travel paths of waves in ice and example of a received waveform. a) Travel paths of electromagnetic waves. An air wave travels directly through the air from transmitter to receiver, at a velocity of *c*. The lateral wave travels through ice in the near-surface air/ice interface, at a velocity determined by the dielectric properties of near-surface ice. The ground wave travels through ice from the transmitter, reflects from the bed surface, and travels back through ice to the receiver. The ground wave conforms to the Law of Reflection, where $\theta_i = \theta_r$. b) Example of a waveform and its components. A waveform indicates the order in which the waves arrive at the receiver and their corresponding travel times and amplitudes. The air wave arrives first, having travelled at the speed of light. The lateral wave is not always detectable in a waveform. The ground wave is reduced in amplitude compared to the air wave, having attenuated along its travel path.

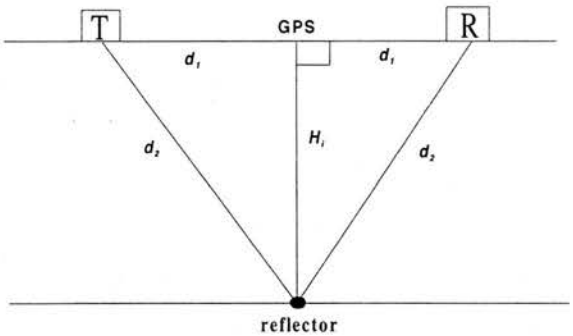

A

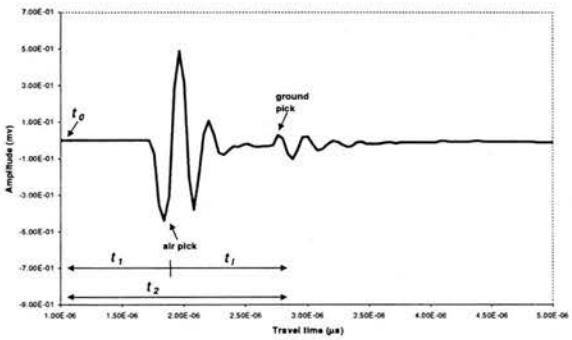

B

$$t_1 = \frac{2d_1}{c}$$

$$t_2 = \frac{2d_2}{v_i}$$

$$t_i = t_2 - t_1$$

where

$2d_1$ = offset distance between transmitter and receiver (m)

$2d_2$ = travel path of EM wave through ice (m)

H_i = ice thickness (m)

c = velocity of EM waves in free space (m μs^{-1})

v_i = velocity of EM waves in ice (m μs^{-1})

t_1 = travel time of air wave from transmitter to receiver (μs)

t_2 = travel time of ground wave from transmitter to receiver (μs)

C

Figure 2.7 Radar sounding geometry. a) Travel paths of an electromagnetic wave transmitted through a dielectric material and reflected from a dielectric interface. H_i represents the depth to reflector or ice thickness in m. A ground wave travels from transmitter to receiver along the path $2d_2$. An air wave travels along the path $2d_1$. b) Example of a received waveform and measurement of travel time. Travel times of air and ground waves are measured on a waveform at the 'pick'. t_1 represents the travel time of the air wave and is calculated as $2d_1/c$, where both parameters are known. t_i is the quantity determined by subtracting the air wave pick from the ground wave pick and is added to t_1 to find the two-way travel time of the ground wave, t_2. c) Explanation of symbols.

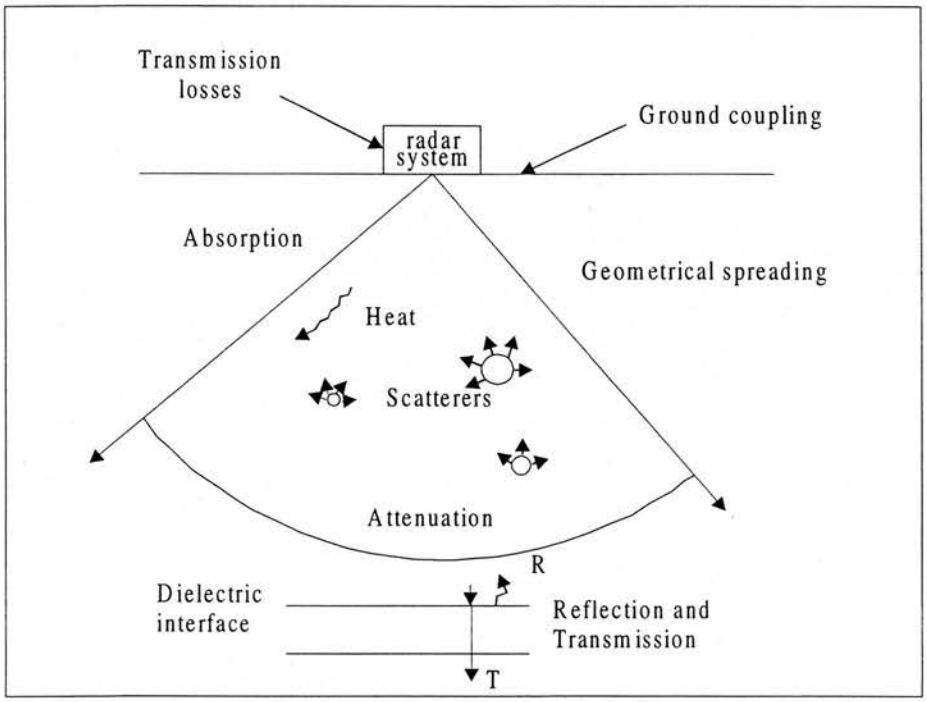

Figure 2.8 Factors which contribute to the attenuation of an electromagnetic wave transmitted through a dielectric material include transmission losses associated with the radar system and antennas, ground-coupling at the air-ice interface, geometrical spreading and absorption within the ice, heat loss, Rayleigh and Mie scattering, and losses associated with reflection and transmission at the bed surface (redrawn from Reynolds, 1997).

Antenna half-lengths (m)	Center frequency (υ_c, MHz)	Wavelength (λ, m)		Vertical resolution (m)
	υ_0 Free space	λ_0 Free space	λ_{ice} Theoretical ($\varepsilon_r = 3.2$)	
10	7.5	40	22	5.5
20	3.8	79	44	11
30	2.5	120	67	17
40	1.9	158	88	22

Table 2.1 Center frequency and wavelength values calculated for the Mark II impulse transmitter and accompanying antennas for electromagnetic wave propagation in free space and theoretical temperate ice. Theoretical maximum vertical resolution is computed for the wavelengths propagating in theoretical temperate ice.

Material	ε_r	v (m μs^{-1})
air	1	300
fresh water	81	33
sea water	81	33
polar snow	1.4 - 3	194 - 252
polar ice	3 - 3.15	168
temperate ice	3.2	167
pure ice	3.2	167
freshwater lake ice	4	150
sea ice	2.5 - 8	78 - 157
granite	5 - 8	106 - 120
basalt (wet)	8	106
quartz	4.3	145

Table 2.2 Relative permittivity values and corresponding electromagnetic wave velocities for a range of dielectric materials (Reynolds, 1997).

2.7 References

Allaby, A., and Allaby, M., 1990. *Oxford Concise Dictionary of Earth Sciences.* Oxford University Press, Oxford, 410 pp.

Annan, A.P., and Davis, J.L, 1977. Radar range analysis for geological materials. Paper 77-1B, Geological Survey of Canada: 117-127.

Benn, D.I., and Evans, D.J.A., 1998. *Glaciers and Glaciation.* John Wiley and Sons, London, 734 pp.

Björnsson, H., Ferrari, R.L., Miller, K.J., and Owen, G., 1977. A 1976 radio echo sounding expedition to the Vatnajökull ice cap, Iceland. Polar Record, 18(115): 375-377.

Clarke, G.K.C., Cross, G.M., and Benson, C.S., 1989. Radar imaging of glaciovolcanic stratigraphy, Mount Wrangell Caldera, Alaska: Interpretation model and results. Journal of Geophysical Research, 94(B6): 7237-7249.

Davis, J.L., and Annan, A.P., 1989. Ground-penetrating radar for high-resolution mapping of soil and rock stratigraphy. Geophysical Prospecting, 37: 531-551.

Dinnis, A.K., 2000. Modelling a radio echo sounding system (Internal Report), University of Edinburgh, Department of Electrical Engineering, 25 pp.

Evans, S., 1965. Dielectric properties of ice and snow - a review. Journal of Glaciology, 5(42): 773-92.

Gogineni, S., Chuah, T., Allen, C., Jezek, K., and Moore, R.K., 1998. An improved coherent radar depth sounder. Journal of Glaciology, 44(148): 659-669.

Jacobel, R.W., Anderson, S.K., and Rioux, D.F., 1988. A portable digital data-acquisition system for surface-based ice-radar studies. Journal of Glaciology, 34(118): 349-354.

Jacobsen, F.M., 1996. A highly reliable mono-pulse radio echo-sounding system for use on temperate valley glaciers. Glacial Geology and Geomorphology (http://ggg.qub.ac.uk/ggg/papers/full/1996/rp02/rp02pr.html).

Jezek, K.C., Clough, J.W., Bentley, C.R., and Shabtaie, S., 1978. Dielectric permittivity of glacier ice measured *in situ* by radar wide-angle reflection. Journal of Glaciology, 21(85): 315-329.

Lowrie, W., 1997. *Fundamentals in Geophysics*. Cambridge University Press, Cambridge, 504 pp.

Mifflin, H. (Editor), 1982. *The American Heritage Dictionary*. Houghton Mifflin, Boston, 1568 pp.

Parasnis, D.S., 1997. *Principles of Applied Geophysics*. Chapman and Hall, London, 429 pp.

Paterson, W.S.B., 1994. *The Physics of Glaciers*. Pergamon, 480 pp.

Reynolds, J.M., 1997. *An Introduction to Applied and Environmental Geophysics*. John Wiley and Sons, Ltd., Chichester, 796 pp.

Robin, G.d.Q., 1975. Velocity of radio waves in ice by means of a bore-hole interferometric technique. Journal of Glaciology, 15(73): 151-159.

Skolnik, M.I., 1969. *Introduction to Radar Systems*. McGraw-Hill, New York, 648 pp.

Strangway, D.W., Simmons, G., LaTorraca, G., Watts, R., Bannister, L., Baker, R., Redman, J.D., and Rossiter, J.R., 1974. Radio-frequency interferometry- a new technique for studying glaciers. Journal of Glaciology, 13(67): 123-132.

Sverrisson, M., Jóhannesson, A., and Björnsson, H., 1980. Radio-echo equipment for depth sounding of temperate glaciers. Journal of Glaciology, 25(93): 477-486.

Watts, R.D., England, A.W., Vickers, R.S., and Meier, M.F., 1975. Radio-echo sounding on South Cascade Glacier, Washington, using a long-wavelength, mono-pulse source. Journal of Glaciology, 27(97): 459-469.

Watts, R.D., and England, A.W., 1976. Radio-echo sounding of temperate glaciers: ice properties and sounder design criteria. Journal of Glaciology, 17(75): 39-48.

Watts, R.D., and Wright, D.L., 1981. Systems for measuring thickness of temperate and polar ice from the ground or from the air. Journal of Glaciology, 27(97): 459-469.

Welch, B.C., Pfeffer, W.T., Harper, J.T., and Humphrey, N.F., 1998. Mapping subglacial surfaces of temperate valley glaciers by two-pass migration of a radio-echo sounding survey. Journal of Glaciology, 44(146): 164-170.

Wu, T.T., and King, W.P., 1965. The cylindrical antenna with non-reflecting resistive loading. IEEE Transactions: Antennas and Propagation, AP-13: 369-373.

Chapter 3: Theoretical Methods

3.1 Introduction

Since the late 1950s, ice radar has been used as a glaciological tool to probe the hitherto inaccessible depths of ice masses. Ice radar surveys have investigated glaciers all over the globe. These surveys have taken many different forms, utilizing a variety of instruments, investigating polar, temperate, and polythermal ice masses at a range of scales and with a number of different objectives. This chapter presents a review of past ice radar surveys, specifically discussing the data collection and post-processing methods required for sounding temperate glaciers. A critical analysis of the survey methods and their subsequent impact on the final resolution and utility of the dataset is presented. Conclusions relevant to the methodological approach taken for the present survey are discussed.

3.2 Factors influencing ice radar survey techniques

Ice radar surveys have been carried out all over the world, on a range of ice masses. ***Table 3.1*** provides a selection of these surveys. The most focussed activity has been in Europe, Antarctica, and North America. The spatial distribution of ice masses roughly corresponds with thermal regime, which, in turn, dictates the data collection methods.

Past surveys have covered an equal division of temperate, polythermal, and cold glaciers (***Table 3.1***). The cold ice masses in the polar regions are typically several hundreds of meters thick, extend hundreds of kilometers in area, maintain a vertically isothermal structure, and are frozen to the bed (Bentley *et al.*, 1998; Dahl-Jensen *et al.*, 1997; Legarsky *et al.*, 1998; Oswald, 1975; Siegert and Ridley, 1998; Tabacco *et al.*, 1998; Vaughan *et al.*, 1999; Walford *et al.*, 1977; Yoshida *et al.*, 1987). Temperate glaciers are more commonly found in the mid-latitudes (Björnsson, 1986; Flowers and Clarke, 1999; Fountain and Jacobel, 1997; Nolan *et*

al., 1995; Saetrang and Wold, 1986; Sharp *et al.*, 1993; Welch *et al.*, 1998; Yamamoto and Yoshida, 1987). These ice masses are, by definition, at the pressure melting point and contain liquid water englacially and at the interface between the ice base and the bed. Temperate glaciers are, as a group, much thinner and cover less area than do cold glaciers. Polythermal glaciers are a combination of the temperate and cold glacier thermal regimes (Björnsson *et al.*, 1996; Kotlyakov and Macheret, 1987; Retzlaff *et al.*, 1993; Schultz *et al.*, 1987; Uratsuka *et al.*, 1996). These ice masses comprise a mixture of cold-based and wet-based spatial zones within the same ice sheet, usually, but not always, exhibiting a temperate interior and a cold snout (Menzies, 1995). When selecting an appropriate type of data collection method for a radar survey, the thermal regime, ice thickness, areal extent, and survey objective are all factors to consider.

3.2.1 Thermal regime and ice thickness

The thermal state of an ice mass prescribes the frequencies that are best employed in a survey. As discussed in *Chapter 2*, the presence of liquid water within an ice mass poses difficulties to radar sounding. The difference in relative permittivity between liquid water and glacier ice is so great that most electromagnetic waves will register a large disturbance (or even be totally reflected) when liquid water is encountered. In order for an electromagnetic wave to bypass an englacial water pocket, the wavelength must be much larger than the diameter of the inhomogeneity. Therefore, long wavelengths (on the order of meters to tens of meters) are needed to successfully probe temperate glaciers. Long wavelengths are produced by low frequencies (< 10 MHz).

The vertical thickness of an ice mass also influences the choice of frequency. In order to sound an ice mass successfully, the power returned from a reflector must be detectable by the receiver. Vertical radar range increases with frequency, allowing waves of shorter wavelength to penetrate deeper and return a detectable signal to the receiver (see *Chapter 2*). The colder ice masses are usually larger and thicker than their temperate counterparts. These cold glaciers require higher

frequencies to sound the ice masses. ***Table 3.2*** indicates the range of frequencies commonly used for ice radar surveys, based on thermal regime.

Typical frequencies for sounding temperate glaciers are usually under 10 MHz. Flowers and Clarke (1999) used a slightly higher frequency at 12 MHz. The major exception is Yamamoto and Yoshida (1987), whose study probed a perennial snow patch, a material which has very different dielectric, conductance, density, and thermal properties than a typical temperate glacier. The snow patch had a maximum thickness of 30 m and had not yet metamorphosed into dense glacier ice. A higher frequency (140 MHz) was required to produce the short wavelengths necessary to resolve the small vertical thickness. The deepest temperate glacier (maximum depth = 1477 meters) sounded to date is the Taku, on the Juneau Icefield in Alaska, using a frequency of 1.7 MHz (Nolan *et al.*, 1995). As mentioned in *Chapter 2*, most radar systems used on temperate glaciers have a range of no more than a few hundred meters, because scattering from internal inhomogeneities obscure the ground reflection. Nolan *et al.* (1995) were able to sound the deep ice of the Taku by supplementing their radar soundings with seismic reflections. The deepest radio echo sounding recorded was 652 m; deeper ice was probed with seismic methods.

Surveys of polythermal and cold glaciers apply frequencies of one to two orders of magnitude higher than temperate surveys. There is also a greater range in frequency chosen to sound cold and polythermal glaciers. The objective of a survey would most likely influence this decision, depending on whether the aim is to investigate the bed or the internal structure of the ice.

Eyjafjallajökull is a temperate glacier and therefore contains a large amount of liquid water. Consequently, low frequencies and long wavelengths are needed to sound the ice cap. The transmission frequencies used for this study are between 2 and 10 MHz.

The ice on Eyjafjallajökull is relatively thin in the areas outside the crater. This is made evident by the ice surface; the bed features are clearly indicated. The ice thickness in the crater is significantly deeper. Therefore, the crater region may require higher sounding frequencies than the rest of the ice cap.

3.2.2 Extent of ice mass and objective of survey

The horizontal extent of an ice mass is another factor to consider when choosing a data collection method. Studies of polar ice masses may encompass areas of hundreds of kilometers, while small-scale surveys of alpine valley glaciers may focus on areas of no more than one or two kilometers. When considering the practicalities involved in collecting radio echo sounding data over a large area, it behooves the researchers of many polar surveys to collect data in continuous transects along a flight path or sledge route. Smaller scale studies allow researchers to collect data in discrete point soundings. Point sounding can produce higher quality data by permitting a researcher to vary the transmitted frequency according to the requirements of the site. However, the area between data points must be interpolated in order to produce a continuous subglacial surface (if that is the objective). This can prove a disadvantage if the survey objective is to identify the size and shape of bed features. Those surveys in which data are collected continuously are able to convert their data into standard seismic formats and utilize commercially available signal processing routines in order to interpret the data. A comparable range of signal processing algorithms does not yet exist for the interpretation of point soundings.

The objective of an ice radar survey usually has a bearing on the mode of data collection adopted. If the aim is to achieve a general sense of the underlying topography, a large point spacing may be chosen in order to accomplish the task within practical means. Yoshida *et al.* (1987), faced with the vastness of Antarctica, separated his transects by 10,000 to 20,000 m. If the aim is to determine the structure of a glacier's hydrological system, then a much smaller point spacing is needed, so that small-scale englacial hydrological features can be resolved. Sharp *et al.* (1993), with this objective in mind, used a separation of about 20 m between points. Practical considerations of data collection such as budget constraints and instrument capabilities may also influence the study objective and method of data collection.

The purpose of the survey at Eyjafjallajökull is to map the bed surface and determine ice thickness and volume. This calls for low transmission frequencies to bypass internal inhomogeneities and a relatively coarse point spacing to obtain a general sense of the underlying topography. The instrument available and the budget constraints necessitate the use of point sounding.

Once a basic radio echo sounding method has been chosen, specific field procedures may be considered. The next section introduces field techniques for low frequency point sounding of temperate glaciers. A review of methods used in the literature is presented, alongside characteristic difficulties which may be encountered. Plans to cope with these difficulties are defined and the field techniques chosen for the current survey are introduced.

3.3 Field techniques of point surveying

The steps taken in the field have a major impact on the ultimate ease of data interpretation and the accuracy and resolution of the final dataset. Techniques used during data collection will ultimately determine the final quality of a subglacial map. The spacing between points, sounding frequencies used, and the accuracy of each point location relative to a datum are all critical to the final resolution and utility of an ice radar survey. If these criteria are not considered in the field, post-processing cannot compensate for the resulting loss of resolution or accuracy.

3.3.1 Point spacing

The spacing between points plays a role in determining the horizontal resolution of a survey. If points are sounded at ten meter intervals across a grid, subglacial roughness of the same order can be determined. However, if the spacing between points is increased to more than 100 meters, only a much longer wavelength of surface roughness can be resolved. The study objective (in addition to field practicalities) usually determines the point spacing. Welch *et al.* (1998) collected point data at a spacing of 5 m, in order to eliminate spatial aliasing from his dataset. Aliasing causes smoothing of reflectors and occurs if spatial sampling is too coarse

(Reynolds, 1997). The measure of coarseness is determined by the size of the first Fresnel zone, or footprint. If the footprints of adjacent points do not overlap or have gaps between them, information is missed between the footprints. For example, if a bed feature is small enough to fit in between adjacent footprints, the feature will not be detected, and subsequent interpolation will not make up for this loss of information. If one wishes to avoid this type of error, point spacing must not be more than one-quarter wavelength ($\lambda/4$) apart (see *Chapter 2*); otherwise, reflector dimensions and slopes will be misrepresented (Welch *et al.*, 1998). A survey transmitting at a frequency of 2.5 MHz, for example, will have wavelengths of approximately 67 m. In order to avoid spatial aliasing, the point spacing would have to be no more than 17 m. Considering the time-consuming nature of collecting ice radar point data, this field technique seems impractical. Most point surveys tend to accept spatial aliasing as an unavoidable, but not overwhelming, error inherent in the radio echo sounding method. Flowers and Clarke (1999) collected data spaced 12.5-25 m apart. This was achieved by extending the survey over a period of several years. Most other researchers separate points by about 100 meters (Knudsen and Hasholt, 1999; Nolan *et al.*, 1995; Retzlaff *et al.*, 1993; Sharp *et al.*, 1993). Retzlaff *et al.* (1993) wanted to know if the locations of Antarctic ice streams were reflected in the bed topography. Nolan *et al.* (1995) wished to determine the relevance of the Taku Glacier's ice thickness to its behavior. Knudsen and Hasholt (1999) required basic geometric data for Mittivakkat Gletscher as modelling input. These studies obtain sufficient coverage for their objectives from 100 m spacing.

The point spacing for the Eyjafjallajökull survey was decided for practical reasons. The main constraint was a small budget which allowed a finite time to collect data and a limited staff to collect it. The objective of obtaining a general sense of the bed surface of the entire system demands a large areal coverage. This large area would have to be covered on foot (skiing). Therefore, a wide point spacing of 200 m was adopted. As a result of this wide spacing, spatial aliasing is introduced from the outset. Therefore, the final horizontal resolution will not be solely a function of the area of the first Fresnel zone.

3.3.2 Waveform averaging

Ease of data interpretation is another important factor when considering field techniques. Once the data have been captured, no amount of signal processing can discern an unidentifiable ground reflection. One must be able to identify the ground wave in a waveform in order to extract ice thickness information. One way to ensure this is to average a number of waveforms for each point in the field. Waveform averaging (sometimes called trace stacking) improves the signal-to-noise ratio, making the ground signal easier to identify relative to other disturbances in the waveform. Most radar systems will do this automatically, averaging 256 or 512 waveforms for each point and displaying the average in real-time on the oscilloscope. Welch *et al.* (1998) average 32 waveforms at each point, Flowers and Clarke (1999) average 256, and Yoshida *et al.* (1987) average either 256 or 512 waveforms per point sounding. Waveform averaging has the added advantage of showing in real time if a waveform is stationary. If a waveform fluctuates too wildly while the system is averaging, adjustments in antenna configuration, offset, or frequency can be made then and there.

The receiving oscilloscope used for the Eyjafjallajökull survey automatically averages 512 waveforms per point sounding.

3.3.3 Point location

Point soundings are useless without knowing their horizontal and vertical position relative to a datum. The location of points, and how accurately it is done, will affect the final resolution and accuracy of the dataset. Positional error is added to all other errors which combine to form the final resolution of a dataset. Most researchers use Global Positioning System (GPS) technology to pinpoint the whereabouts of their radio echo soundings (Flowers and Clarke, 1999; Fountain and Jacobel, 1997; Gogineni *et al.*, 1998; Jezek and Thompson, 1982; Knudsen and Hasholt, 1999; Kotlyakov and Macheret, 1987; Nolan *et al.*, 1995; Sharp *et al.*, 1993; Taylor, 1997; Welch *et al.*, 1998). Individual instrument capabilities and differential post-processing determine the positional accuracy.

The Eyjafjallajökull survey uses GPS to determine the location of point soundings. The system is described in *Chapter 5*.

Once the data have been collected, the point soundings and GPS positions must be processed before ice depth and locational information can be extracted. The following section describes the techniques involved.

3.4 Post-processing techniques of point surveying

Post-processing techniques aim to correct and interpret the collected data, so that the sought after information may be extracted. Corrections include calculations which account for near-surface velocity differences in the firn layer and misplaced bed slopes. Waveform interpretation is the critical step of identifying the basal reflection and determining the two-way travel time of the ground wave from transmitter to receiver. Post-processing is also needed to correct GPS positions scrambled by Selective Availability. Post-processing techniques, just like data collection, have an enormous impact on the utility and plausibility of the final dataset.

3.4.1 Migration

Migration is a post-processing technique which corrects the location of misplaced reflectors, a phenomenon caused by spherical propagation of electromagnetic waves. Electromagnetic waves reflect from an area, not from a point. The disturbance in a waveform often assumed to be the reflection from a point on the ground vertically beneath the midpoint between transmitter and receiver is actually a combination of all the energy reflected from an area. If the bed is sloping, the travel-time to the upslope area will be shorter than the travel-time to the area directly beneath the midpoint. Therefore, the depth of the ice at that point will be calculated to be shallower than it actually is and its location will be incorrectly assumed to be directly below the midpoint. Migration repositions dipping reflection events to lie beneath their true surface locations at corrected vertical two-way travel times (Allaby and Allaby, 1990).

Migration uses adjacent soundings to correctly position and represent the slopes of reflecting surfaces. The method makes use of the entire dataset so that results are not biased by pre-migration interpretation of reflectors (Welch *et al.*, 1998). The requirement of using adjacent soundings makes this an ideal method for surveys where data have been collected continuously. Just like the signal processing software available to these surveys, migration routines are also available. Langley (2000) migrated her data by computer, as did Welch *et al.* (1998). Both of these studies collected continuous data.

The need to migrate data is most intense if the survey area covers steeply dipping terrain or is surrounded by steep slopes which produce lateral reflections. These sites are usually alpine-style valley glaciers, occupying U-shaped valleys hemmed in by steep rock walls. These relatively small, usually temperate glaciers are also typically sounded by point surveys. Unless the point spacing is small, the use of adjacent soundings to migrate the data is difficult. In addition, migration routines available for continuous data are hard to adapt for point data. Researchers approach these issues in different ways. Knudsen and Hasholt (1999) take a qualitative approach. In order to check whether reflectors are reasonably located, he compares several adjacent profiles to see if the topography is similar. Sharp *et al.* (1993) assume a reflection originates from directly below the midpoint of the transmitter-receiver array. Flowers and Clarke (1999) choose not to migrate their data, explaining that it is not necessary because the glacier flows unconfined over its bed and steeply dipping valley walls are not present. Driedger and Kennard (1986) migrate their point data, collected on the steep slopes of Cascade stratovolcanoes, by utilizing knowledge of the bed slope obtained from adjacent upslope data points.

The current survey does not employ migration post-processing techniques for a number of reasons. Eyajafjallajökull is a summit icecap and therefore not valley-confined. The slopes are not generally steep. Lastly, the point spacing is too wide to justify the use of adjacent soundings to correct bed positions.

3.4.2 Firn correction

Another correction to consider is that which takes into account the firn layer present on the surface of many glaciers. Firn is a layer of surface snow more than a year old, but which has not yet metamorphosed into glacier ice. The permittivity of firn differs from that of glacier ice because it contains more liquid water and air, and is therefore less dense. As discussed previously (*Chapter 2*), a change in the relative permittivity of a medium will alter the propagation velocity of radio waves, and a correction must be made when calculating depth. Correcting for the presence of firn is uncommon amongst surveys on temperate glaciers because a typical firn layer does not make up a large enough percentage of the total ice thickness to make a noticeable difference in the corrected two-way travel time. Many alpine glaciers, like the Haut Glaciar d' Arolla (Sharp *et al.*, 1993), do not even have a continuous layer of firn during the ablation season when most surveys take place. Firn corrections tend to be used on thick, polythermal or cold glaciers (Bentley *et al.*, 1998; Retzlaff *et al.*, 1993).

Firn correction is not used in this survey. Gigjökull has no firn during the summer and neither do the lower flanks. The firn layer may be more significant in the crater. These implications are discussed in *Chapter 4*.

3.4.3 Differential correction

GPS post-processing corrects for Selective Availability, the intentional signal degradation by the United States Department of Defense. Global Positioning satellites were placed in orbit for the use of the US Armed Forces, but the government has allowed the rest of the world to obtain positional fixes as well, albeit at a possible 30-100 m reduced accuracy (Dana, 1994)[1]. However, this accuracy can be improved with the use of differential post-processing. If a GPS receiver at a

[1] Selective Availability was switched off by President Clinton on May 2, 2000, instantly improving the accuracy of every hand-held GPS by a factor of ten (*Geography.about.com, 2000).*

known location collects data at the same time as a remote receiver, a correction can be made by comparing the two files. The Selective Availability bias errors at the remote location are corrected by the measured bias errors at the known location (Dana, 1994). This calculation can improve the range error from 60 m to 6 m.

There are two types of GPS, pseudo-range navigation and carrier-phase tracking. The latter is more accurate (to a mm scale), but requires longer collection times. This survey intends to use differential correction, using a pseudo-range navigation GPS. The resolution of the radar data precludes the necessity of the sub-centimeter resolution of carrier-phase tracking.

3.4.4 Waveform interpretation

Waveform interpretation is the most important step in post-processing. If one is to extract depth information from a waveform, one must be able to identify clearly the air wave and the ground wave. The two-way travel time is determined from the elapsed time between the arrival of the air wave and the arrival of the ground wave at the receiver. The depth information is only useful if the interpretation is accurate and repeatable. The identification of an airwave is quite simple, but an accurate and confident identification of a ground wave can be difficult. The difficulties arise from the variable transmission frequencies used, ground-coupling effects of ice, and a lack of practical validation techniques.

3.4.4.1 Effects of varied frequency

As discussed previously (*Section 3.2.2*), point sounding may produce higher quality data than continuous sounding, because the transmitted frequency can be modulated according to site requirements. The varying depths and densities of the ice, as well as the surrounding topography, call for a variety of frequencies to obtain clear reflections. As a result, received waveforms vary in shape and amplitude. The variations make it difficult to create homogeneous processing algorithms for all waveforms.

By swapping antenna lengths, the transmission frequency of the Mark II impulse radar may be varied. In the field it is possible to alter the frequency until one is found that produces an interpretable waveform.

3.4.4.2 Effects of antenna separation

In addition to modifying the frequency according to the requirements of each specific site, the separation distance (or offset) between the antennas attached to the transmitter and receiver can be varied to obtain clearer reflections. The shape and amplitude of the airwave varies considerably when the separation distance is altered. The shape changes as a result of the interference of waves at the air-ice interface taking different paths as the pulse moves from the transmitter to the receiver (Dinnis, 2000). The amplitude of the air wave decreases as the separation distance increases. These effects pose difficulties for waveform interpretation.

This survey systematically tested equipment configurations in order to determine ideal antenna separations for different sections of the ice cap. There is a discussion and examples of the experiments in *Chapter 4*.

3.4.4.3 Effects of ground-coupling

Ground-coupling changes the form of a transmitted wave as it enters the ice. The medium of ice alters the shape and amplitude of a downgoing wave (Reynolds, 1997). Ice decreases both the wavelength and the amplitude of a signal (Dinnis, 2000). Ice may also cause a delay in the arrival of an airwave at the receiver. These effects are caused by the interference of three air wave components near the air-ice interface: spherical waves which travels through air and ice, a lateral wave which travels through the ice very near to the air-ice boundary, and an inhomogeneous wave. Ice depths are calculated from parameters including the transmitted frequency and the travel time of an air wave from transmitter to receiver. If the frequency is actually lower than estimated and the air wave has been delayed for an unknown amount of time, then the calculation of ice depth may be incorrect. Ground coupling effects have serious impacts on waveform interpretation.

There is not much that can be done about ground-coupling effects except to recognize their existence. Further discussion of the observed effects and implications of ground-coupling occurs in *Chapter 4*.

3.4.4.4 Picking

As early as 1976, Watts and England determined that the major waveform interpretation problem was the identification of the ground signal (Watts and England, 1976). Reynolds (1997) concurs, noting that defining the onset position of a ground reflection is subjective.

The true ground signal must be identified and not confused with internal reflectors. In order to calculate ice thickness from a received signal, the two-way travel time (the time it takes for the pulse to travel from the transmitter through the ice to the bedrock and back to the receiver) must be determined. The two-way travel time is measured as the time elapsed between the onset of the air wave and the onset of the ground wave, plus the air wave travel time. Choosing (or picking) the onset of reflection has traditionally been the least quantitative part of the radio echo sounding method. The inherent difficulty and subjectivity of the picking procedure is well documented (Flowers and Clarke, 1999; Knudsen and Hasholt, 1999; Taylor, 1997).

Many papers do not mention how the waveforms are interpreted and do not explain the picking method (Nolan *et al.*, 1995; Sharp *et al.*, 1993; Taylor, 1997). By ignoring, or not explicitly communicating, this, it is difficult to assess the accuracy of the results. A large part of dataset error results from waveform interpretation. Even if a method is generally qualitative, an effort to quantify the repeatability of the method is needed.

Knudsen and Hasholt (1999) give examples of raw waveforms, indicating where the picks are set (***Figure 3.1a***). One example interprets a very shallow depth (36 m), one which is notoriously difficult to sound because it borders the minimum detectable range of most radar instruments. Most radar systems used on temperate ice have a minimum range of about 30 m. Knudsen and Hasholt set the pick before the end of the air wave, where the ground signal is masked by the tail of the air wave. However, it is not clear why the pick is set here. There is no clear ground signal and

no adjacent waveforms with which to compare. The method is subjective, establishing no estimated margin of error for the picking. Without validation, such as a borehole depth, it is difficult to establish confidence in the interpreted ice depth.

Cassasa (1992) also gives examples of raw waveforms and the picking method used (***Figure 3.1b***). The dataset is small (12 point soundings), so each waveform is discussed individually. Some of the calculated ice depths are expressed as a range and displayed with an error bar. The ranges represent the uncertainty in picking when a "double reflection" appears (Cassasa, 1992).

Flowers and Clarke (1999) give the best explanation of an attempt to quantify waveform interpretation error (***Figure 3.1c***). First, they explain where the ground wave is picked: at the time of the first detectable energy of the bed echo. Second, they rank the waveforms in order of data quality and uncertainty in arrival picks and quantifies their confidence in the interpretation by calculating an index which represents the number of oscilloscope pixels of uncertainty in arrival location (Flowers and Clarke, 1999).

Unlike Knudsen and Hasholt, Flowers and Clarke reject shallow data, deciding that it is uninterpretable. They instead make a general statement excusing the lack of shallow depths from the data set: "...areas of thin ice are underrepresented in the original data because reflected radar signals often occur within the tail of the direct wave, becoming indistinguishable" (Flowers and Clarke, 1999). This approach could be problematic. Collecting discrete point data is time consuming, so the datasets are not large. If data are hard to come by, it is desirable to obtain as much information from the waveforms as possible and avoid throwing out 'bad' data, or underrepresenting shallow areas.

Reynolds (1997) notes that, in general, the signal processing that has been developed so far is not as sophisticated as the instruments, creating a serious gap between technology and user, or application.

> "Despite the recent upsurge in interest in the method, general experience in data processing and interpretation within the engineering community in particular has not kept pace with advances in technology or computer capabilities." (Reynolds, 1997).

It is proposed to cope with waveform interpretation difficulties in the current study by sounding more than once at each point with different frequencies. By replicating waveforms it may be possible to establish if picking is repeatable. In addition, experiments undertaken to investigate the behavior of received waveforms may provide further insight into how to interpret waveforms. These two methods aim to determine a picking error and address the problem of subjectivity.

3.5 Summary

Ice radar surveys have been taking place for over four decades and a number of techniques designed to obtain, interpret, and resolve radio echo soundings have been developed. Initial factors which influence the choice of ice radar survey method include the survey objective and the thermal regime, thickness, and areal extent of the ice mass to be surveyed. Field techniques to consider include sampling density, transmission frequency, waveform averaging, and horizontal positioning. Post-processing techniques such as migration, firn correction, differential correction, and waveform interpretation all contribute to the final accuracy and resolution of a dataset.

After considering the theoretical methods presented above, the methodology for the current study was chosen. Eyjafjallajökull is a temperate ice cap, 100 km^2 in area, and has estimated ice thicknesses no greater than a few hundred meters. The limitations of the budget preclude the adoption of a survey of the entire ice cap, so the crater was chosen as the focus of the study, in addition to any data that could be collected on accessible flanks. A low frequency, point sounding survey is chosen, with a sampling density of 200 m. Horizontal and vertical positions of point soundings are determined by pseudo-range navigation GPS. GPS positions are differentially corrected during post-processing.

The main focus of the waveform interpretation method is the development of a picking technique that is quantifiable and repeatable. There is a lack of borehole validation, for practical reasons, so a way of assessing confidence in the identification of the ground signal and estimating the error of calculated ice depth is sought.

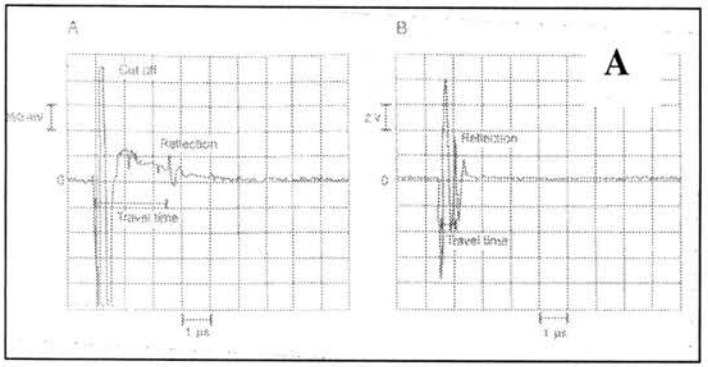

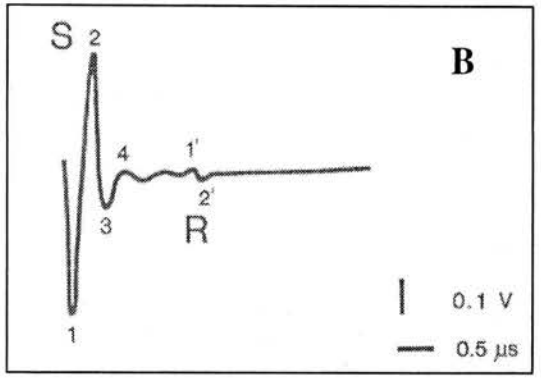

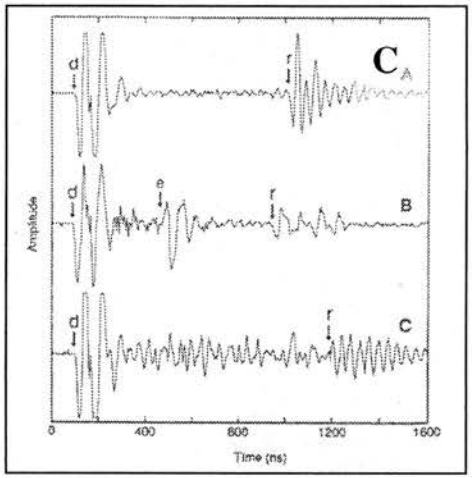

Figure 3.1 Examples of picking techniques from the literature: a) Picking method of Knudsen and Hasholt (1999). Waveform on the right shows a ground wave picked in the tail of the air wave. b) Picking method of Cassassa (1992). Air wave and ground wave picks are set at 1 and 1', respectively. c) Picking method of Flowers and Clarke (1999); r indicates position of ground wave pick.

Location	Glacier type	Thermal state	Reference
Trapridge Glacier, Canada	alpine	temperate	Flowers and Clarke (1999)
Worthington Glacier, Alaska	valley	temperate	Welch *et al.* (1998)
South Cascade Glacier, USA	alpine	temperate	Fountain and Jacobel (1997)
Taku Glacier, Alaska	valley	temperate	Nolan *et al.* (1995)
Solheimajökull, Iceland	valley	temperate	Taylor (1997)
Hofsjökull, Vatnajökull, Iceland	ice cap	temperate	Björnsson (1986)
Haut Glaciar d'Arolla, Switzerland	valley	temperate	Sharp *et al.* (1993)
Jostedalsbreen, Norway	ice cap	temperate	Saetrang and Wold (1986)
Storglaciaren, Sweden	valley	temperate	Björnsson (1981)
Kuranosuke, Japan	perennial snow patch	temperate	Yamamoto and Yoshida (1987)
Mittivakkat Gletscher, Greenland	valley	temperate	Knudsen *et al.* (1999)
Svalbard	valley, ice cap	polythermal	Kotlyakov and Macheret (1987)
Svalbard	valley	polythermal	Björnsson *et al.* (1996)
Sor Rondane Mtns., Antarctica	ice shelf	polythermal	Uratsuka *et al.* (1996)
Ice Streams A,B,C Antarctica	ice stream	polythermal	Bentley *et al.* (1998); Retzlaff *et al.* (1993); Schultz *et al.* (1987)
Devon Island, Canada	ice cap	cold	Walford *et al.* (1977)
Greenland	ice cap	cold	Dahl-Jensen *et al.* (1997); Legarsky *et al.* (1998)
Dome C, Antarctica	ice cap	cold	Siegert and Ridley (1998)
East Dronning Maud Land	ice sheet	cold	Yoshida *et al.* (1987)
Fletcher Promontory, Antarctica	ice cap	cold	Vaughan *et al.* (1999)
Ridge BC, West Antarctica	ice sheet	cold	Bentley *et al.* (1998)
Dome C, East Antarctica	ice sheet	cold	Tabacco *et al.* (1998)
Antarctica	ice sheet	cold	Oswald (1975)

Table 3.1 Example selection of ice radar surveys.

Source	MHz	Thermal regime	Survey type
Nolan *et al.* (1995)	1.7	temperate	point
Knudsen and Hasholt (1999)	1.25-5	temperate	point
Sharp *et al.* (1993)	1-10	temperate	point
Björnsson (1986)	2-5	temperate	continuous
Björnsson (1981)	2-5	temperate	continuous
Taylor (1997)	2-5	temperate	point
Welch *et al.* (1998)	5	temperate	point
Saetrang and Wold (1986)	8	temperate	continuous
Flowers and Clarke (1999)	12	temperate	point
Yamamoto and Yoshida (1987)	140	temperate	continuous
Björnsson *et al.* (1996)	5-20	polythermal	continuous
Bentley *et al.* (1998)	50	polythermal	point
Retzlaff *et al.* (1993)	50	polythermal	point
Schultz *et al.* (1987)	50	polythermal	continuous
Uratsuka *et al.* (1996)	179	polythermal	continuous
Kotlyakov and Macheret (1987)	440, 620	polythermal	continuous
Walford, *et al.* (1977)	60	cold	point
Oswald (1975)	60	cold	continuous
Tabacco *et al.* (1998)	60	cold	continuous
Vaughan *et al.* (1999)	100	cold	continuous
Dahl-Jensen *et al.* (1997)	150	cold	continuous
Legarsky *et al.* (1998)	150	cold	continuous
Yoshida *et al.* (1987)	179	cold	point

Table 3.2 Range of frequencies commonly used for ice radar surveys, based on thermal regime.

3.6 References

Allaby, A., and Allaby, M., 1990. *Oxford Concise Dictionary of Earth Sciences.* Oxford University Press, Oxford, 410 pp.

Bentley, C.R., Lord, N., and Liu, C., 1998. Radar reflections reveal a wet bed beneath stagnant Ice Stream C and a frozen bed beneath ridge BC, West Antarctica. Journal of Glaciology, 44(146): 149-156.

Björnsson, H., 1981. Radio-echo sounding maps of Storglaciaren, Isfallsglaciaren and Rabots Glaciar, Northern Sweden. Geografiska Annaler, 63 A: 225-229.

Björnsson, H., 1986. Surface and bedrock topography of ice caps in Iceland, mapped by radio echo-sounding. Annals of Glaciology, 8: 11-18.

Björnsson, H., Gjessing, Y., Hamran, S-E.,Olav Leistol, J.O.H., Pálsson, F., and Erlingsson, B., 1996. The thermal regime of sub-polar glaciers mapped by multi-frequency radio-echo sounding. Journal of Glaciology, 42(140): 23-32.

Cassasa, G., 1992. Radio-echo sounding of Tyndall Glacier, southern Patagonia. Bulletin of Glacier Research, 10: 69-74.

Dahl-Jensen, D., Gunderstrup, N.S., Keller, K., Johnsen, S.J., Gogineni, S.P., Allen, C.T., Chuah, T.S., Miller, H., Kipfstuhl, S., and Waddington, E.D., 1997. A search in North Greenland for a new ice-core drill site. Journal of Glaciology, 43(144): 300-306.

Dana, P.H., 1994. Global Positioning System Overview. Geography Department, University of Texas, www.utexas.edu/depts/grg/gcraft.

Dinnis, A.K., 2000. Modelling a radio echo sounding system (Internal Report), University of Edinburgh, Department of Electrical Engineering, 25 pp.

Driedger, C.L., and Kennard, P.M., 1986. Ice volumes on Cascade Volcanoes: Mount Rainier, Mount Hood, Three Sisters, and Mount Shasta. US Geological Survey Professional Paper, 1365: 1-28.

Flowers, G.E., and Clarke, G.K.C., 1999. Surface and bed topography of Trapridge Glacier, Yukon Territory, Canada: digital elevation models and derived hydraulic geometry. Journal of Glaciology, 45(149): 165-174.

Fountain, A.G., and Jacobel, R.W., 1997. Advances in ice radar studies of a temperate alpine glacier, South Cascade Glacier, Washington, USA. Annals of Glaciology, 24: 303-308.

Geography.about.com, 2000. President Turns Off GPS Selective Availability. http://geography.about.com/science/geography/library/weekly/aa050400a.htm?once=true&.

Gogineni, S., Chuah, T., Allen, C., Jezek, K., and Moore, R.K., 1998. An improved coherent radar depth sounder. Journal of Glaciology, 44(148): 659-669.

Jezek, K.C., and Thompson, L.G., 1982. Interpretation of mono-pulse ice radar soundings on two Peruvian glaciers. IEEE Transactions on Geoscience and Remote Sensing, GE-20(3): 243-249.

Knudsen, N.T., and Hasholt, B., 1999. Radio-echo sounding at the Mittivakkat Gletscher, Southeast Greenland. Arctic, Antarctic, and Alpine Research, 31(3): 321-328.

Kotlyakov, V.M., and Macheret, Y.Y., 1987. Radio echo-sounding of sub-polar glaciers in Svalbard: some problems and results of Soviet studies. Annals of Glaciology, 9: 151-159.

Legarsky, J., Wong, A., Akins, T., and Gogineni, S.P., 1998. Detection of hills from radar data in central-northern Greenland. Journal of Glaciology, 44(146): 182-184.

Menzies, J.E., 1995. Glaciers and Ice Sheets. In: J. Menzies (Editor), *Modern Glacial Environments: Processes, Dynamics and Sediments*. Butterworth-Heinemann, Oxford, 621 pp.

Nolan, M., Motkya, R.J., Echelmeyer, K., and Trabant, D.C., 1995. Ice-thickness measurements of Taku Glacier, Alaska, U.S.A., and their relevance to its recent behavior. Journal of Glaciology, 41(139): 541-553.

Oswald, G.K.A., 1975. Investigation of sub-ice bedrock characteristics by radio-echo sounding. Journal of Glaciology, 15(73): 75-87.

Retzlaff, R., Lord, N., and Bentley, C.R., 1993. Airborne radar studies: Ice Streams A, B, and C, West Antarctica. Journal of Glaciology, 39(133): 495-506.

Reynolds, J.M., 1997. An Introduction to Applied and Environmental Geophysics. John Wiley and Sons, Ltd., Chichester, 796 pp.

Saetrang, A.C., and Wold, B., 1986. Results from the radio echo-sounding on parts of the Jostedalsbreen Ice Cap, Norway. Annals of Glaciology, 8: 156-158.

Schultz, D.G., Powell, L.A., and Bentley, C.R., 1987. A digital radar system for echo studies on ice sheets. Annals of Glaciology, 9: 206-209.

Sharp, M., Richards, K., Willis, I., Arnold, N., Nienow, P., Lawson, W., and Tison, J-L., 1993. Geometry, bed topography and drainage system structure of the Haut Glacier D'Arolla, Switzerland. Earth Surface Processes and Landforms, 18: 557-571.

Siegert, M.J., and Ridley, J.K., 1998. Determining basal ice-sheet conditions in the Dome C region of East Antarctica using satellite radar altimetry and airborne radio-echo sounding. Journal of Glaciology, 44(146): 1-8.

Tabacco, I.E., Passerini, A., Corbelli, F., and Gorman, M., 1998. Determination of the surface and bed topography at Dome C, East Antarctica. Journal of Glaciology, 44(146): 185-191.

Taylor, F.M., 1997. Interpolation of the surface and bed topography of an Iceland glacier: using GIS, GPS, and radio-echo sounding. Unpublished MSc Thesis, University of Edinburgh, Department of Geography.

Uratsuka, S., Nishio, F., and Mae, S., 1996. Internal and basal ice changes near the grounding line derived from radio-echo sounding. Journal of Glaciology, 42(140): 103-109.

Vaughan, D.G., Corr, H.F.J., Doake, C.S.M., and Waddington, E.D., 1999. Distortion of isochronous layers in ice revealed by ground-penetrating radar. Nature, 398: 323-326.

Walford, M.E.R., Holdorf, P.C., and Oakberg, R.G., 1977. Phase-sensitive radio-echo sounding at the Devon Island ice cap, Canada. Journal of Glaciology, 18(79): 217-229.

Watts, R.D., and England, A.W., 1976. Radio-echo sounding of temperate glaciers: ice properties and sounder design criteria. Journal of Glaciology, 17(75): 39-48.

Welch, B.C., Pfeffer, W.T., Harper, J.T., and Humphrey, N.F., 1998. Mapping subglacial surfaces of temperate valley glaciers by two-pass migration of a radio-echo sounding survey. Journal of Glaciology, 44(146): 164-170.

Yamamoto, K., and Yoshida, M., 1987. Impulse radar sounding of fossil ice within the Kuranosuke perennial snow patch, Central Japan. Annals of Glaciology, 9: 218-220.

Yoshida, M., Yamashita, K., and Mae, S., 1987. Bottom topography and internal layers in East Dronning Maud Land, East Antarctica, from 179 MHz radio echo-sounding. Annals of Glaciology, 9: 221-224.

Chapter 4: Field Experiments

4.1 Introduction

It is desirable to avoid assumptions about the physical properties of ice when surveying a glacier by radio echo sounding. Empirical derivation of electromagnetic wave propagation velocity on site may increase the accuracy of ice thickness estimation. It is also important to test the capabilities of the radar instrument. Experimental testing may not only indicate the most efficient use of the instrument, but may provide a method of depth validation. If a measure of uncertainty can be applied to waveform picking, then a level of confidence in the depth estimation can be produced, bolstering the plausibility of the final map.

Watts and Wright (1981) stressed that "experiments need to be carried out for *each* [ice radar] system". Glaciers vary a great deal in form, structure, and density, and the various ice radar instruments employed to survey them have differing capabilities. Obtaining interpretable waveforms from sounding such varied material is a bit of an art. Ideal antenna separation distances and frequencies required to produce these waveforms need to be determined prior to launching the bulk of the survey. It would also be helpful to make a local estimate of the ice properties at Eyjafjallajökull by determining the wave propagation velocity, as opposed to relying on a theoretical value. It was hoped, in this study, to improve both the method of collection and interpretation by making experimental measurements.

This section introduces the experimental sites on Eyjafjallajökull and the equipment testing that was undertaken at each. A waveform interpretation method developed from the experiments is discussed, as is a method of depth validation. Theoretical values for electromagnetic wave velocity in ice are considered and experiments from the literature which have measured these values in the field are critically reviewed. Field experiments for the current study are then introduced, detailing calculations used to derive empirical values for electromagnetic wave velocity in ice at Eyjafjallajökull.

4.2 Experimental sites

Three representative sites on the ice cap were chosen for the experiments: the eastern flank, the crater, and the foot of Gigjökull (***Figure 4.1***). Each provided a different glaciological regime, ice depth, and surface type. It was hoped that the dielectric properties of the ice at each site would be significantly different.

4.2.1 Gigjökull

Gigjökull is an outlet glacier whose snout is approximately 200 m above sea level. The surface, being in the ablation zone, is blue ice and contains a high volume of water during the height of the ablation season (early July), when the experiments took place. Water pools on the surface, flows through supraglacial, englacial, and subglacial streams, and drains from the surface to the bed through moulins. Crevassing is widespread and tephra is scattered on the surface. The ice thicknesses are typically less than 100 m. It is difficult to locate a large flat area on the snout of Gigjökull which is not too close to reflecting walls or overly crevassed. A site was chosen at the base of the icefall, in the center of the glacier. A second experiment at Gigjökull, located in a slightly different place, was carried out in 2000 by Nick Hulton and Ross Purves (Hulton, N., 2000, *pers. comm.*).

4.2.2 East flank

The experimental site on the eastern flank is at an elevation of about 1200 m, 100 m above the equilibrium line altitude (ELA). The site is on a flat plateau, 50 m north of a nunatak. The glacier surface consisted of a soft, saturated granular snow. The ice thicknesses are about 100 m.

4.2.3 Crater

A flat site about 200 m from the center of the east rim was chosen for the crater experiment. This site is not in the deepest part of the crater, but was judged to

be representative of typical conditions. At 1500 m, this is the heart of the accumulation zone. Ice depths are typically about 200 m. The crater experiment took place on a surface of melting snow (fresh within the past week).

At each site, a center point on flat ice was chosen, in an area where crevassing and slopes were at a minimum and where no reflecting vertical walls were within 50 m. Starting at a 20 m separation distance between transmitter and receiver, each antenna (or frequency) combination and orientation was tested. The separation distance was increased by 20 m for each iteration, up to a maximum of 80 m. On the flank, the experiment was repeated in the perpendicular direction.

4.3 Equipment characterization

The radar instrument was tested in order to determine the ideal antenna orientations, separations, and transmission frequencies required to produce interpretable waveforms at sites with different thicknesses, densities, and water content. It was expected that the best antenna orientation would be a parallel setup and that an antenna separation of at least 50 m would be required at each site. The lowest frequencies (1-2 MHz) were expected to be most successful at the thin, wet Gigjökull site. It was found that sometimes the slightest change in orientation or offset between antennas could make the difference between an interpretable waveform and one which contained no decipherable ground wave.

4.3.1 Antenna orientation

A variety of antenna orientations were tested in order to determine which produced the most interpretable waveforms. ***Figure 4.2*** describes the three orientations: parallel, perpendicular, and end-to-end. The most successful of these orientations was the parallel setup. The perpendicular and end-to-end orientations produced unusual, mostly non-stationary waveforms (***Figure 4.3***). These orientations produce waveforms an order of magnitude less in amplitude than those

produced with the parallel orientation. The weak signal, with a low signal-to-noise ratio, makes it difficult to identify the ground wave.

4.3.2 Antenna separation

Different antenna separations were systematically tested in order to determine the offset distance that produced the clearest waveforms. Offset is measured as the distance between the transmitter and receiver across the ice. At Gigjökull, the best waveform was produced using a 60 m offset. Swapping the transmitter and receiver between antennas generated nearly identical waveforms (***Figure 4.4***). An offset of 80 m produced the clearest waveforms at the flank experimental site (***Figure 4.5***). *At least* a 60 m offset is needed in order to produce a clear ground signal in the crater (***Figure 4.6***). At a separation distance less than this, the waveforms are characterized by massively different trigger times and ascending limbs (***Figure 4.7***). This shape interferes with the detection of the ground wave.

4.3.3 Frequency

Various frequency combinations were also systematically tested at the experimental sites. Transmission frequency is changed by altering the lengths of antenna attached to the transmitter and receiver. ***Figure 4.8*** shows the configurations which produced the clearest waveforms. These combinations were subsequently used throughout the survey. The black antennas (2.0 MHz) produced decent waveforms at most sites, while the black and blue combination (1.5 MHz) was most successful at probing the shallower ice depths at Gigjökull. The red antennas (4 MHz) were, unfortunately, not tested in the crater. Theoretically, the highest frequency should produce the clearest waveforms in the deepest ice. The 4 MHz antennas performed well at the flank and Gigjökull. At Gigjökull, all the frequency combinations yielded some interpretable ground signals, revealing no ideal frequency combination. This indicates that the ice mass at Gigjökull is irregular and contains numerous inhomogeneities on the same scale of the transmitted wavelengths (about 20-90 m, *Chapter 2*).

4.4 Waveform interpretation

The uncertainty involved with the waveform interpretation, or picking, is an important parameter to quantify. The experiments provide multiple measurements of ice depth at different offsets and frequencies from which an interpretation error is estimated.

4.4.1 Identifying the ground wave

Travel times of both air waves and ground waves are determined by picking. A point of reflection (usually the onset) must be chosen, or 'picked', in way which can be replicated for all waveforms. There is a 180° phase reversal of an electromagnetic wave upon reflection at the bed, causing the sign of a ground wave to be opposite that of an air wave (Watts and England, 1976). When identifying a ground wave, the first peak (amplitude maxima or minima) of a reflection is always more obvious than the onset of the first incidence of reflection. Therefore, this maxima or minima can be chosen with confidence for all air waves and ground waves. This picking method was adopted for ease of repeatability.

There is sometimes ambiguity in determining which part of a waveform represents the ground wave (*Chapter 3*). ***Figure 4.9*** gives some examples. In each of these waveforms, there is more than one candidate for the ground wave. The ghost wave[1] can be quickly eliminated; it is usually similar in shape to the air wave and does not have the phase reversal of a ground wave. However, each echo that does have a phase reversal could be the ground wave, an internal reflection, or a secondary wave. Reflections which have encountered englacial water should have larger amplitudes than ground waves, because the difference in relative permittivity between water and ice is greater than that between rock and ice. Therefore, choosing

[1] A disturbance in a waveform possibly caused by a lack of impedance matching between antennas (Dinnis, 2000). The ghost wave does not occur with all antennas, but when it does, always has a travel time of greater than 3 μs.

the reflection with the largest amplitude (aside from the air wave) could be incorrect. Identifying the penultimate reflection (before the ghost wave) may be incorrect also, because secondary waves, which are essentially repetitions of ground waves, can occur after a ground wave has arrived.

It seems the best way to cope with these ambiguities is to identify a ground wave from multiple soundings taken with different frequencies. By comparing more than one sounding, the ground wave usually becomes apparent. Different frequencies produce disparate waveforms; for example, a 1 MHz antenna may show just two waves (air and ground) in a waveform, while a 5 MHz antenna may show a ghost wave and internal relections in addition to the air and ground waves. With both waveforms derived from the same sounding point, similar ground wave picking times will validate the identification. This is confirmation that the identification of a ground reflection is repeatable.

4.4.2 Picking error and depth validation

If two frequencies can produce interpretable waveforms at each point, then multiple measurements can be made, validating the depth measurement. The experiments establish that similar depths can be produced from different frequencies (***Figures 4.10-4.13***). It was not practically possible to drill boreholes in the ice cap to validate the depth measurements, so the estimated uncertainty in the waveform interpretation is used as validation instead. Precision error of waveform interpretation is quantified by taking multiple frequency soundings at each point. Data on the flank were collected with both 2 and 4 MHz antenna combinations, while data in the crater were collected with frequencies of 2 and 1.5 MHz. Gigjökull data were collected at 2 MHz.

Table 4.1 presents the estimated means and range of error for ground wave picking in the experimental dataset. The quantities compared are the values for t_i, the travel time of the ground wave pick subtracted from the air wave pick. Note that the scope resolution only allows a picking precision of 0.04 μs (Fluke, 1996).

When looking at the breakdown of uncertainty between experimental sites, it is clear once again how important antenna separation is to waveform interpretation.

The uncertainty is higher at all sites when estimated at a single frequency with a spread of separations, whereas the uncertainties are very low for a single separation at a variety of frequencies (***Figure 4.14***). Therefore, during subsequent data collection, it was decided to sound each point at the same offset and to sound it twice, using two different frequencies. Thus, the uncertainty in ground wave picking is reduced to the error for individual frequencies given in ***Table 4.1***, about 2-3 %.

The total error for the Gigjökull and crater sites are greater than those on the flank. This would be expected for Gigjökull, because the material in the ablation area is much more variable than elsewhere on the ice cap. There is much less data for the crater site, a factor which may increase the uncertainty. The error for the flank is quite low, except for the Flank A set, if the 4 MHz antenna data are included. Flank A has a fractional uncertainty of 17%, a relatively large margin of error when compared to the rest of the dataset. These data could be considered outliers and excluded from the calculations. First, however, there are implications which must be considered.

Much of the survey data collected on the flanks were sounded using the 2 and 4 MHz antenna combinations. If the high levels of picking uncertainty from Flank A are rejected, then the error estimation for the flank data may be underestimated. On the other hand, the 4 MHz uncertainty calculated for the first flank experimental set is low, similar to levels of uncertainty calculated for the crater and Gigjökull experiments. Furthermore, when analyzing the waveforms for Flank A, it seems that the picking error results from internal waves being picked which do not show up on the Flank waveforms. Perhaps the perpendicular change in orientation preferentially aligned the antennas with englacial inhomogeneities which the first experiment did not encounter.

The calculated picking error equals about 3 m in equivalent ice depth. The greatest error which could arise from picking is about 25 m depth equivalent, if the 4 MHz Flank A data are included. The picking uncertainty contributes to the total dataset error which includes the radar range, GPS, and interpolation error.

4.5 Estimation of electromagnetic wave velocity in ice

In order to determine ice thickness from two-way travel times of electromagnetic waves in ice, the propagation velocity of these waves must be known. Laboratory experiments have produced theoretical values for "pure" ice, and field experiments have gathered empirical velocity values as well. However, most of the velocities are derived for cold, polar ice, which have very different physical properties than temperate ice (*Chapter 3*). The density, vertical structure, liquid water content, and internal inhomogeneities in temperate ice determine the velocity of the electromagnetic waves which travel through them. The paucity of empirical and theoretical data for describing these velocities suggests that the physical properties of temperate ice need to be studied in greater detail. If ice depths are to be determined accurately, then velocities must be measured.

4.5.1 Theoretical values

Table 4.2 provides a selection of velocity values derived from field and laboratory experiments for cold ice, firn, "pure" ice, and temperate ice. The range of values for cold ice are similar for both field and lab studies, from about 167-170 m μs^{-1} (Auty and Benson, 1952; Jiracek and Bentley, 1971; Robin, 1975). Velocity values for firn are typically much higher, because the lower densities of the media allow electromagnetic waves to propagate faster. Velocities for temperate ice are considerably lower, at about 160 m μs^{-1} (Macheret *et al.*, 1993). Also note that the range of error is much higher for one of the temperate velocity values, at $\pm$ 6.9 m μs^{-1}. The variations between the values for cold and temperate ice could be measurement error or, more likely, could reflect real variations in ice properties. As a body, temperate ice has much greater spatial variation in density and liquid water content, both vertically and horizontally, than polar ice. For example, the ablation zone of a temperate glacier will typically have no firn layer during the melt season (when ice radar surveys usually take place) and will contain high volumes of liquid

water, supraglacially, englacially, and subglacially. In comparison, the accumulation zone of the same glacier may have a substantial layer of firn and a much lower mean liquid water content. The wave velocities through each of these contrasting zones will be significantly different. If one was to calculate all the ice thicknesses with the same velocity value, the conclusions would be considerably inaccurate.

4.5.2 Methods for estimating velocity

Table 4.2 also shows the variety of experimental methods available to empirically measure wave velocity in ice. ***Borehole interferometry*** is perhaps the most precise, allowing the vertical layering of an ice body to be investigated, but drilling boreholes is impractical for many researchers. ***Wide-angle reflection (WAR)***, commonly used in seismic sounding, is a straightforward method in which a transmitter is placed in a fixed position and the receiver is moved away at even increments. Soundings are taken at each separation and wave velocity is derived from the difference in two-way travel time relative to the offset. The disadvantage to the WAR method is that errors in the velocity estimation occur if the bed surface is not flat. The bed slope angle must be known for the estimation to be accurate. If there are no means to determine the bed slope angle, then it is better to use the ***common-midpoint sounding (CMP)*** method. Similar in theory to WAR, CMP sounding requires that both the transmitter and receiver are moved away from a midpoint at equal increments (***Figure 4.15***). This method diminishes errors which result from a sloping bed because the same point is theoretically being measured at each offset. For this reason, the CMP method was chosen for the present study.

4.6 Common-midpoint sounding experiments

CMP experiments were performed at Eyjafjallajökull at each of the three experimental sites, according to the method described above. From the data collected, electromagnetic wave velocity in ice at each site was calculated. The velocity estimation proved difficult, because the small antenna separation distances required for sounding temperate ice limited the use of linear estimation. The

velocities were eventually derived in a qualitative manner, by bracketing the empirical data between theoretical offset/travel-time curves.

4.6.1 Velocity estimation

The velocity of wave propagation may be determined from Pythagorean geometry (***Chapter 2, Figure 2.7***). $2d_2$ is the distance in meters that a ground wave travels from transmitter to receiver through ice. If the ice depth is unknown, then the distance travelled is unknown. The distance travelled can be determined by multiplying the travel time of the ground wave (t_2) by the wave propagation velocity. However, the velocity is unknown. What is known is the distance in meters between the transmitter and the receiver, as well as the velocity of the air wave (c). If one considers a right-angled triangle, where d_2 is the hypotenuse, Pythagorean geometry states that $(d_1)^2 + (H_i)^2 = (d_2)^2$. This equation can be written $(2d_1)^2 + (2H_i)^2 = (2d_2)^2$ to incorporate both sides of the travel path. Then, the velocity and travel time components are substituted for the distance parameters, giving

$$(v_i t_2)^2 = (ct_1)^2 + (2H_i)^2,$$

Equation 4.1

where

$v_i t_2 = 2d_2$

$ct_1 = 2d_1$.

For this equation, there are two known parameters, t_1 and t_2. t_1, the travel time of the air wave, is calculated by dividing the offset by the speed of light, c. t_2 is determined from the received signal (***Figure 2.7b***). The measured travel time of the ground wave (t_i) plus the calculated time of the air wave (t_1) equals t_2, the two-way travel time. Since the arrival of the airwave at the receiver triggers the oscilloscope sweep, some time has elapsed since the transmission of the ground wave before the receiver starts measuring the time.

In order to determine the two unknowns, v_i and H_i, the previous equation may be substituted into the equation of a line:

$$v_i^2 t_2^2 = c^2 t_1^2 + (2H_i)^2 .$$

Equation 4.2

If t_2^2 is plotted on a graph as a function of t_1^2, the data should form a straight line. The slope and intercept values from the equation of the best-fit line can then be used to calculate the unknown velocity and depth parameters:

$$t_2^2 = \frac{c^2}{v_i^2} t_1^2 + \frac{(2H_i)^2}{v_i^2},$$

Equation 4.3

where the gradient equals $\frac{c^2}{v_i^2}$ and the y-intercept is at $\frac{(2H_i)^2}{v_i^2}$.

There is some discussion in the literature (Jiracek and Bentley, 1971; Robin *et al.*, 1969) that the interference between the air wave and the lateral wave causes the air wave to propagate at a velocity other than *c*. However, Jezek *et al.* (1978) state that this phenomenon only occurs on solid ice (for example, on blue ice in the ablation zone of a temperate glacier) and not on ice that has a top layer of snow or firn. The difference in density between the overlying firn and underlying ice causes the velocity to decrease with depth which in turn causes the downward refraction of the lateral wave. Thus, it will not interfere with the air wave. The implication of this discussion is that in a place like the accumulation area of a temperate glacier where there is a layer of firn, it can be safely assumed that the air wave travels at the velocity of propagation in air (*c*). On the other hand, in the ablation zone, where no firn layer is present, this cannot be assumed. The air wave triggers the oscilloscope, so the actual travel time of the direct wave cannot be measured nor can the velocity of the air wave be empirically determined. Since the air wave is used as a reference for all time measurements, a basic error is introduced for all the depth calculations at these sites. At locations like the ablation area of Gigjökull, there will be a delay in the arrival of the air wave (Dinnis, 2000). Velocities will be overestimated and relative permittivities underestimated. The actual delay cannot be quantified at this time (Dinnis, 2000).

The previous discussion goes a long way towards explaining the difficulties encountered when deriving velocities from the experimental data using the linear estimation method. This method is not investigated for temperate ice in the literature. Very small separations are needed to produce clear waveforms in thin, temperate ice. When the separation is increased (from, say, a 40 m offset to an 80 m offset), the distance travelled by the air wave increases by 40 m, while the distance travelled by the ground wave (in an ice thickness of 150 m) only increases by about 7 m (Dinnis, 2000). The difference between the air wave and the ground wave therefore becomes smaller. When the air wave travel time (t_1) is added to t_i to get t_2, the two-way travel time, the resulting values should indicate that, as separations increase, the ground wave travel times increase. However, if the assumption that the air wave always travels at the speed of light (c) is incorrect, then the t_2 times will also be incorrect. If the air wave is actually travelling at a slower velocity than c, as a result of interference with the lateral wave, then the t_2 times will be underestimated.

Almost 30% of the experimental data plotted at t_2^2 against t_1^2 for the linear estimation have negative slopes, a result which is physically unmeaningful, since it requires the calculation of the square root of a negative number (***Figure 4.16***). ***Table 4.3*** summarizes the velocities calculated for the three experimental sites using linear estimation.

If t_i is plotted against x (antenna separation or offset in m), then the experimental data matches that of theoretical curves calculated for a range of velocities and depths based on Laws of Reflection and Pythagorean geometry (***Figure 4.17***). Travel time decreases with offset until the antenna separation approaches that of the ice depth, when it then increases. If the experimental t_i values match the theoretical values, but the t_2 values do not, then there must be something amiss with the assumptions governing the quantity t_1, which is added to t_i to equal t_2. Essentially, the assumption is that the air wave travels at c, but it actually does not. At this time, the discrepancy cannot be quantified, so the t_2 time cannot be used to estimate the velocities.

It was decided to use the t_i times to estimate the velocities, therefore eliminating the incorrect t_1 assumptions from the calculation. The t_i data for each site were plotted with the theoretical t_i curves. By plotting the empirical data, along

with error bars representing the ground wave picking error, amongst a group of theoretical curves which represent a range of velocities and depths, then an estimate of the empirical velocity and depth can be made. The theoretical curves provide a bracket for the empirical data.

Strangway *et al.* (1974) did something similar, by computing theoretical power-frequency curves for various dielectric constants, loss tangents, and depths. The theoretical curves were compared with the field curves and a best fit was chosen. The authors do establish a caveat:

> "Such an interpretation [comparing theoretical curves to field data and determining a best fit] is not always unambiguous. There may be several different combinations of parameters which appear to fit the data equally well. In such cases the redundancy of several components and several frequencies comes into play. The criterion of consistency is applied to select the correct determination from various possibilities." (Strangway *et al.*, 1974)

A similarly qualitative approach was applied to the selection of the best bracketing curves. ***Figures 4.18 - 4.21*** show the theoretical curves which bracket the experimental data from each site.

4.6.2 Experimental values

Table 4.4 states the electromagnetic wave propagation velocities derived for each experimental site. The Gigjökull and flank sites have similar depths (t_i times) and estimated velocities. These values are much lower than the velocity and depth estimated for the crater. One would expect the velocity of the ice at Gigjökull to be lower than that of the flank and the crater because the measurements were taken on blue ice, a material denser as a whole than ice bodies which contain portions of firn. The ablation area contains numerous englacial water channels and surface water, and the ice is more compacted than that in the accumulation zone. The crater most likely has a significant firn layer of less dense ice, which would increase the average velocity of waves propagating through the material. The material at the flank site is in a transitional zone at the equilibrium line altitude and should thus have velocities

somewhere in between the two extremes of the crater and Gigjökull sites. However, the results indicate that the material at the flank site is much more similar to the material at Gigjökull than anticipated.

The velocity derived for the Gigjökull site is 138 ± 10 m μs^{-1} (or ± 7 %). It should be expected that the velocity values fluctuate a great deal according to the frequency used, because the scale of inhomogeneities is less than that of the distance between antenna separation iterations. The density at this site will vary a great deal spatially, but the objective is to get a good idea of the bulk density of the ice body as a whole. The glacier at this site is more of a mixture, of ice, liquid water, and other inhomogenities, such as tephra, than at the other sites, so the velocity should vary more.

The velocity derived for the crater site is 187 ± 23 m μs^{-1} (or ± 12 %). This was the site where the least amount of experimental testing was done, unfortunately, as a result of practical concerns, such as the enormous amount of time it took to get there and the personal hazards involved. The major omission of the experiment was not testing with the 4 MHz antennas. They provide the highest frequency and are therefore the most obvious choice to sound the thickest and driest part of the glacier. The data are sparse here for the velocity derivation, a fact reflected in the high uncertainty. This is an obvious place where more work needs to be done.

The velocity derived for the flank site is 140 ± 8 m μs^{-1} (or ± 6 %). The results for this site are the most surprising, because the velocity values were expected to be higher than those at Gigjökull. Perhaps the differences in material are not significant enough to discern with the velocity estimation method employed.

4.7 Summary

The experimental data provide the means to determine the electromagnetic wave propagation velocities in ice at representative sites on Eyjafjallajökull. The measured velocities give site-specific accuracy to the depth determinations and provide insight into the physical properties of the ice. There seem to be two discrete spatial zones of ice at Eyjafjallajökull: thin, dense ice on the volcano flanks and at

the toe of Gigjökull, and thicker ice with a lower bulk density contained within the crater.

Each of these sites requires different offset distances between transmitter and receiver and different transmission frequencies to obtain interpretable waveforms. The varying depth and presence of liquid water seem to have the greatest impact on the radar configuration.

Clearly, more work needs to be done in determining what happens with the air wave in the near surface air/ice interface and what implications the supposed interference with the lateral wave has for the estimation of velocity. However, it makes sense theoretically and practically that thin temperate ice in ablation areas will have lower propagation velocities than accumulation areas because the former have more varied material composition.

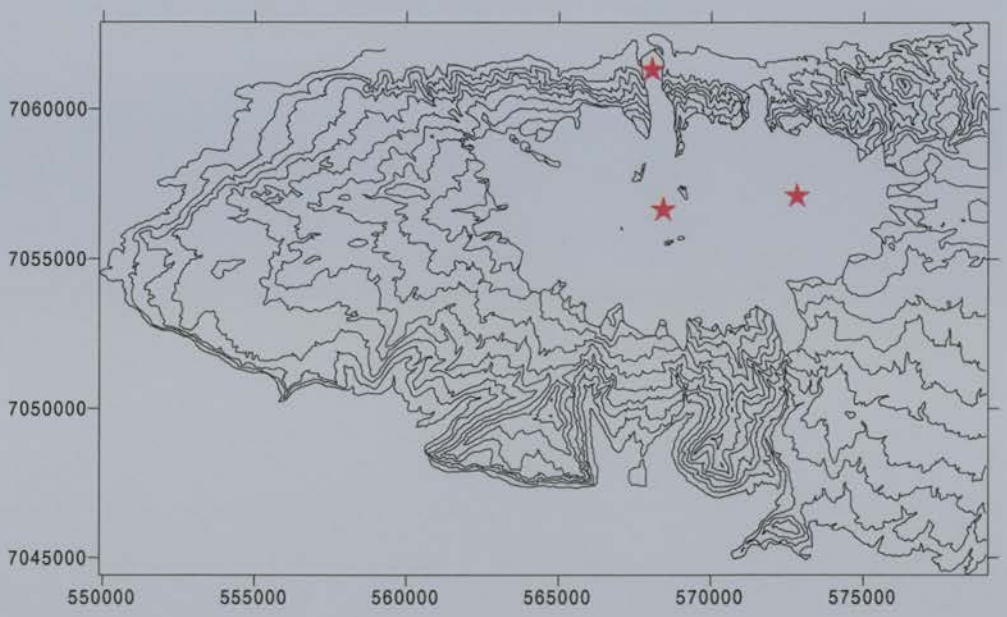

Figure 4.1 Location of common midpoint sounding (CMP) experiments (stars) on Eyjafjallajökull. Experiments were performed in the crater, on the east flank, and at the base of Gigjökull.

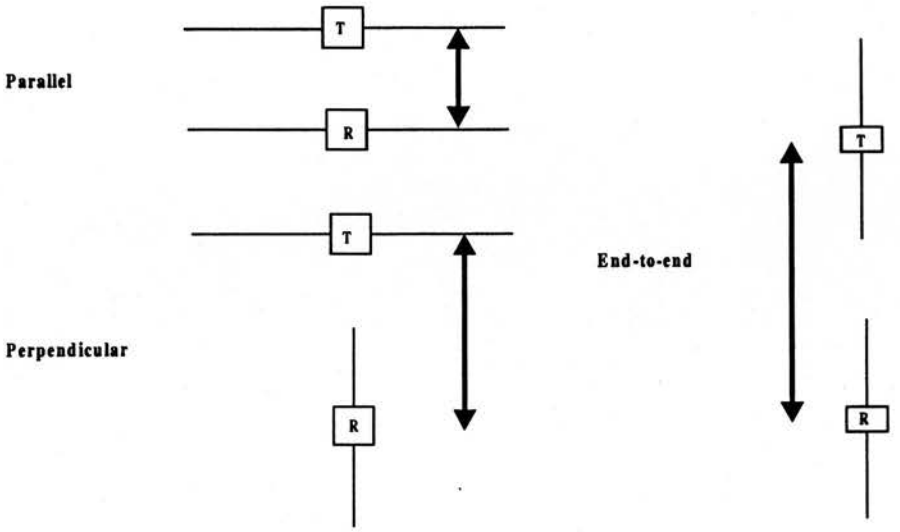

Figure 4.2 Antenna orientations tested in field experiments: parallel, perpendicular, and end-to-end. Offset is measured as the distance between transmitter and receiver, indicated by arrows.

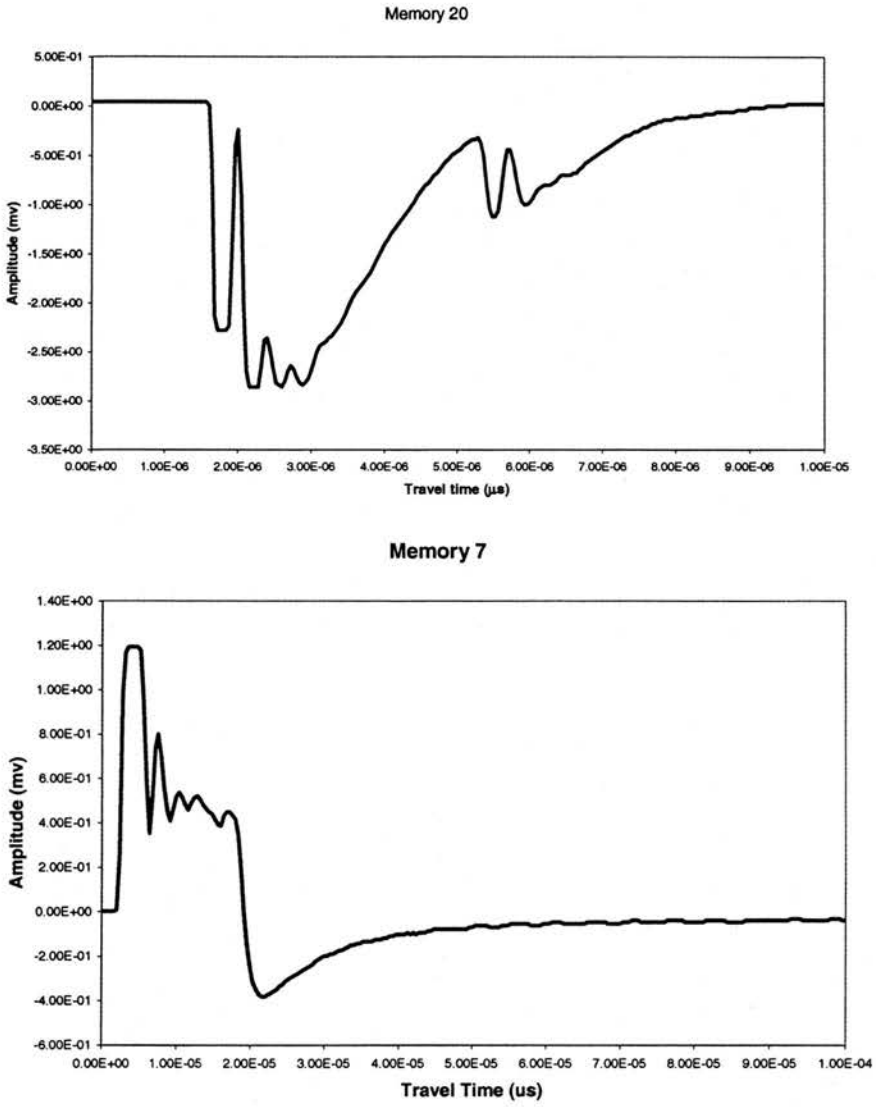

Figure 4.3 Two waveforms produced using a perpendicular antenna orientation. Ground waves cannot be identified in either waveform, rendering them uninterpretable.

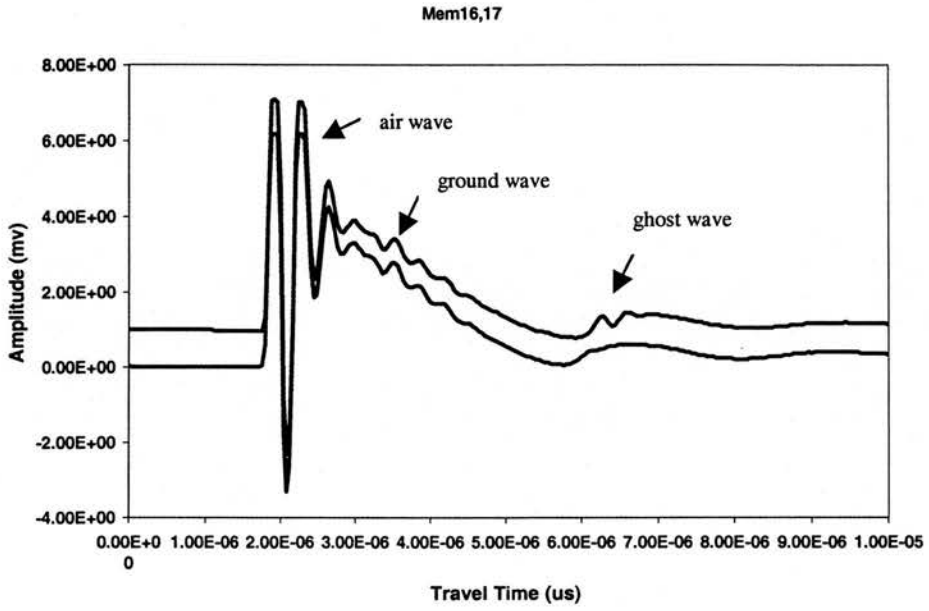

Figure 4.4 Example of nearly identical waveforms produced by swapping the transmitter and receiver between antennas (Gigjökull experimental site, 20 m offset, 2 MHz). Air and ground waves are very similar, but one ghost wave is more detailed than the other.

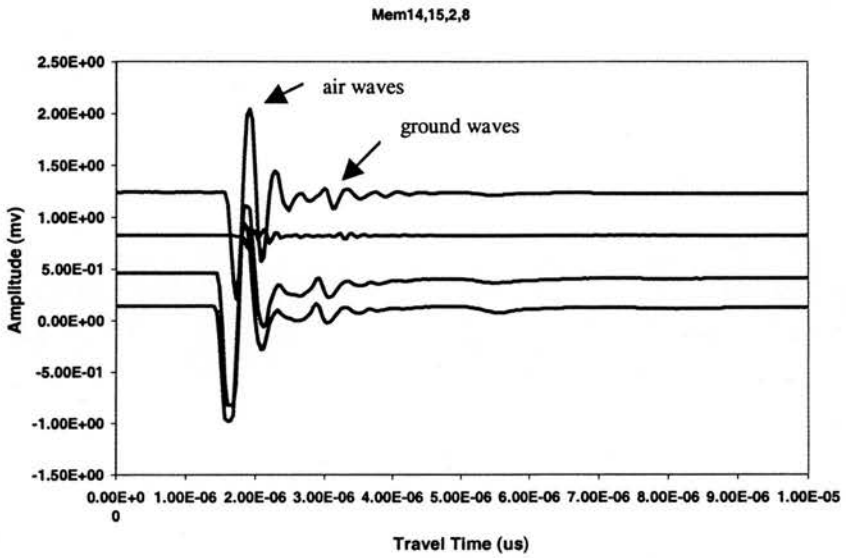

Figure 4.5 Example of clearest waveforms produced at flank experimental site with an 80 m antenna separation at a range of frequencies. Air waves and ground waves are clearly identifiable in each waveform.

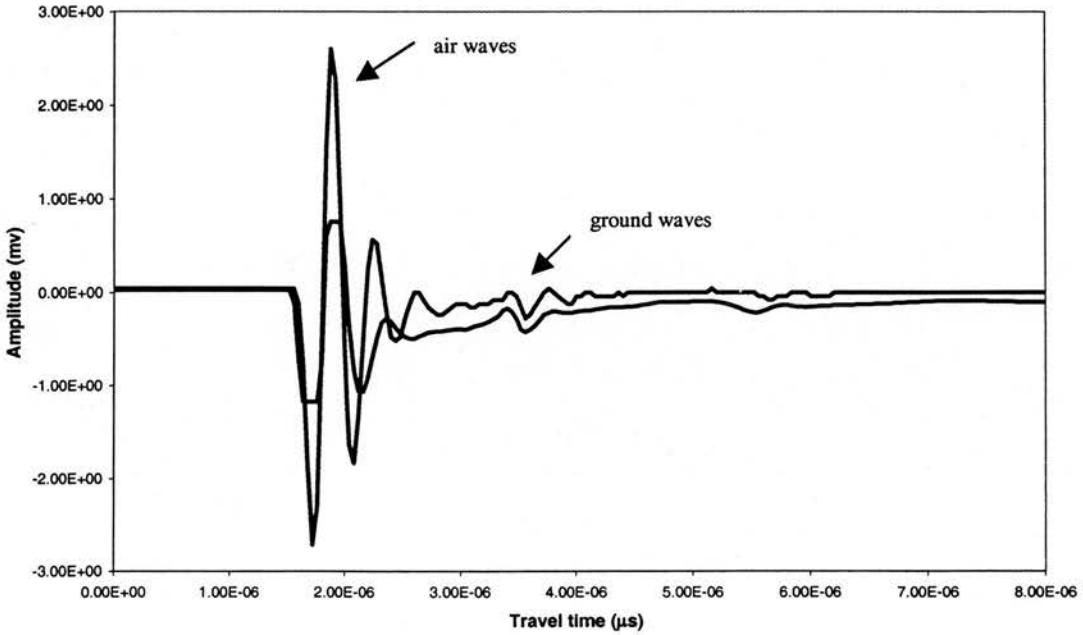

Figure 4.6 Example of clearest waveforms produced at crater experimental site with a 60 m antenna separation and different frequencies. The shape of both waveforms is similar, but the air wave in one has a smaller amplitude.

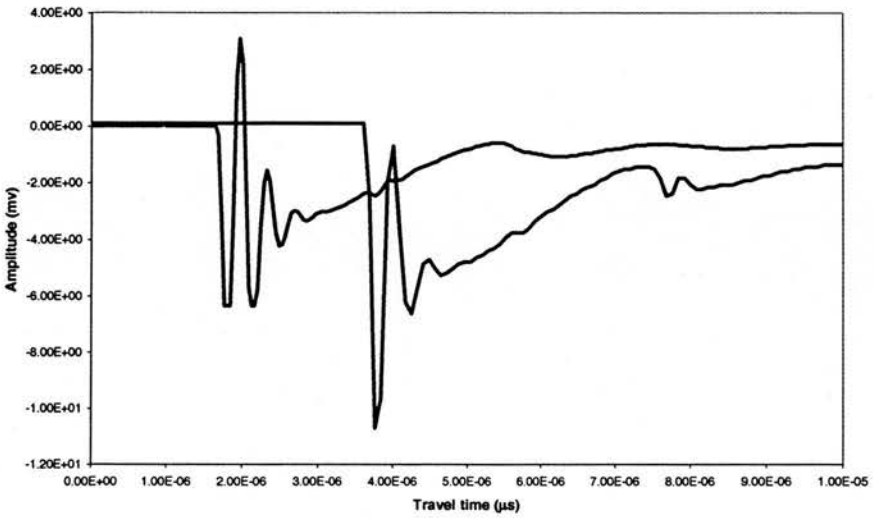

Figure 4.7 Example of poor waveforms produced at crater experimental site with a 20 m antenna separation and different frequencies. Ground waves are not obvious features of either waveform.

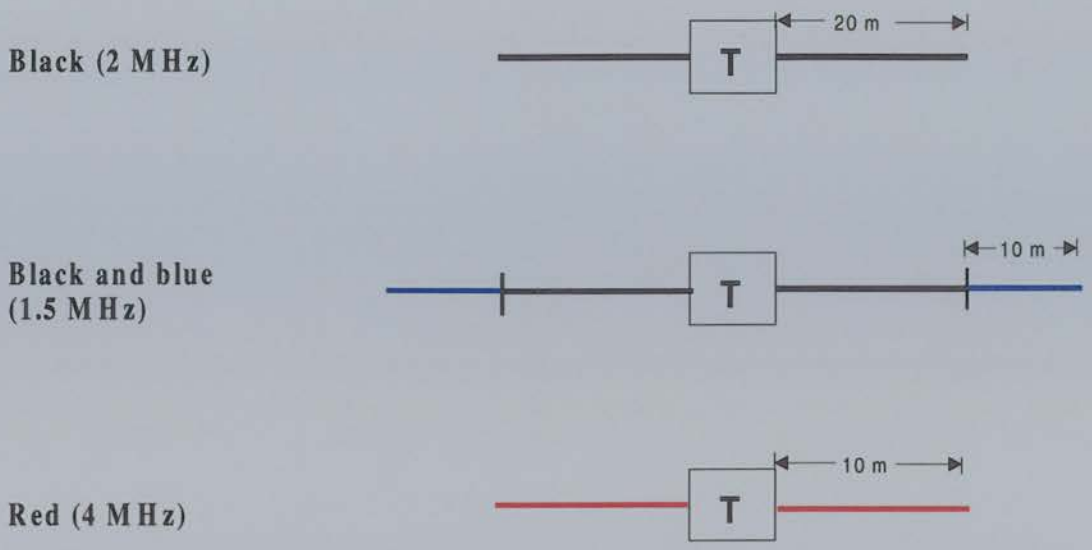

Figure 4.8 Antenna configurations used in the survey. Dimensions of antenna half-lengths are given.

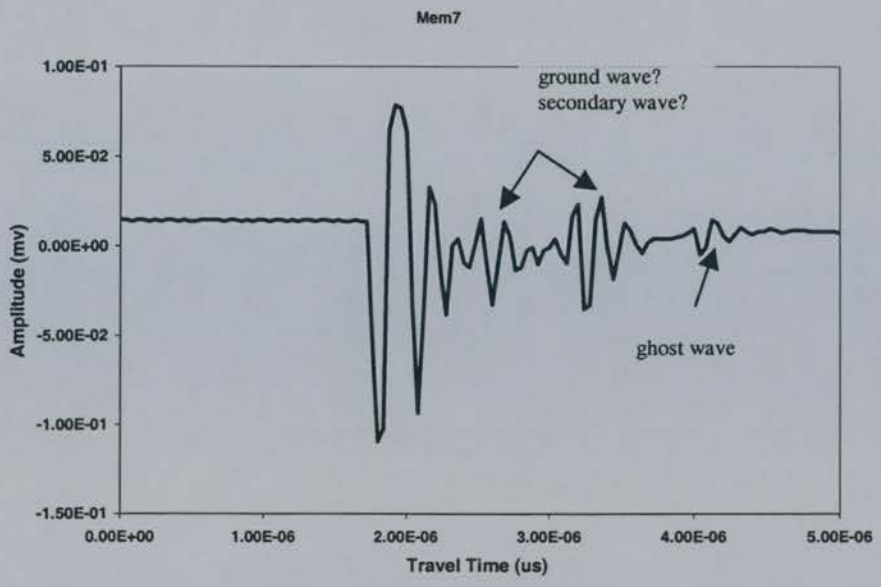

Figure 4.9 Examples of secondary and ghost waves, additional waves which may appear in a waveform and increase the difficulty of identifying the ground wave. Ghost waves only appear when using the black antennas, either alone or in combination with the blue antennas (1.5 - 2 MHz), and always have a travel time of greater than 3 μs. Secondary waves are rare; they only appear in waveforms sounded on the east flank.

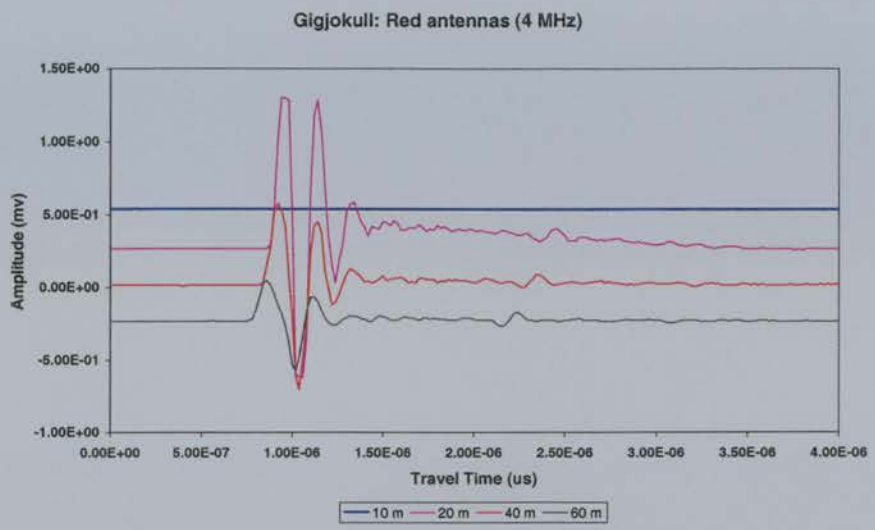
Gigjokull: Red antennas (4 MHz)
1.50E+00
1.00E+00
5.00E-01
0.00E+00
-5.00E-01
-1.00E+00
Amplitude (mv)
0.00E+00
5.00E-07
1.00E-06
1.50E-06
2.00E-06
2.50E-06
3.00E-06
3.50E-06
4.00E-06
Travel Time (us)
10 m
20 m
40 m
60 m

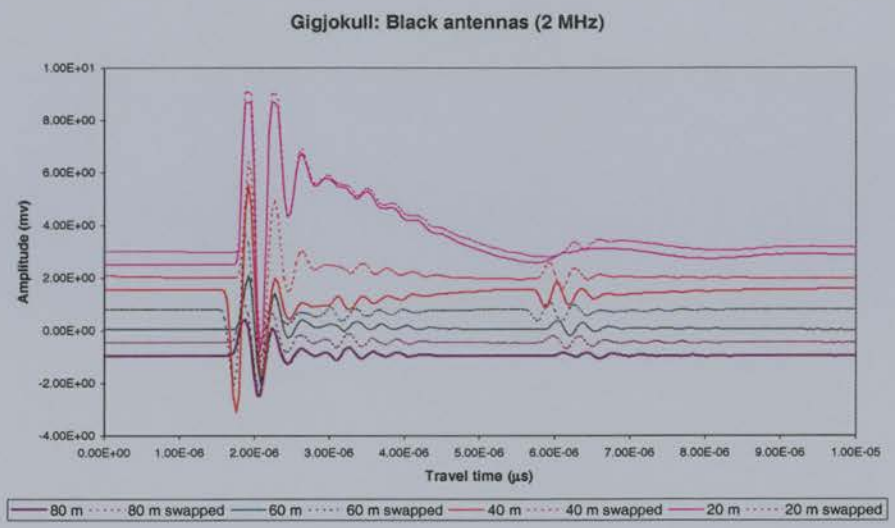
Gigjokull: Black antennas (2 MHz)
1.00E+01
8.00E+00
6.00E+00
4.00E+00
2.00E+00
0.00E+00
-2.00E+00
-4.00E+00
Amplitude (mv)
0.00E+00
1.00E-06
2.00E-06
3.00E-06
4.00E-06
5.00E-06
6.00E-06
7.00E-06
8.00E-06
9.00E-06
1.00E-05
Travel time (µs)
80 m
80 m swapped
60 m
60 m swapped
40 m
40 m swapped
20 m
20 m swapped

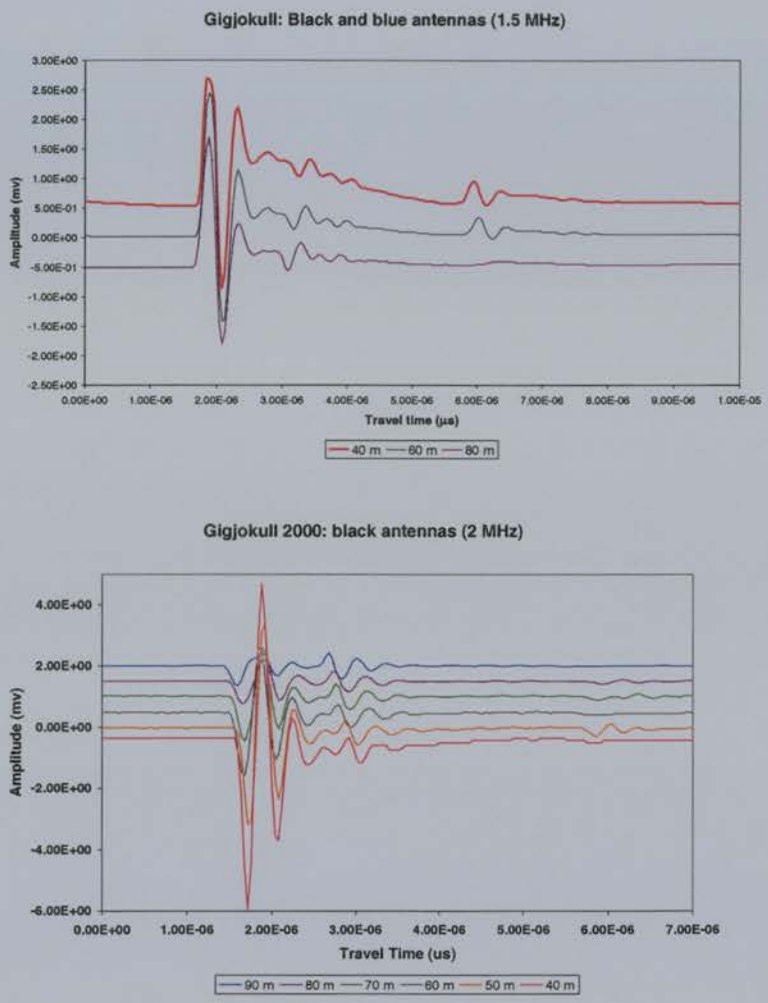

Figure 4.10 Stacked waveforms for Gigjökull experiments. Each stack represents the same point sounded by one frequency at increasing offsets and illustrates the repeatability of depth measurements. The Gigjökull 2000 stack measures a different point than the Gigjökull 1999 stacks.

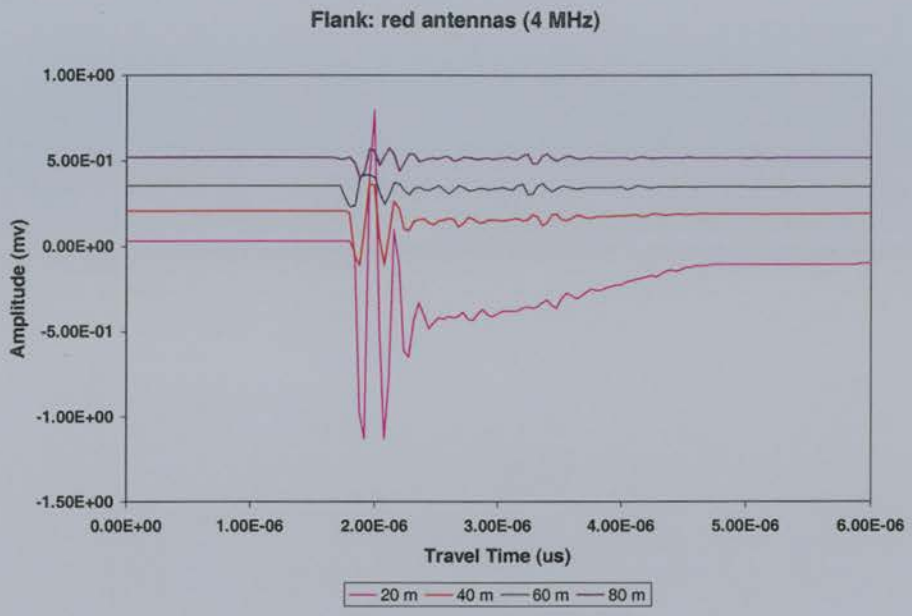
Flank: red antennas (4 MHz)
1.00E+00
5.00E-01
0.00E+00
-5.00E-01
-1.00E+00
-1.50E+00
Amplitude (mv)
0.00E+00
1.00E-06
2.00E-06
3.00E-06
4.00E-06
5.00E-06
6.00E-06
Travel Time (us)
20 m
40 m
60 m
80 m

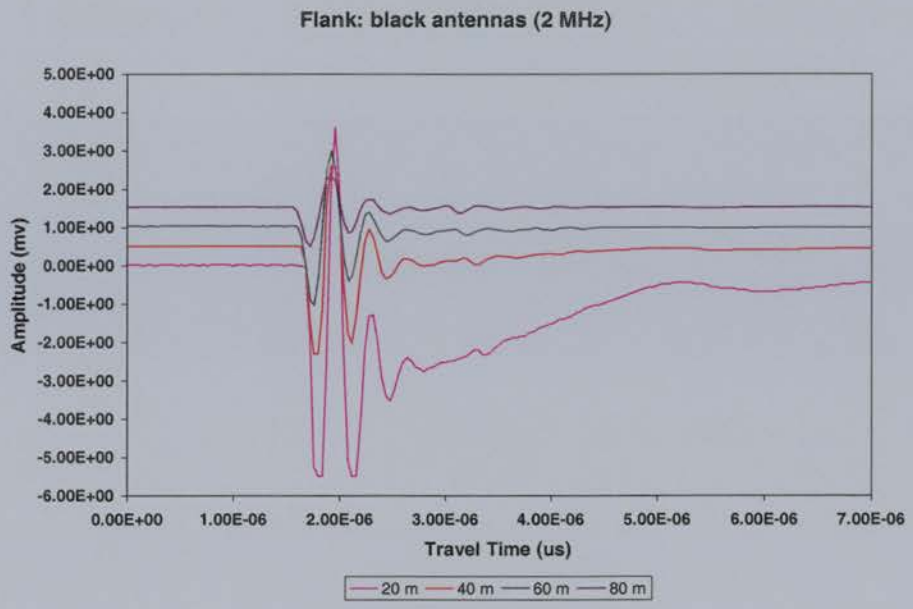
Flank: black antennas (2 MHz)
5.00E+00
4.00E+00
3.00E+00
2.00E+00
1.00E+00
0.00E+00
-1.00E+00
-2.00E+00
-3.00E+00
-4.00E+00
-5.00E+00
-6.00E+00
Amplitude (mv)
0.00E+00
1.00E-06
2.00E-06
3.00E-06
4.00E-06
5.00E-06
6.00E-06
7.00E-06
Travel Time (us)
20 m
40 m
60 m
80 m

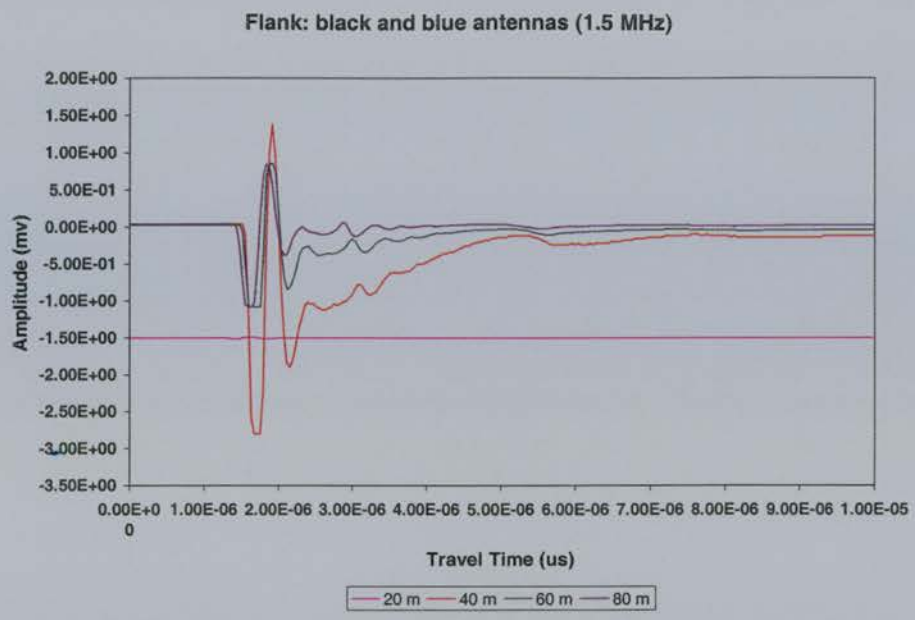

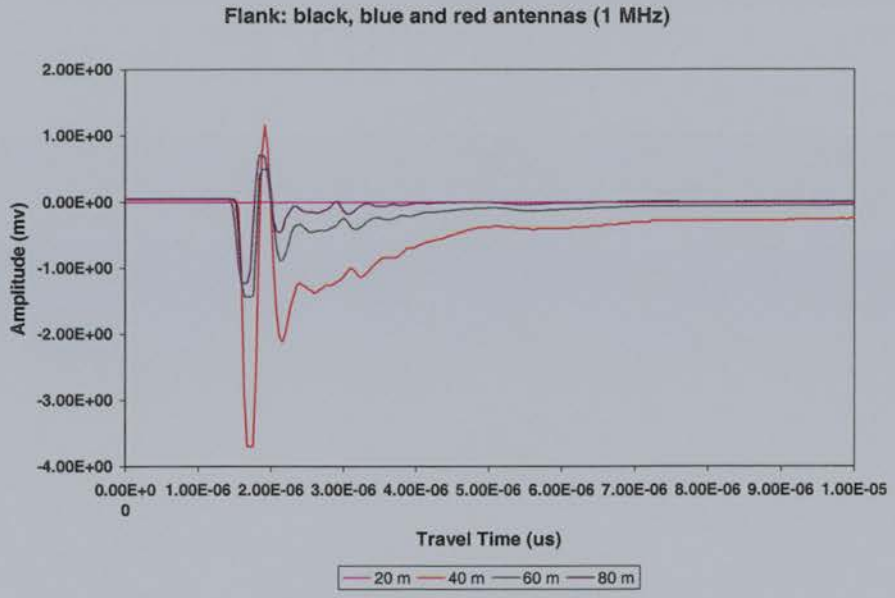

Figure 4.11 Flank experiment stacked waveforms: Antennas perpendicular to flow. Each stack represents the same point sounded by one frequency at increasing offsets and illustrates the repeatability of depth measurements.

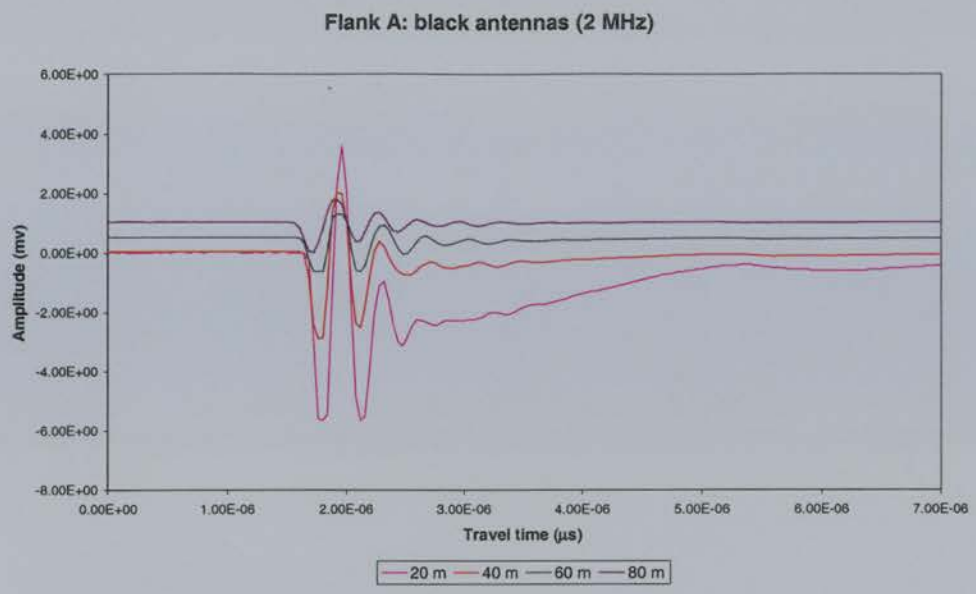
Flank A: black antennas (2 MHz)
6.00E+00
4.00E+00
2.00E+00
0.00E+00
-2.00E+00
-4.00E+00
-6.00E+00
-8.00E+00
Amplitude (mv)
0.00E+00
1.00E-06
2.00E-06
3.00E-06
4.00E-06
5.00E-06
6.00E-06
7.00E-06
Travel time (µs)
20 m
40 m
60 m
80 m

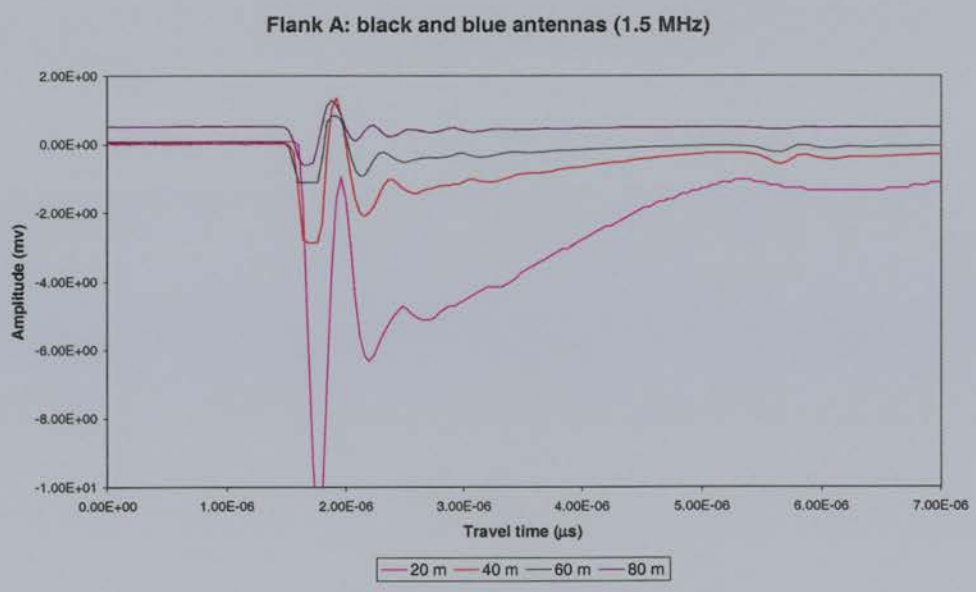
Flank A: black and blue antennas (1.5 MHz)
2.00E+00
0.00E+00
-2.00E+00
-4.00E+00
-6.00E+00
-8.00E+00
-1.00E+01
Amplitude (mv)
0.00E+00
1.00E-06
2.00E-06
3.00E-06
4.00E-06
5.00E-06
6.00E-06
7.00E-06
Travel time (µs)
20 m
40 m
60 m
80 m

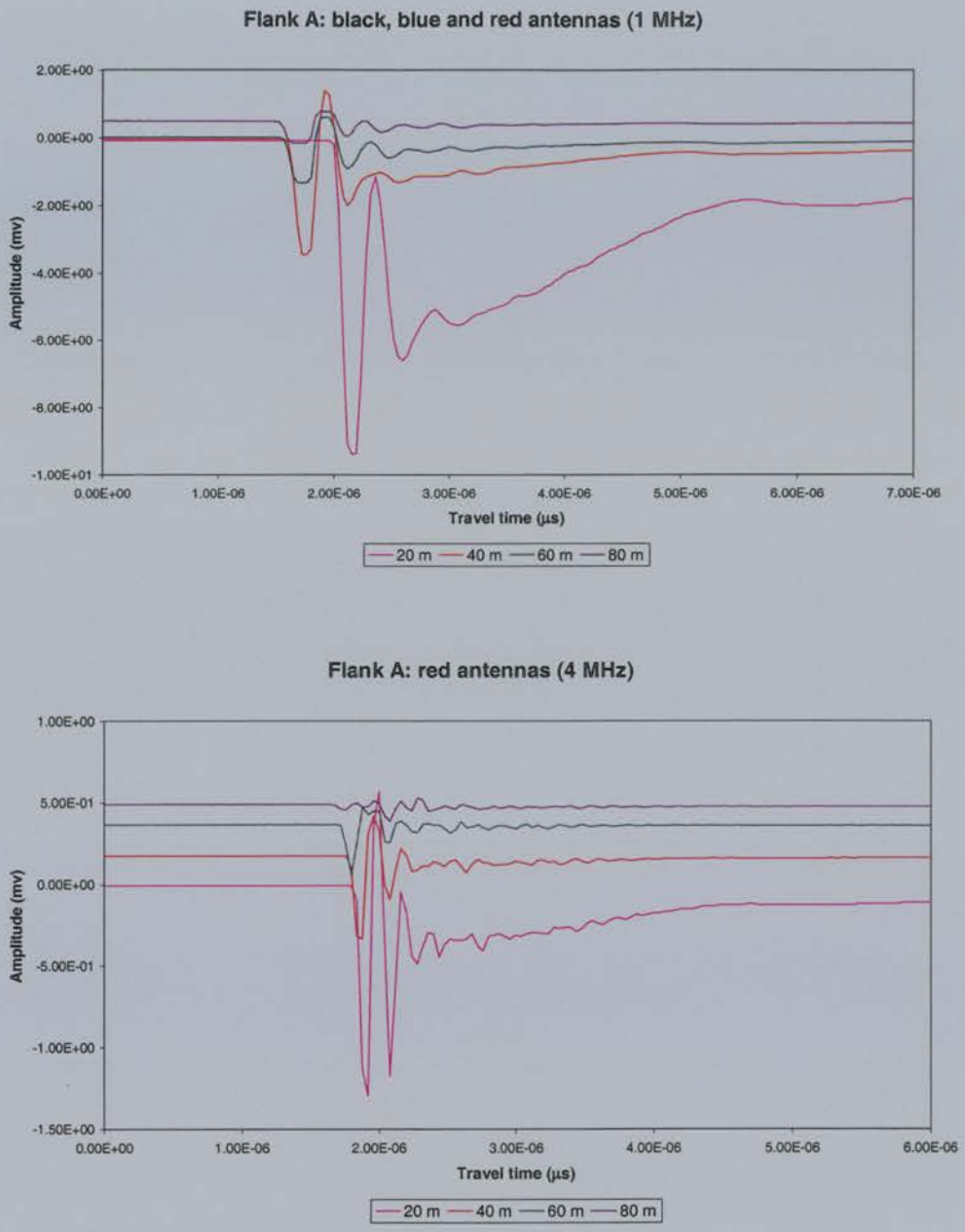

Figure 4.12 Flank experiment stacked waveforms: Antennas parallel to flow. Each stack represents the same point sounded by one frequency at increasing offsets and illustrates the repeatability of depth measurements.

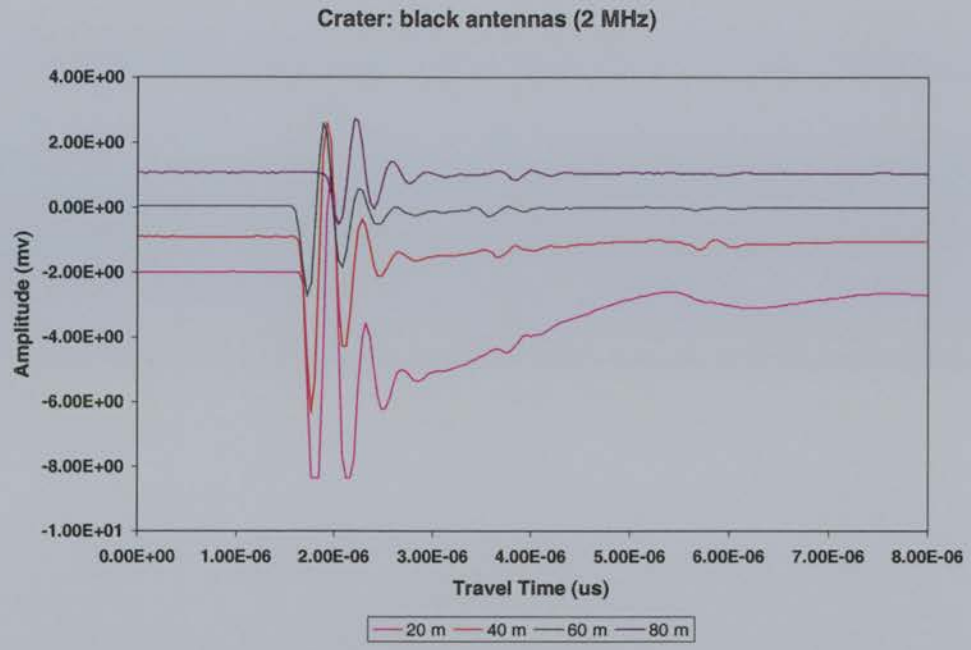

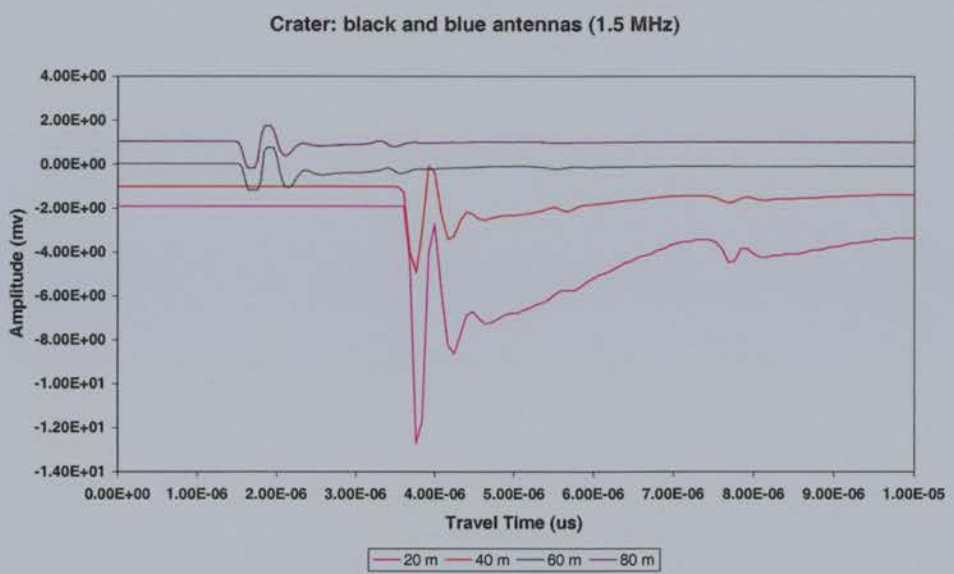

Figure 4.13 Crater experiment stacked waveforms. Each stack represents the same point sounded by one frequency at increasing offsets and illustrates the repeatability of depth measurements.

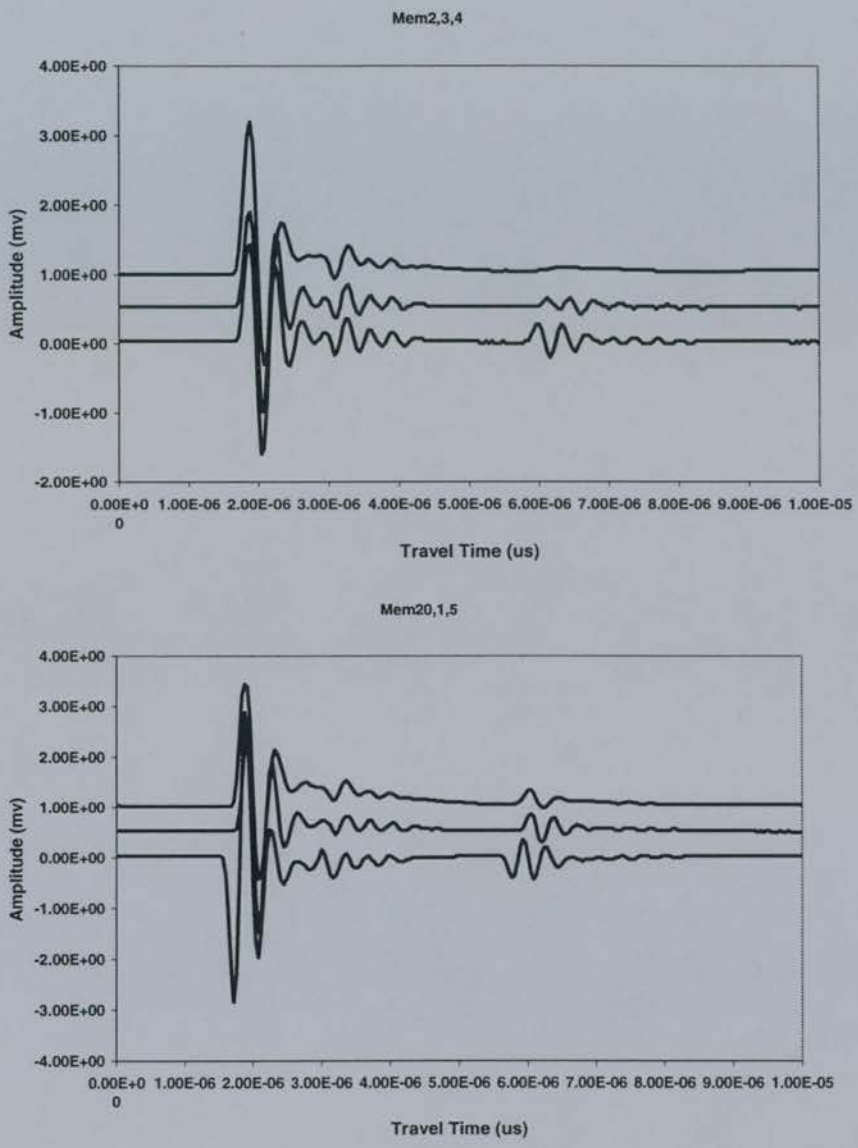

Figure 4.14 Examples of groups of waveforms measuring the same point at the same offset, using different frequencies. Common midpoint soundings (CMP) also show differences between waveforms produced at the same point and offset, with different frequencies. In both examples, the change in ghost wave with frequency is evident.

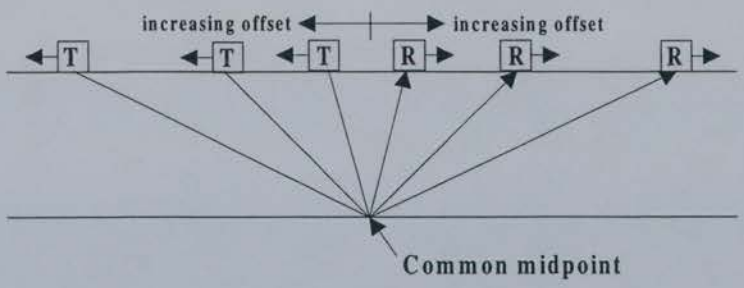

Figure 4.15 Common midpoint sounding (CMP) setup (redrawn from Reynolds, 1997). The transmitter and receiver are placed at equal distances on either side of a common midpoint. The offset is increased at equal intervals and a sounding taken at each iteration.

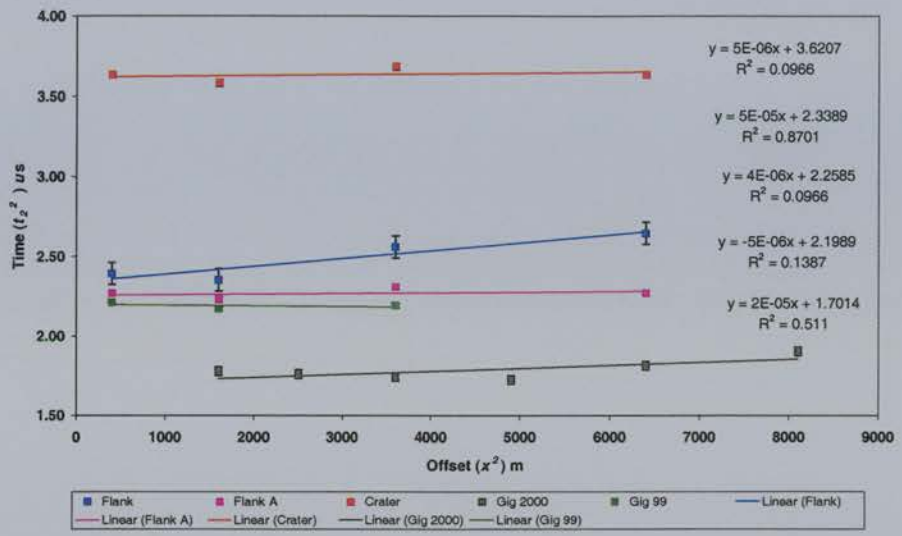

Figure 4.16 Examples of linear estimation method for deriving electromagnetic wave velocity in ice. Two-way travel time data (t_2) from each experimental site are plotted against antenna separation (x). Slope values from best-fit lines are used to calculate velocity.

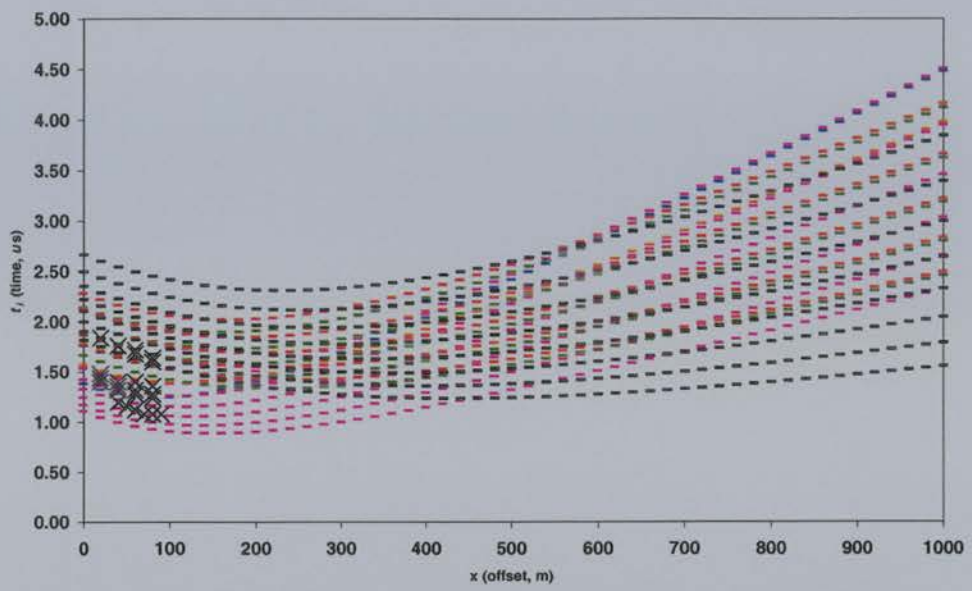

Figure 4.17 Theoretical curves (multicolored) and experimental data (crosses) of antenna separation (x) plotted as a function of travel time (t_i). Theoretical curves are calculated for a variety of ice depths (H_i) and velocities (v_i). t_i is defined as the travel time of the ground wave (t_{ground}) minus the travel time of the air wave (t_{air}), where $t_{air} = \frac{x}{c}$ and $t_{ground} = \frac{2}{v_i}\sqrt{H_i^2 + \frac{x^2}{4}}$. Note travel times decrease with increased offset at very small offsets, but eventually increase. All Eyjafjallajökull experimental data were collected at small offsets, a requirement for sounding temperate ice.

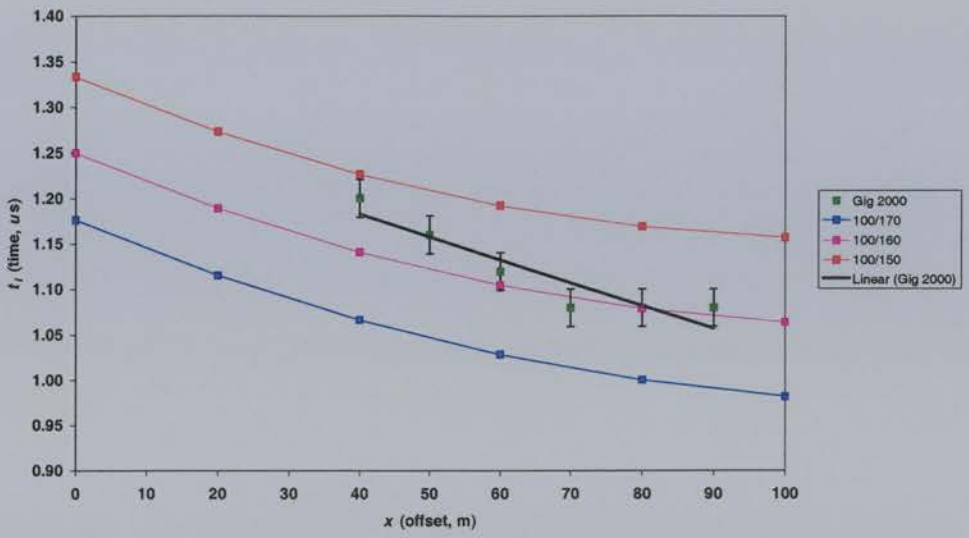

Figure 4.18 Gigjökull 2000 experimental data bracketed by theoretical offset/travel time curves. Legend indicates ice thickness (H_i) and velocity (v_i) values used in the calculation of each theoretical curve. For example, 100, 170 means H_i = 100 m and v_i = 170 m μs^{-1}.

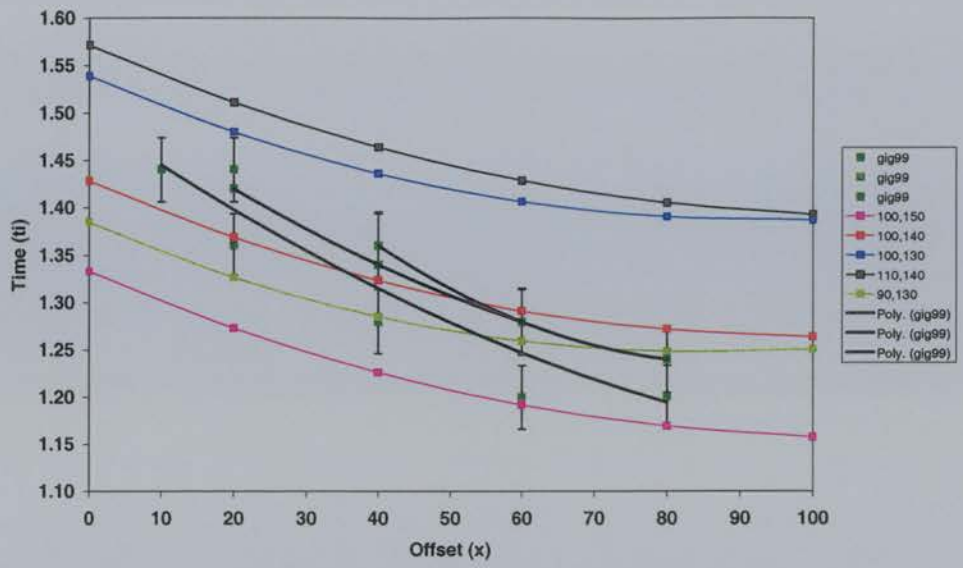

Figure 4.19 Gigjökull 1999 experimental data bracketed by theoretical offset/travel time curves. Legend indicates ice thickness (H_i) and velocity (v_i) values used in the calculation of each theoretical curve. For example, 100, 170 means H_i = 100 m and v_i = 170 m μs^{-1}.

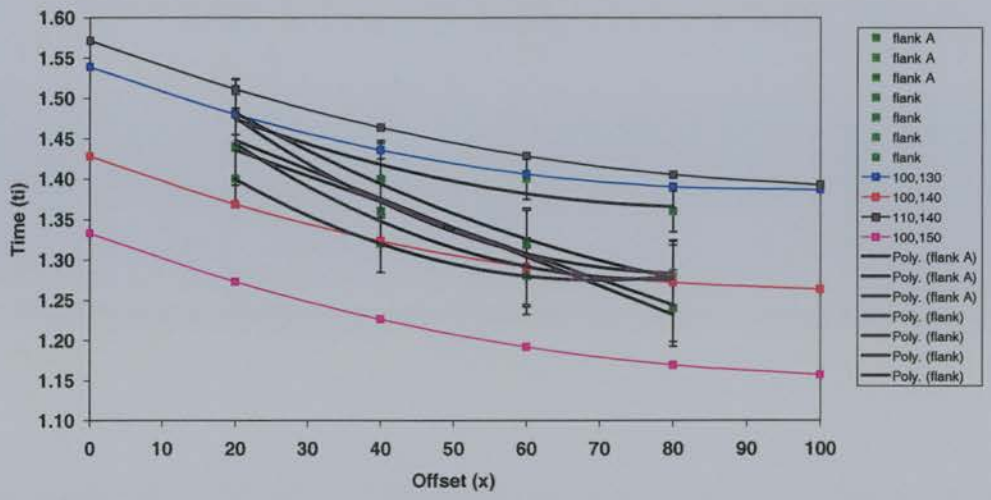

Figure 4.20 Flank experimental data bracketed by theoretical offset/travel time curves. Legend indicates ice thickness (H_i) and velocity (v_i) values used in the calculation of each theoretical curve. For example, 100, 170 means H_i = 100 m and v_i = 170 m μs^{-1}.

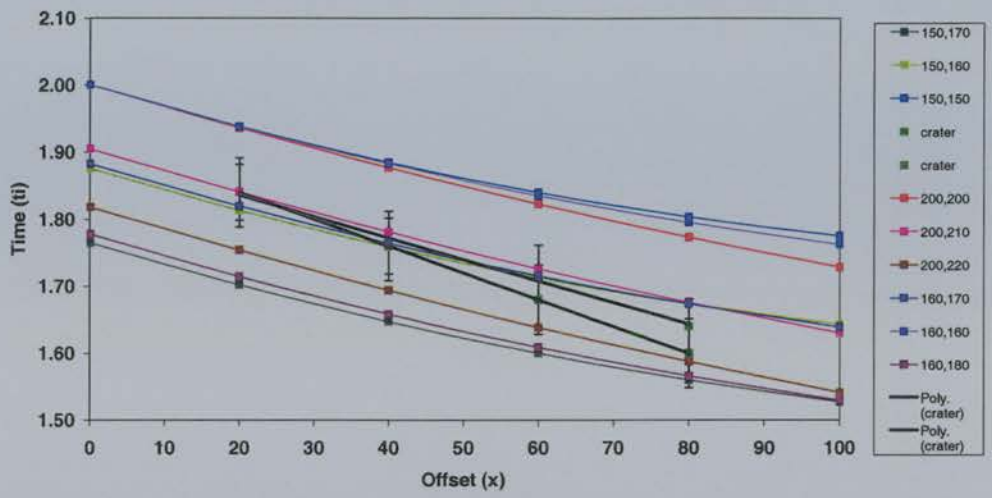

Figure 4.21 Crater experimental data bracketed by theoretical offset/travel time curves. Legend indicates ice thickness (H_i) and velocity (v_i) values used in the calculation of each theoretical curve. For example, 100, 170 means H_i = 100 m and v_i = 170 m μs^{-1}.

Site	Frequency or offset	Mean (μs)	Standard Deviation ($\pm\mu$s)	Fractional Error ($\pm$ %)
Gigjökull				
all offsets	black (2 MHz)	1.32	0.03	2
	black and blue (1.5 MHz)	1.29	0.04	3
	red (4 MHz)	1.35	0.04	3
all frequencies	20 m	1.43	0.01	0
	40 m	1.36	0.01	0
	60 m	1.28	0.00	0
	80 m	1.21	0.01	0
	Total	**1.32**	**0.02**	**2**
Crater				
all offsets	black	1.72	0.05	3
	black and blue	1.77	0.04	2
all frequencies	20 m	1.84	0.00	0
	40 m	1.76	0.00	0
	60 m	1.70	0.02	1
	80 m	1.62	0.02	1
	Total	**1.73**	**0.03**	**2**
Flank				
all offsets	black	1.37	0.04	3
	black and blue	1.36	0.04	3
	black, blue and red (1 MHz)	1.33	0.04	3
	red	1.41	0.03	2
all frequencies	20 m	1.48	0.00	0
	40 m	1.39	0.01	0
	60 m	1.34	0.02	1
	80 m	1.30	0.02	2
	Total	**1.37**	**0.02**	**1**
Flank A				
all offsets	black	1.34	0.04	3
	black and blue	1.34	0.04	3
	black, blue and red	1.34	0.05	4
	red	**0.89**	**0.15**	**17**
all frequencies	20 m (excluding red)	1.44	0.00	0
	40 m (excluding red)	1.37	0.01	0
	60 m (excluding red)	1.29	0.01	0
	80 m (including red)	1.27	0.02	2
	Total (excluding red)	**1.34**	**0.02**	**1**

Table 4.1 Uncertainties calculated for ground wave picking. The errors indicate the expected uncertainty in determining ice depth. Measured ice depth at Eyjafjallajökull can be determined with no more precision than the values given in the table.

Reference	Medium	Velocity (m μs^{-1})	Method
Robin (1975)	cold ice (-20° C)	170.0 ± 1.0	borehole interferometry
	cold ice (-20° C)	168.6 ± 0.2	
	cold ice (-20° C)	169.9 ± 0.3	
	cold ice (-20° C)	168.8 ± 0.2	
	firn	198 - 225	
Jiracek and Bentley (1971)	cold ice	168.5 ± 1.0	wide-angle reflection (WAR)
	pure cold ice	167.4	theoretical estimate
Auty and Benson (1952)	pure cold ice (-11° C)	169 - 173 ± 1.0	laboratory experiment
Macheret *et al.* (1993)	temperate (ablation zone)	160.3 ± 1.0	common-midpoint (CMP)
	temperate (basal ice of accumulation zone)	161.3 ± **6.9**	
	temperate (firn layer of accumulation zone)	182.3 ± 1.6	
	nearby snowpack/firn	190	

Table 4.2 Experimental and theoretical velocity values from the literature.

Site	Best Fit Line	R^2	Velocity (m μs^{-1})
Gigjökull 2000	$y = 2 \times 10^{-5}x + 1.70$	0.51	224
Gigjökull 1999	$y = -2 \times 10^{-5}x + 2.27$	0.97	-
	$y = 1 \times 10^{-5}x + 2.19$	0.34	316
	$y = -5 \times 10^{-6}x + 2.20$	0.14	-
Flank	$y = 4 \times 10^{-7}x + 2.36$	0.001	1581
	$y = 9 \times 10^{-6}x + 2.31$	0.08	333
	$y = 1 \times 10^{-5}x + 2.31$	0.34	316
	$y = 5 \times 10^{-5}x + 2.34$	0.87	141
Flank A	$y = 4 \times 10^{-6}x + 2.26$	0.10	500
	$y = 2 \times 10^{-5}x + 2.21$	0.38	224
	$y = -8 \times 10^{-6}x + 2.29$	0.10	-
	$y = 3 \times 10^{-4}x + 0.28$	0.87	58
Crater	$y = -2 \times 10^{-5}x + 3.63$	0.97	-
	$y = 5 \times 10^{-6}x + 3.62$	0.10	447

Table 4.3 Experimental velocities calculated by the linear estimation method.

Site	Depth (m)	Velocity (m μs^{-1})	Average Velocity (m μs^{-1})
Gigjökull	90	130	**138 ± 10 (or ±7%)**
	100	150	
	100	130	
	100	140	
Flank	100	130	**140 ± 8 (or ±6%)**
	110	140	
	100	150	
	100	140	
Crater	160	170	**187 ± 23 (or ±12 %)**
	150	160	
	200	200	
	200	220	
	160	180	
	150	170	
	200	210	

Table 4.4 Experimental velocities determined by qualitatively bracketing the experimental data with theoretical curves.

4.8 References

Auty, R.P., and Benson, C.S., 1952. Dielectric properties of ice and solid D_2O. Journal of Chemical Physics, 20(8): 1309-14.

Dinnis, A.K., 2000. Modelling a radio echo sounding system (Internal Report), University of Edinburgh, Department of Electrical Engineering, 25 pp.

Fluke, 1996. Fluke 92B/96B/99B/105B Scopemeter Series II User's Manual. Fluke Corporation, Netherlands.

Jezek, K.C., Clough, J.W., Bentley, C.R., and Shabtaie, S., 1978. Dielectric permittivity of glacier ice measured *in situ* by radar wide-angle reflection. Journal of Glaciology, 21(85): 315-329.

Jiracek, G.R., and Bentley, C.R., 1971. Velocity of electromagnetic waves in Antarctic ice. Antarctic Research Series, 16: 199-208.

Macheret, Y.Y., Moskalevsky, M.Y., and Vasilenko, E.V., 1993. Velocity of radio waves in glaciers as an indicator of their hydrothermal state, structure, and regime. Journal of Glaciology, 39(132): 373-384.

Reynolds, J.M., 1997. *An Introduction to Applied and Environmental Geophysics*. John Wiley and Sons, Ltd., Chichester, 796 pp.

Robin, G.d.Q., Evans, S., and Bailey, J.T., 1969. Interpretation of radio echo sounding in polar ice sheets. Philosophical Transactions of the Royal Society of London, 265(116): 437-505.

Robin, G.d.Q., 1975. Velocity of radio waves in ice by means of a bore-hole interferometric technique. Journal of Glaciology, 15(73): 151-159.

Strangway, D.W., Simmons, G., LaTorraca, G., Watts, R., Bannister, L., Baker, R., Redman, J.D., and Rossiter, J.R., 1974. Radio-frequency interferometry- a new technique for studying glaciers. Journal of Glaciology, 13(67): 123-132.

Watts, R.D., and England, A.W., 1976. Radio-echo sounding of temperate glaciers: ice properties and sounder design criteria. Journal of Glaciology, 17(75): 39-48.

Watts, R.D., and Wright, D.L., 1981. Systems for measuring thickness of temperate and polar ice from the ground or from the air. Journal of Glaciology, 27(97): 459-469.

Chapter 5: Practical Methods

5.1 Introduction

This chapter describes how the data were collected, processed and interpreted. The methods of map preparation and interpolation are discussed.

5.2 Data Collection

The data were collected in two field seasons during the summers of 1998 and 1999. Some of the data for Gigjökull were collected during the summer of 2000 by Nick Hulton and Ross Purves (Hulton, N., 2000, *pers. comm.*). A total of 425 points at 256 locations were sounded on the east and west flanks of the ice cap, inside the crater, on the crater rim, and at the base of Gigjökull (***Figure 5.1***).

5.2.1 Ice radar

Point depths were measured by placing the transmitter and receiver on the ice surface a set distance apart, with two antennas attached to both transmitter and receiver. The offset distance (usually about 60 m) was varied according to the requirements of the site, based on the conclusions derived from the experiments in *Chapter 4*. The transmitter and receiving oscilloscope were switched on and the amplitude and time scales adjusted manually to display the clearest waveform. If the waveform was unstable (unstationary), the amplitude scales on the oscilloscope were toggled, then the antenna lengths, offset, and orientation were changed until a stable waveform was produced. Instability occurs if the multiple travel paths of reflections averaged into a waveform are too varied. Sometimes no satisfactory waveform could be produced at all and the location and terrain were noted. This usually occurred when the ice was too thin (< 30 m) or too crevassed. The radar instrument has a minimum range of 30 m; crevasses introduce noise into waveforms which obscures ground reflections.

Satisfactory waveforms were saved as digital files on the oscilloscope and downloaded onto a laptop computer at the end of each day, using Flukeview software (Fluke, 1994). The files, in comma delimited format (.csv), were imported into Excel. The digital signals were then graphed, recreating the waveforms as seen originally in the field on the oscilloscope.

5.2.2 Ice radar post-processing

The subjectivity and ambiguity involved in identifying ground reflections were overcome by taking two soundings of varying frequencies at each point, using the method developed in *Chapter 4*. The waveforms were then overlaid and analyzed. When the two-way travel times of the waveform pair were compared, those that had a discrepancy greater than the margin of error determined by the experiments were discarded. About 3% of the total waveforms were discarded for this reason. Waveforms that contained no identifiable ground reflection were also rejected. As a result, the thickest and thinnest measured depths are underrepresented on the final map because these waveforms are the hardest to interpret and are most likely to be discarded. The 1998 and 1999 Gigjökull data were collected before the validation method was decided, so only single soundings at each point were taken. For these data, only the most obvious ground waves were picked and any ambiguous ones were rejected.

Of the total number of waveforms collected, 186 were deemed interpretable. Since more than one waveform was collected at each location, when all the processing was complete, there remained a total of 135 radar data points with which to create the map.

When the two-way travel times of the waveforms were determined, the ice thicknesses were calculated using the velocities calculated from the experiments in *Chapter 4* and *Equation 2.11*.

5.2.3 GPS

The horizontal and vertical location of the ice surface was determined with a Global Positioning System (GPS). x, y, and z surface coordinates were recorded by a Magellan ProMARK X hand-held GPS.

For each sounding, the GPS receiver was placed on the ice surface at the center point between the radar transmitter and receiver, in order to most accurately locate the bottom reflector on the horizontal plane and to measure the ice surface height. The remote receiver logged for three minutes at each point. Coordinates were then written down as well as saved digitally.

A GPS base station logged continuously throughout the day. A sub-meter antenna was mounted on the roof of Fimmvörðuskali (a hut on Fimmvörðuháls). The hut's position was determined by differentially processing locational files obtained simultaneously from the nearest known trigonometric point (at the farm between Seljalandsfoss and Heimaland).

Coordinates were logged in UTM, Zone 27, in order to assess the plausibility of the position received when moving from point to point, compared to the published maps (Iceland Geodetic Survey, 1990a; Iceland Geodetic Survey, 1990b). The altitude reference used was height above ellipsoid (HAE), based on the WGS-84 datum. These standards were used during both field seasons on remote and base station receivers, and were checked daily to ensure compliance.

5.2.4 GPS post-processing

At the end of each day, the remote receiver files were downloaded onto a laptop computer which contained the base station files, using the Magellan software MCOMM (Magellan, 1996a). Another Magellan software package, MSTAR (Magellan, 1996b), was then utilized to process the matching files and calculate the differential files. Three files were used for the calculation: the remote file, the base file, and the control point, which was determined from the original differential calculation using the known trigonometric point. The times between the remote file and the base file were matched up and the correction made. The UTM x, y, and z

coordinates were then extracted from the new differential files and matched with the correct radar points.

During the 1999 field season, the base station receiver failed on a number of days, as a result of battery discharge. The GPS data collected with the remote receiver could therefore not be differentially corrected for those days. Consequently, the inclusion of the uncorrected GPS points increases the possible positional uncertainty from 10 m (15 m RMS error) to 100 m with RMS errors of about 60 m. These are maximum values, however. The actual uncertainty for the Eyjafjallajökull dataset is closer to 30 m with RMS errors of about 9 m (***Figure 5.2***). Since the error for the uncorrected z values are much greater than the x and y errors, the radar-defined ice thicknesses were subtracted from the heights of the digitized ice contours to place the basal surface relative to the ice surface and the WGS-84 ellipsoid.

5.3 Data Interpolation

In order to produce a continuous surface from point data, interpolation is required. The method chosen should consider the intended use of the interpolated surface, the need to honor data points, and the necessity of data smoothing. A selection of local estimators was tested and compared. Kriging, a geostatistical method, was chosen because it honors original data points, does not over-smooth sparse data sets, and utilizes local weighting functions. The kriging method has been previously applied to radio echo sounding surveys (Flowers and Clarke, 1999; Knudsen and Hasholt, 1999; Taylor, 1997).

The interpolation was performed in Surfer (Golden, 1999) by combining the radar data with data digitized from map contours. Nunataks were also digitized from maps (Iceland Geodetic Survey, 1990a; Iceland Geodetic Survey, 1990b). Since the radar data are concentrated in the center of the ice cap, it was necessary to estimate ice thicknesses for the periphery, in order to avoid a too rapid thinning of ice towards the glacier edge. Ice thickness was estimated from the ice surface slope, based on the principle of basal shear stress (Paterson, 1994),

$$\tau_b = \rho g h \sin\alpha,$$

Equation 5.1

where

τ_b = basal shear stress (100 kPa)

ρ = density of ice (0.9 g m^{-3})

g = acceleration due to gravity (9.8 m s^{-2})

h = ice thickness (m)

α = ice surface slope.

The assumption of a constant basal shear stress is based on Nye's theory that flowing ice is a perfectly plastic material (Paterson, 1994). The relation implies that ice is thinner on steep surfaces and thicker on surfaces with shallow slopes. The surface slope is determined from a contour map of the ice surface at the main flow-line. The slope is calculated as an average value over a distance which is several times the ice thickness, thus negating the effect of small-scale features.

An initial interpolation of the ice surface, using default point kriging, was used to divide the ice cap into ice drainage basins. Longitudinal flowlines were estimated from each and surface slopes calculated. The resulting ice thicknesses calculated from the shear stress relation and their horizontal positions along the flow line of each drainage basin were added to the dataset to create the final interpolation (***Figure 5.3a, b***).

A comparison between depths estimated by the shear stress equation and measured by radio echo sounding was made where overlap existed. The west flank transect coincided with part of a flowline used for the estimation. It was found that the average root mean square (RMS) error between the calculated depths and measured profiles was 21 m. The maximum RMS error was 46 m or about a 50 % discrepancy. In addition, it is clear from the ice thickness map (***Figure 6.5***) that a portion of the east flank is overestimated by as much as 100 m. This is quite a large margin of error, but the shear stress equation is the best method of estimation available at present.

5.3.1 Choosing the interpolation method

The main assumption inherent in interpolation is spatial autocorrelation; two points close to each other are more likely to have similar values than two points far apart. Thus it is appropriate to use only data points lying within a local neighborhood around the point to be interpolated, instead of using the entire dataset to interpolate each point. Global estimators use all the data points, whereas local estimators utilize only those nearby. Local estimation methods include kriging, nearest neighbor, inverse distance weighting, triangulation, minimum curvature, and spline fitting.

Other considerations which need to be taken into account when assessing an interpolation method bear in mind the use of the final interpolated surface: to what use will the data be applied? If data points need to be honored exactly, an exact interpolator, like point kriging, should be chosen. If there is low confidence in the repeatability of the measurements, it may be necessary to smooth the data. Some interpolation methods are better at reducing the effect of small-scale variablity than others. Other interpolators produce less of a 'bull's eye' effect, and should be selected if this effect needs to be avoided.

The strengths and weaknesses of a selection of the most common local interpolation methods with regard to the present data set are summarized as follows. ***Nearest neighbor*** assigns the value of the nearest data point to each grid node using Thiessen polygons. It is useful for filling gaps in regularly spaced data. The data collected for Eyjafjallajökull are regularly spaced in transects, not a grid. They are concentrated in small areas in comparison to the rest of the massif, so nearest neighbor may not be an appropriate method. ***Inverse distance weighting*** is a weighted average interpolator; the influence of a point declines with distance from a grid node. The bull's eye effect can be reduced by smoothing and the weighting power can be varied. It is desirable to avoid the bull's eye effect in the Eyjafjallajökull dataset so that bed features are not exaggerated. ***Triangulation*** creates Delauney triangles between data points. Values at grid nodes are then

estimated using linear interpolation. Data are closely honored, which is desirable for the present dataset. However, the final surface may look faceted as a result of the triangles. ***Minimum curvature*** aims to fit a surface through all data points without creating any kinks or creases, like "fitting a metal sheet through all data points" (Murray, M., 1999, *pers. comm.*). Data are closely honored. It is a method widely used in the earth sciences. ***Kriging*** is a geostatistical method which explicitly models spatial variation at a range of scales. It can be an exact interpolator and allows spatial trends to be recognized. Kriging is generally recognized as providing the best linear unbiased estimate for sparse, irregularly spaced data.

Figures 5.4 - 5.12 show interpolations of the ice surface of Eyjafjallajökull derived from a variety of interpolation methods. An initial qualitative, visual assessment makes clear that the best interpolations are inverse distance weighting, triangulation, radial basis function, natural neighbor, and point and block kriging. Nearest neighbor creates blocky, regularly spaced contours which bear very little resemblance to the published map (Iceland Geodetic Survey, 1990a; Iceland Geodetic Survey, 1990b) (***Figure 5.13***). Minimum curvature creates a combination of overly smoothed contours in the region of the ice cap and divides many of the features on the western flank into discrete bits. Again this interpolation method bears little resemblance to the published map. The Modified Shepard's method does not link up the digitized contours even though the density of points is high. Blank spaces are left on the interpolated surface where areas between the radar data and digitized contours have not been interpolated. From this initial visual qualitative assessment, the interpolation methods of nearest neighbor, minimum curvature, and Modified Shepard's method are rejected.

The remaining interpolation methods may be further assessed by quantitatively comparing interpolated z values with real z values, both in terms of elevation and position. ***Table 5.1*** compares each method with the measured data points through descriptive statistics. The mean values of the interpolated data sets are well within 100 m of the measured mean, with the exception of triangulation and natural neighbor. These two produce extremely high maximum values which increase the mean and are therefore rejected. Three out of the six interpolation

methods produce a minimum value which is the same as the measured minimum. Inverse distance calculates the most accurate maximum value.

When the maximum values of those interpolation methods which gave reasonable values (inverse distance, radial basis function, point and block kriging) are plotted on a map with the maximum measured value, they all fall on the same position, offset slightly to the northeast of the measured maximum. This is perhaps an artifact of the gridding procedure in the software. However, it is mysterious that so-called exact interpolators do not exactly reproduce either the value or location of the measured maximum.

Perhaps a better way to assess the locational and formational accuracy of an interpolation method is to overlay the digitized outer contours with the interpolated contours and see how they match up. By assessing the contours on a visual, qualitative basis, it is apparent that all the interpolation methods reproduce the digitized contours in a similar manner. ***Figures 5.14 - 5.17*** demonstrate this.

By comparing a variety of interpolation methods it seems clear that, amongst a few, it does not make a huge difference which method is chosen. However, kriging seems to be the most flexible and allows the interpolation to be customized according to expert knowledge of the dataset. Trends can be accounted for and weightings can be adjusted according to confidence in certain data points. The Eyjafjallajökull data are therefore interpolated with point kriging. Block kriging is not necessary because the coarseness of the spacing between data points forces the use of large blocks anyway.

5.3.2 Kriging

Kriging is based on the Theory of Regionalized Variables. Data points are defined as continuous, spatially-dependent, and random. Regionalized Variable Theory assumes that the spatial variation of any variable can be expressed as the sum of three components: deterministic, stochastic, and residual (or structured, random, and noise). This relationship is represented by the equation,

$$Z(x) = m(x) + \varepsilon'(x) + \varepsilon''(x),$$

Equation 5.2

where

Z = a random variable at position x in one, two, or three dimensions

$m(x)$ = structural, deterministic component (mean value in sampling area)

$\varepsilon'(x)$ = random, stochastic component (locally varying, but spatially-dependent)

$\varepsilon''(x)$ = residual, spatially-independent noise component

Regionalized Variable Theory contains an intrinsic hypothesis which states that once the structural component, $m(x)$, of the spatial variation of the variables has been accounted for, then the remaining spatial variation of the variables is solely a function of the distance between them. The intrinsic hypothesis demands that two assumptions be made in order for it to be true. The stationarity of difference assumption states that the average or expected difference between any two points, x and $x+h$ (where h is the distance that separates the two points), is zero. In equation form:

$$E[z(x)-z(x+h)]=0.$$

Equation 5.3

The variance of differences assumption states that the variance of differences between any two points, x and $x+h$, depends only on the distance (h) between them. Mathematically:

$$E[\{z(x)-z(x+h)\}2]=$$
$$E[\{\varepsilon'(x)-\varepsilon'(x+h)\}2]=2\gamma(h)$$

Equation 5.4

where

$\gamma(h)$= semivariance.

If the two assumptions required by the intrinsic hypothesis can be made, then the following equation represents the spatial variation of the regionalized variable,

$$Z(x)=m(x)+\gamma(h)+\varepsilon'',$$

Equation 5.5

where

$\gamma(h) = \varepsilon'$.

However, the intrinsic hypothesis assumptions are not easily made, especially that of stationarity. By definition, a variable is stationary only if there is no significant drift within the sample window (Swan and Sandilands, 1995). Drift describes trend in the local means and variances of the data. The entire method of kriging has been debated, concerning the appropriateness of using a technique that depends on assuming non-drifting data, whereas many earth science data do have trends. Specifically, the calculation of drift from the semivariogram is objectionable. According to the argument, the kriging technique cannot be valid if drift in the data can only be calculated from the range defined by the semivariogram, while the semivariogram can only be created once stationarity (or lack of drift) of data has been assumed. This tautology invalidates the method.

On the other hand, within the window of the sampling area, data that indicate trend over a large area can be relatively homogeneous. Since the assumption of stationarity only applies to the data within the sampling area, the drift can be negligible and assumption of stationarity safely made. The local stationarity assumed by kriging methods is often a viable assumption even in data sets for which global stationarity is clearly inappropriate (Isaaks and Srivastava, 1989).

Drift in the dataset is assessed by variogram modelling. Variograms were created for both the Eyjafjallajökull surface and subsurface datasets and a linear model was fit to each (***Figure 5.18***). Where the model does not fit well is beyond 6 km, meaning that data points separated by 6 km or more will not be considered spatially dependent in the interpolation. The parameters derived from the variograms was used as input for the interpolation gridding procedure.

5.4 Summary

The radar survey at Eyjafjallajökull took place during the summers of 1998-2000. A total of 425 points were collected at the base of Gigjökull, on the east and west flanks, and in the crater. The positions of radar soundings were determined

with a hand-held GPS. Collected waveforms were processed using the methods described in *Chapter 3* and developed in *Chapter 4*. Both corrected and uncorrected GPS positions are included in the dataset. The surface and subsurface maps were interpolated using the point kriging method in Surfer.

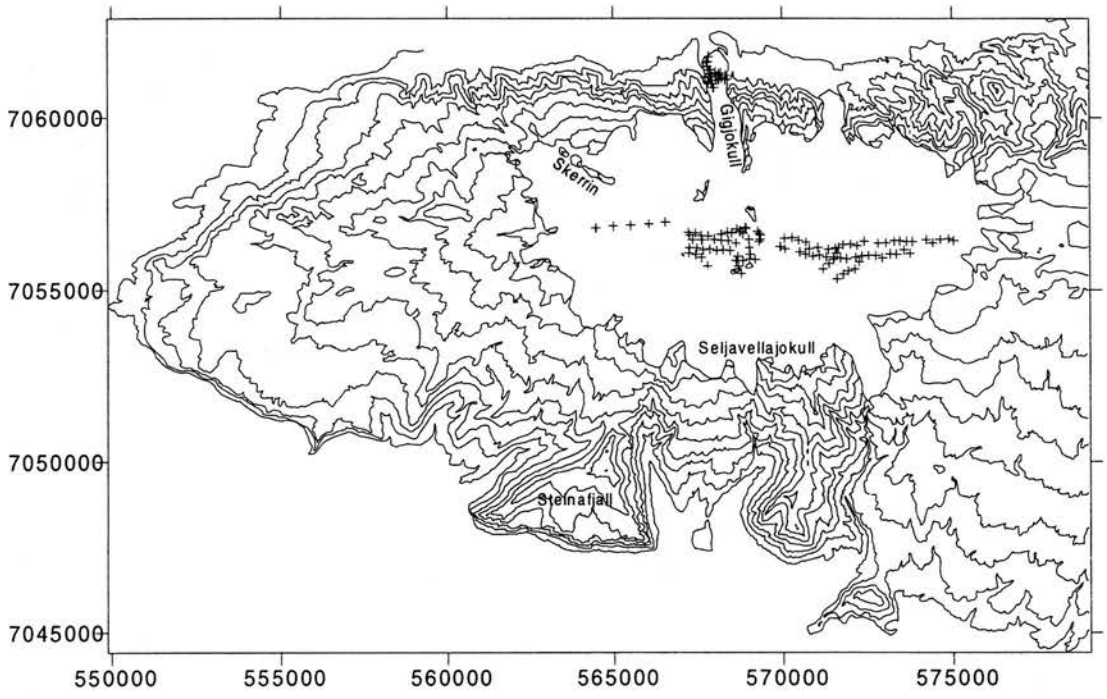

Figure 5.1 Location of radar soundings (crosses) on Eyjafjallajökull.

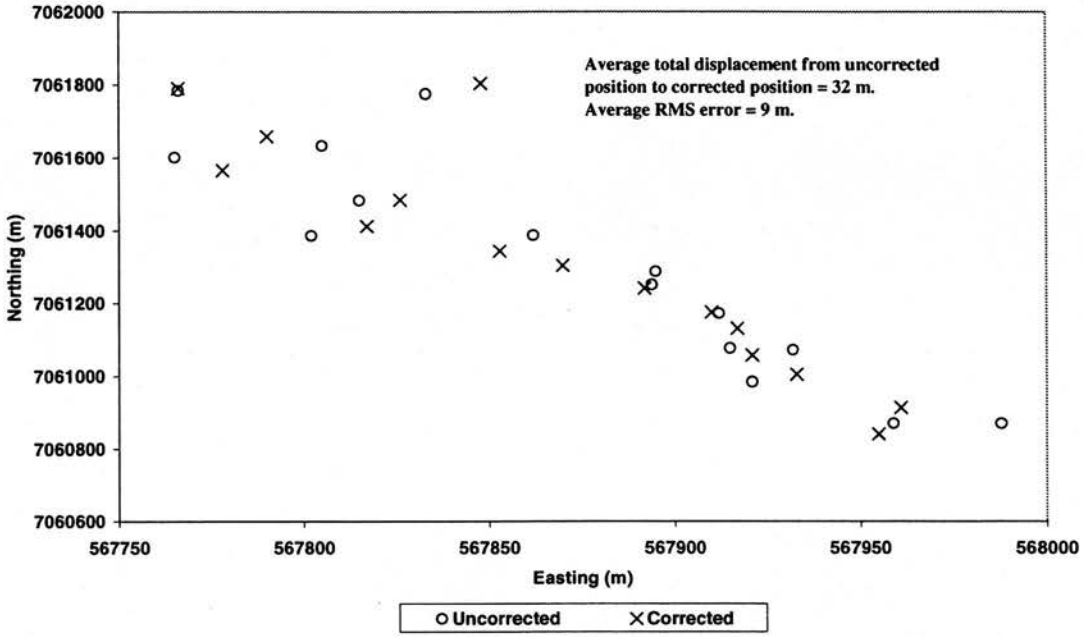

Figure 5.2 Displacement of corrected GPS locations from their uncorrected positions.

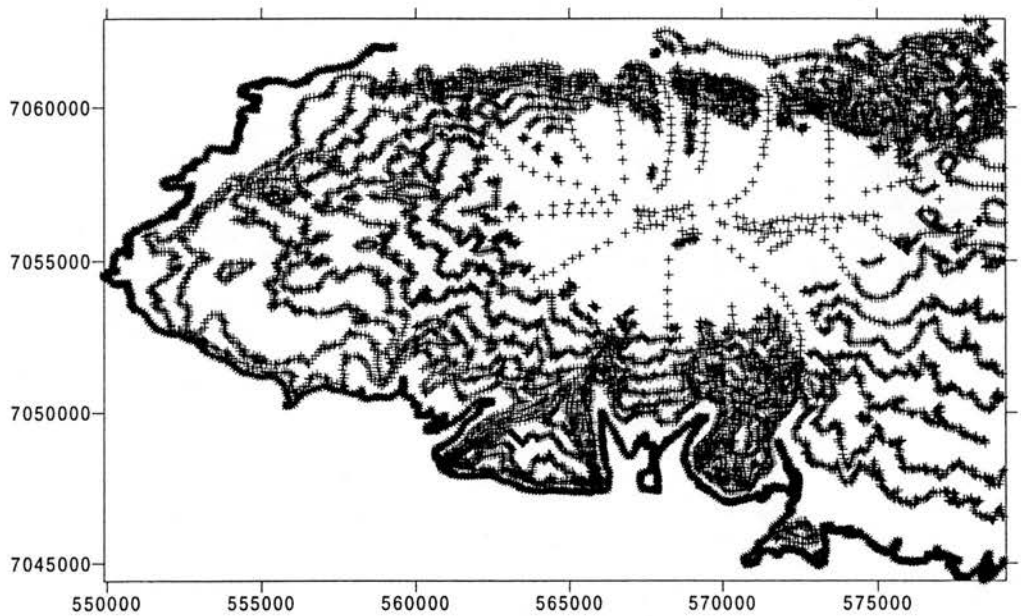

Figure 5.3a All data points used in the *basal* interpolation: radar points, digitized contours and nunataks, and points estimated from the basal shear stress relation.

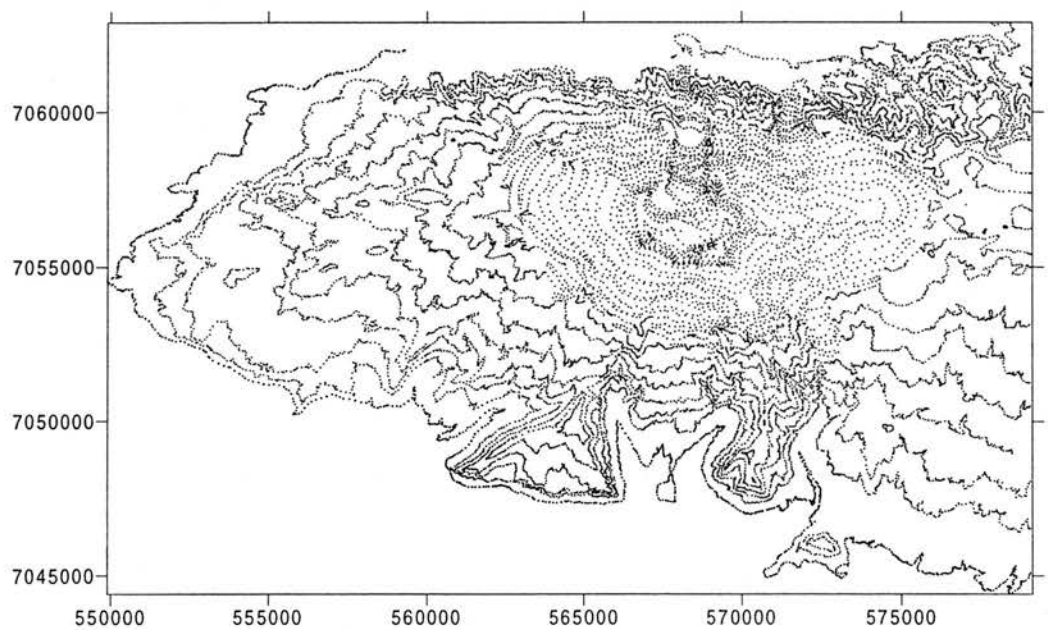

Figure 5.3b All data points used in the *surface* interpolation: radar points, digitized contours (deglaciated and ice) and nunataks.

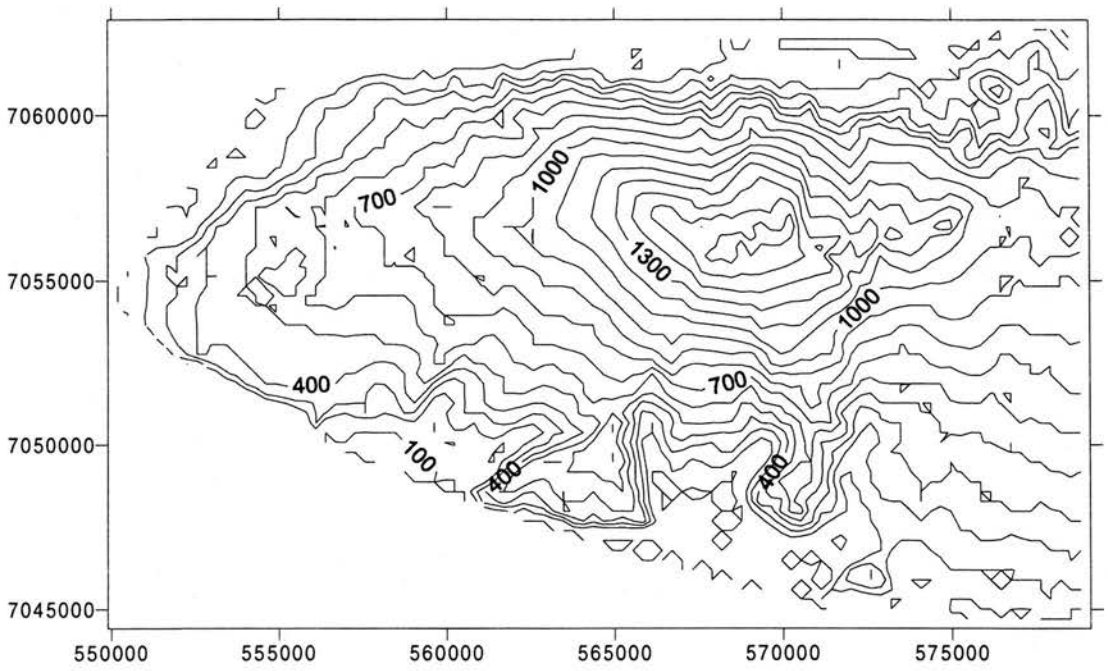

Figure 5.4 Eyjafjöll ice surface contour map interpolated by triangulation method (100 m contour interval).

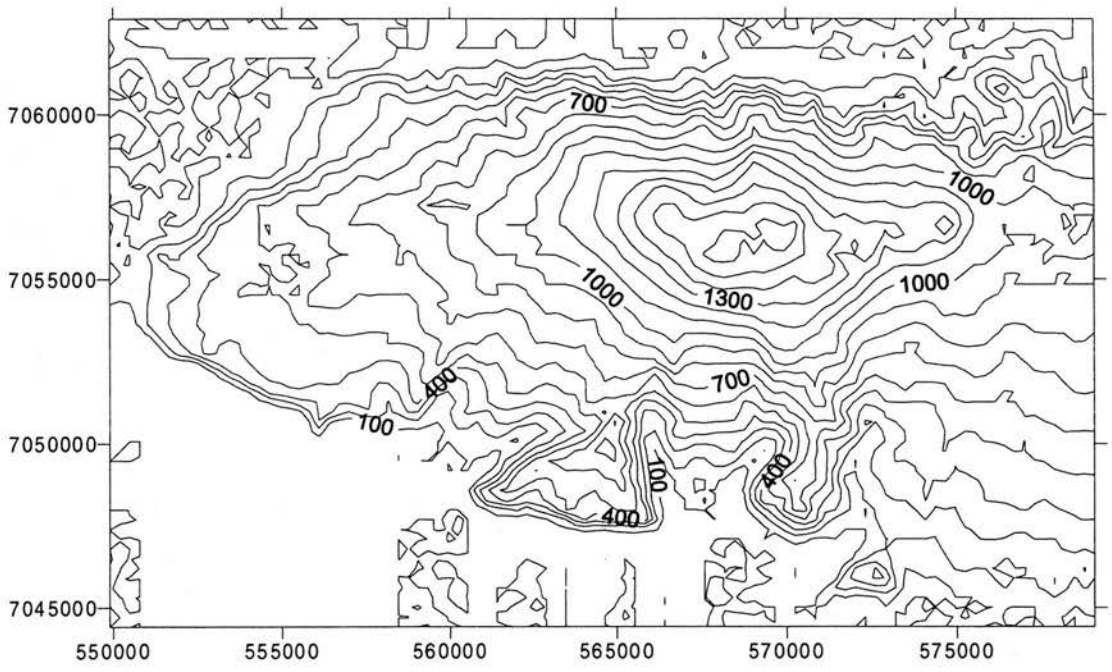

Figure 5.5 Eyjafjöll ice surface contour map interpolated by radial basis function method (100 m contour interval).

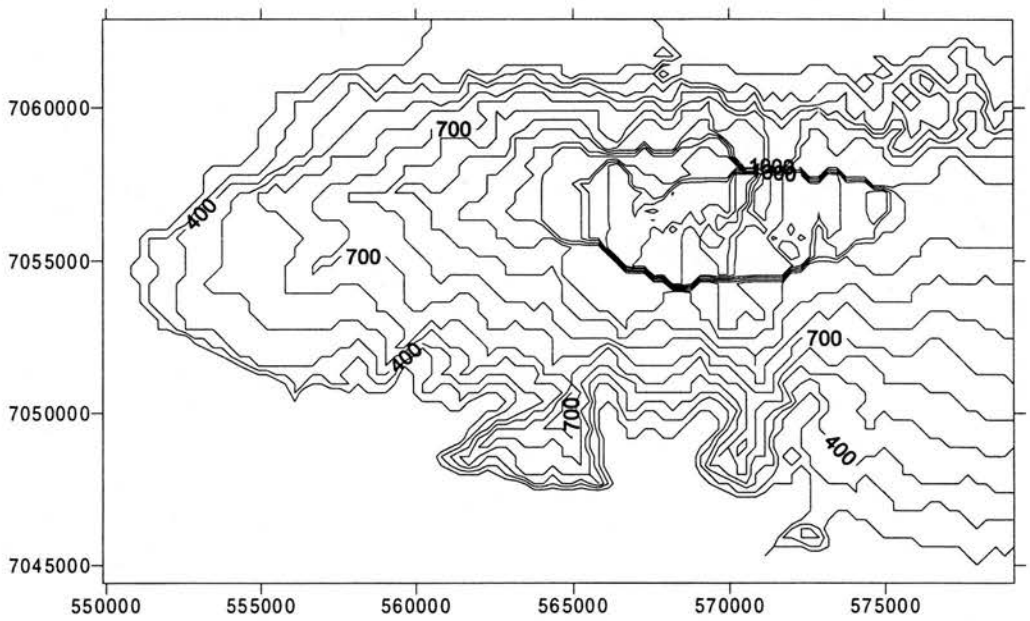

Figure 5.6 Eyjafjöll ice surface contour map interpolated by nearest neighbor function method (100 m contour interval).

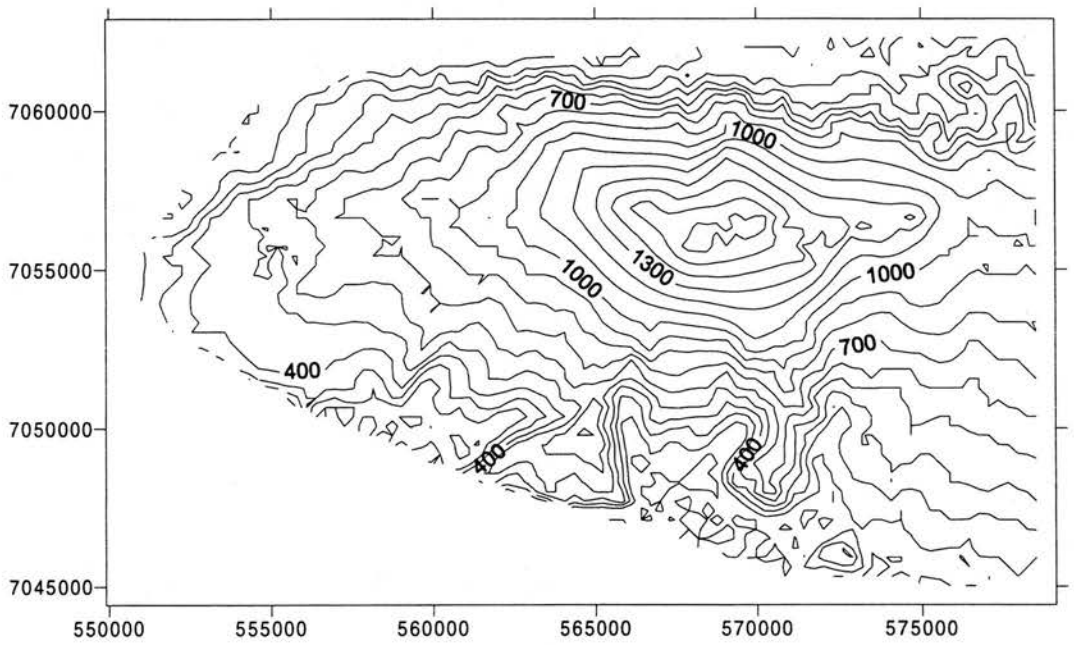

Figure 5.7 Eyjafjöll ice surface contour map interpolated by natural neighbor function method (100 m contour interval).

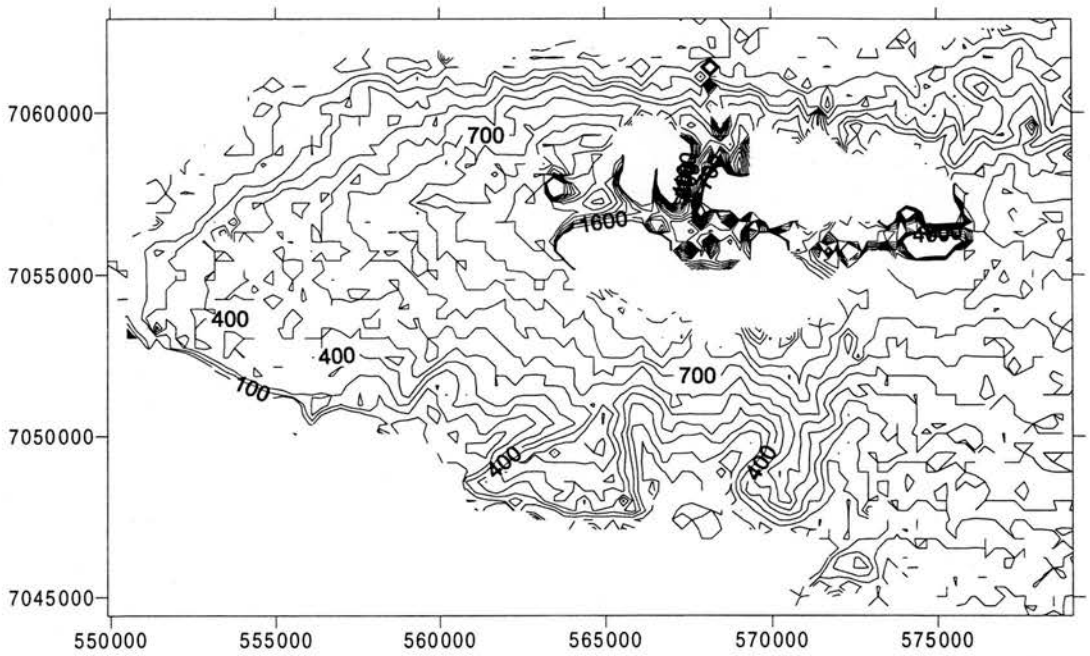

Figure 5.8 Eyjafjöll ice surface contour map interpolated by Modified Shepard's method (100 m contour interval).

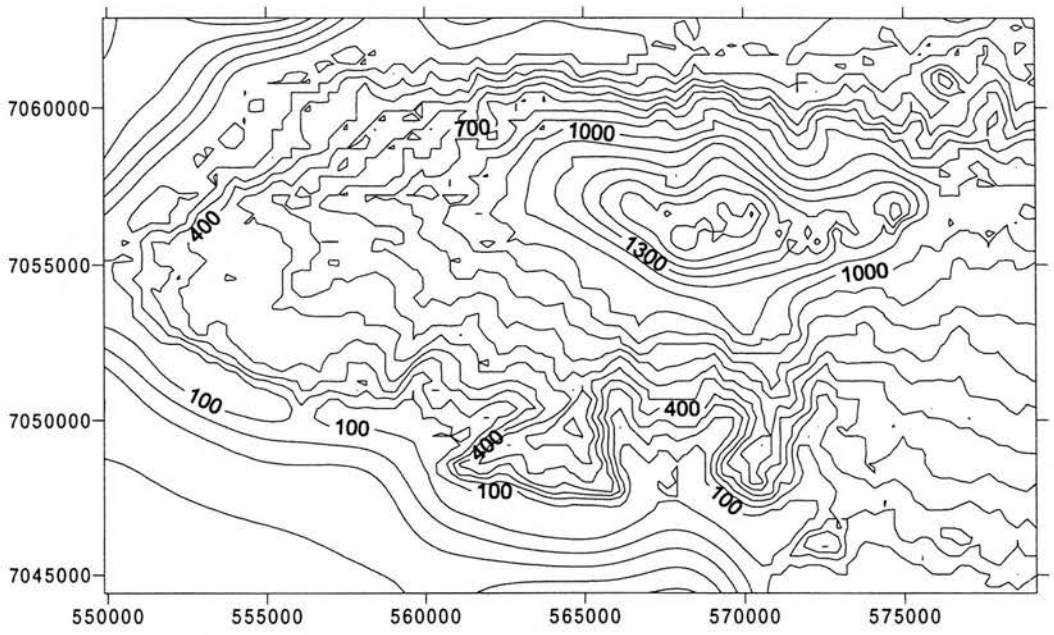

Figure 5.9 Eyjafjöll ice surface contour map interpolated by minimum curvature method (100 m contour interval).

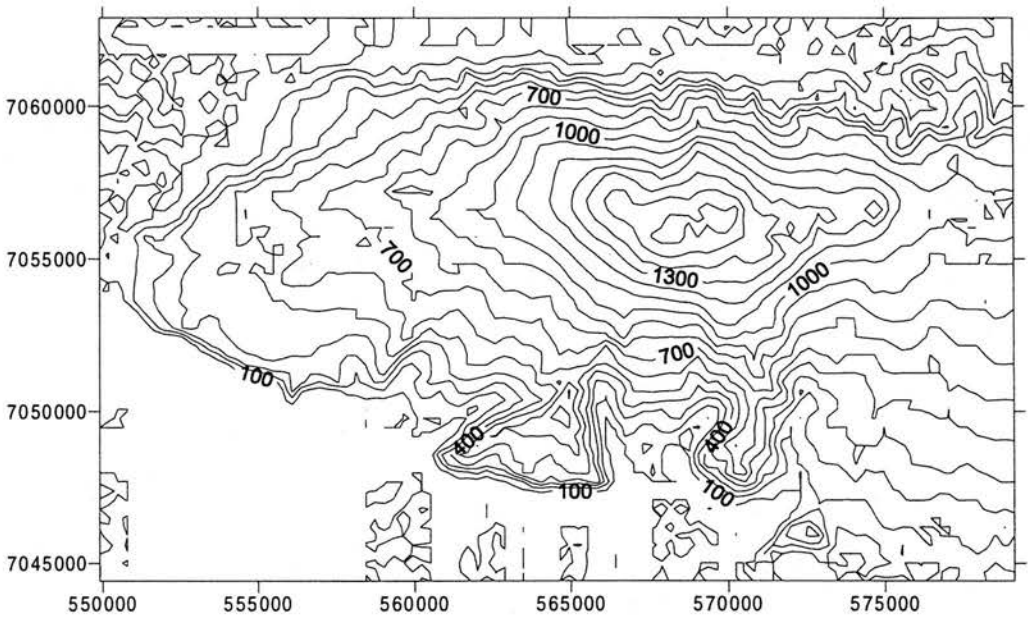

Figure 5.10 Eyjafjöll ice surface contour map interpolated by default linear point kriging method (100 m contour interval).

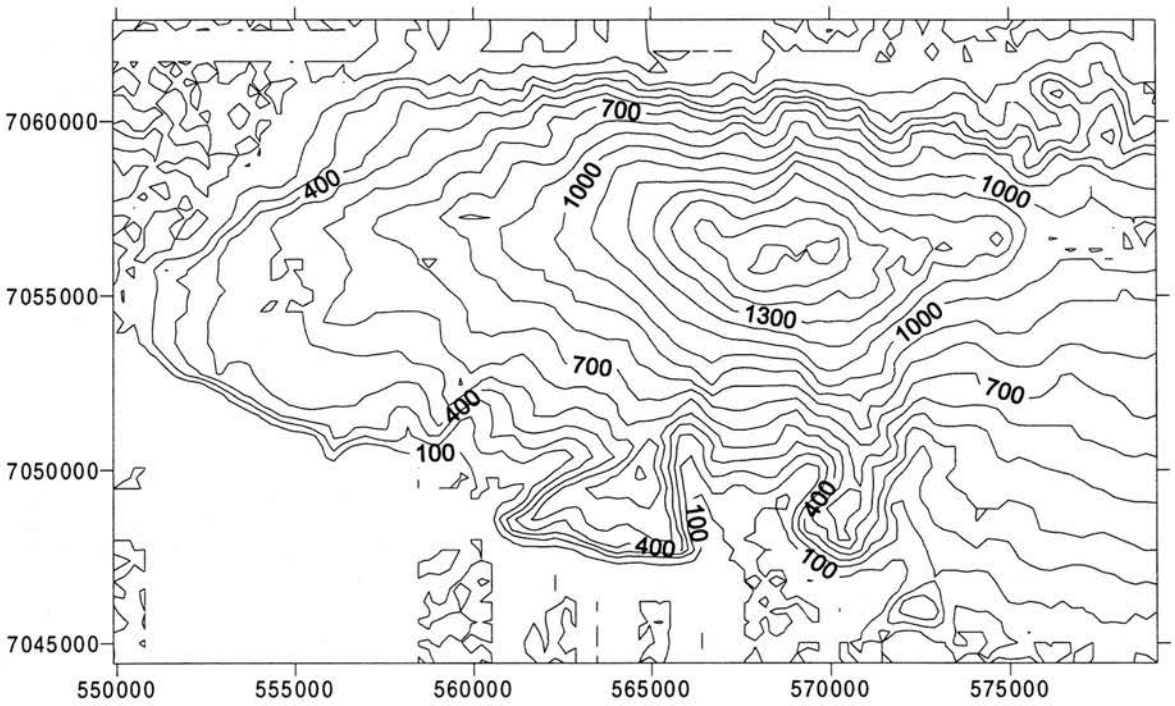

Figure 5.11 Eyjafjöll ice surface contour map interpolated by default linear block kriging method (100 m contour interval).

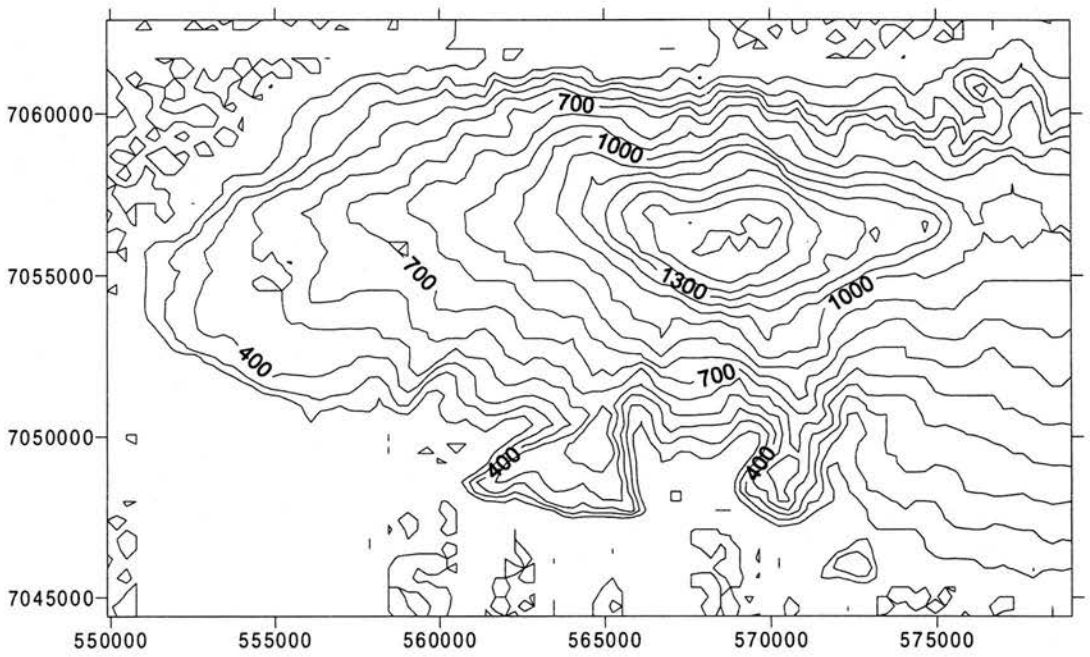

Figure 5.12 Eyjafjöll ice surface contour map interpolated by inverse distance method (100 m contour interval).

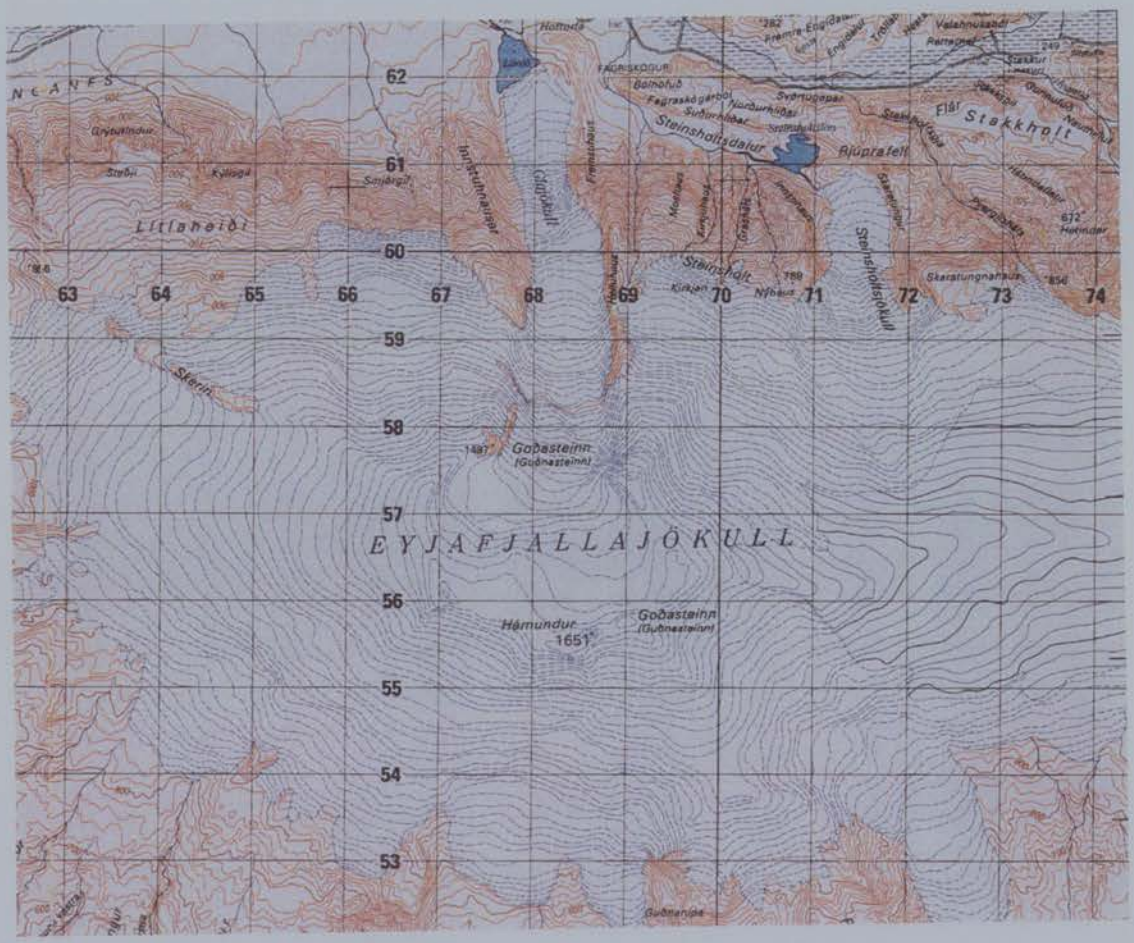

Figure 5.13 Published 1:50,000 map of Eyjafjallajökull (Iceland Geodetic Survey, 1990a).

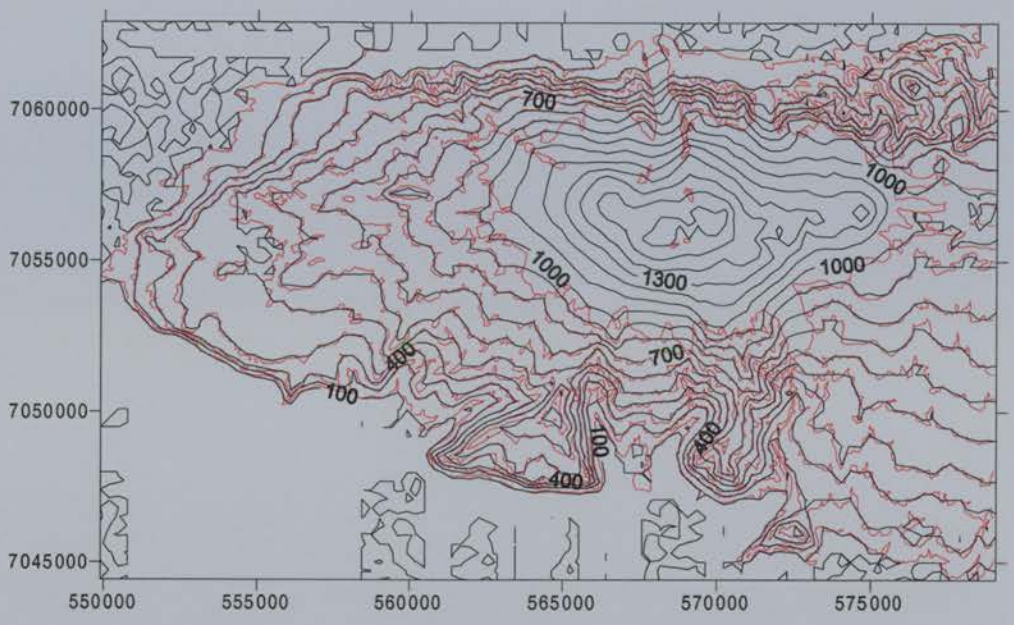

Figure 5.14 Radial basis function interpolation method (black lines) compared to digitized contours (red lines).

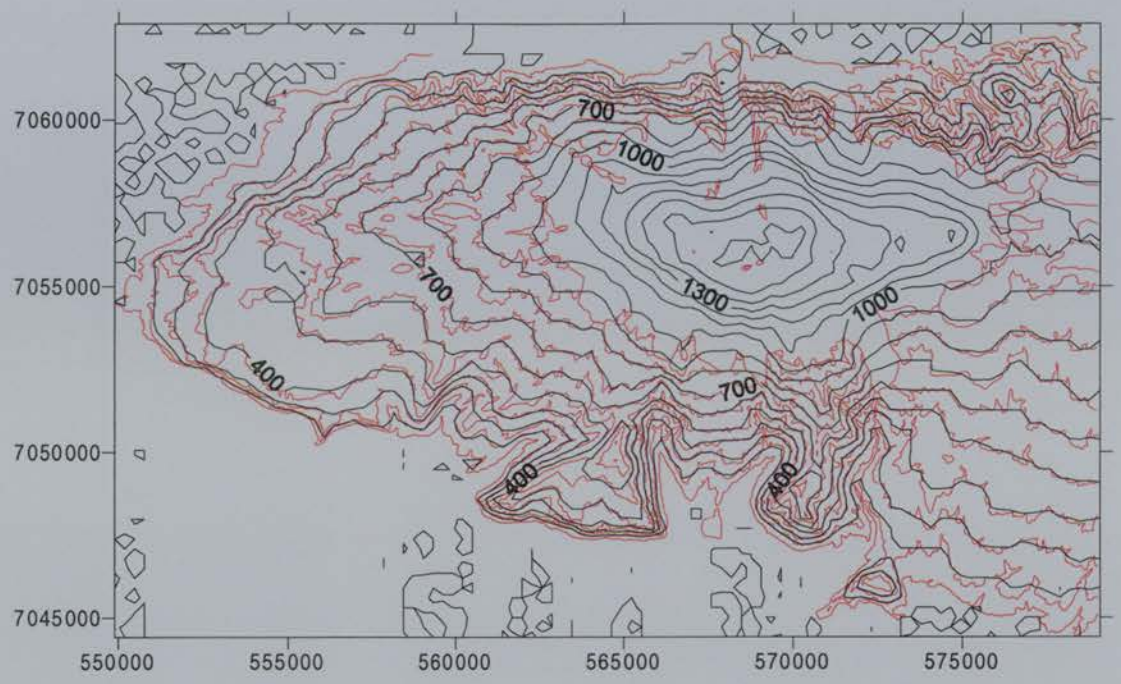

Figure 5.15 Inverse distance interpolation method (black lines) compared to digitized contours (red lines).

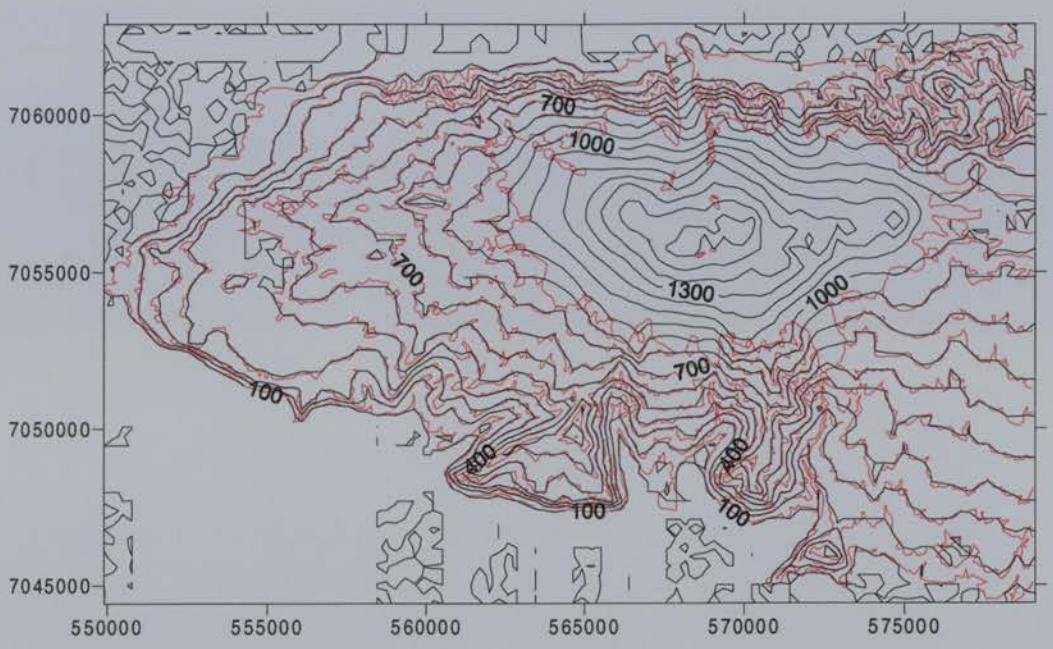

Figure 5.16 Point kriging interpolation method (black lines) compared to digitized contours (red lines).

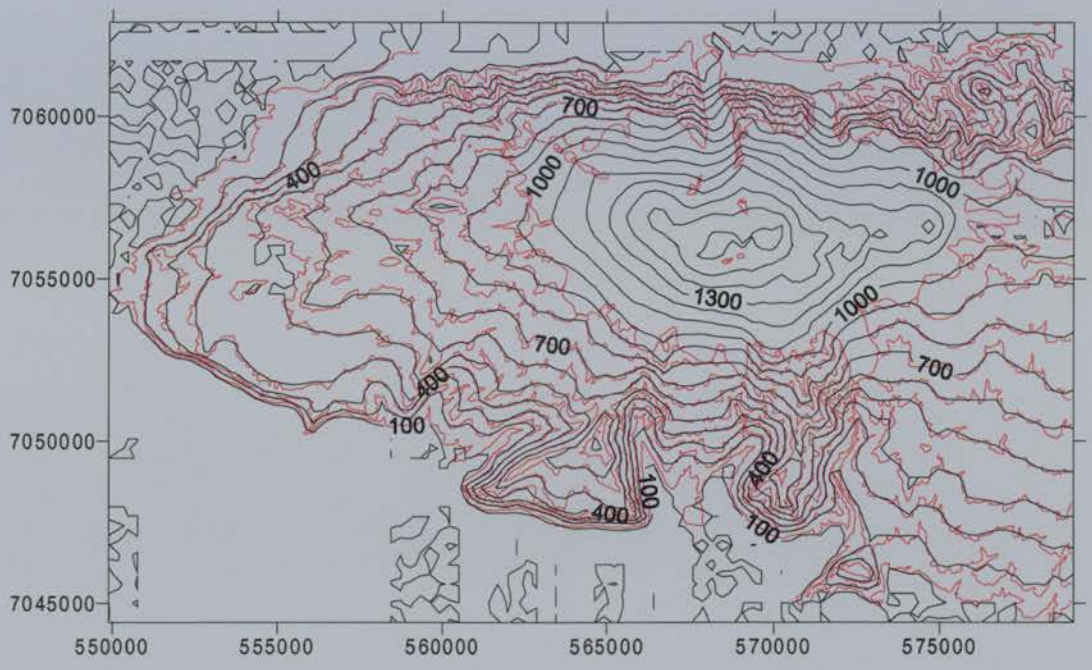

Figure 5.17 Block kriging interpolation method (black lines) compared to digitized contours (red lines).

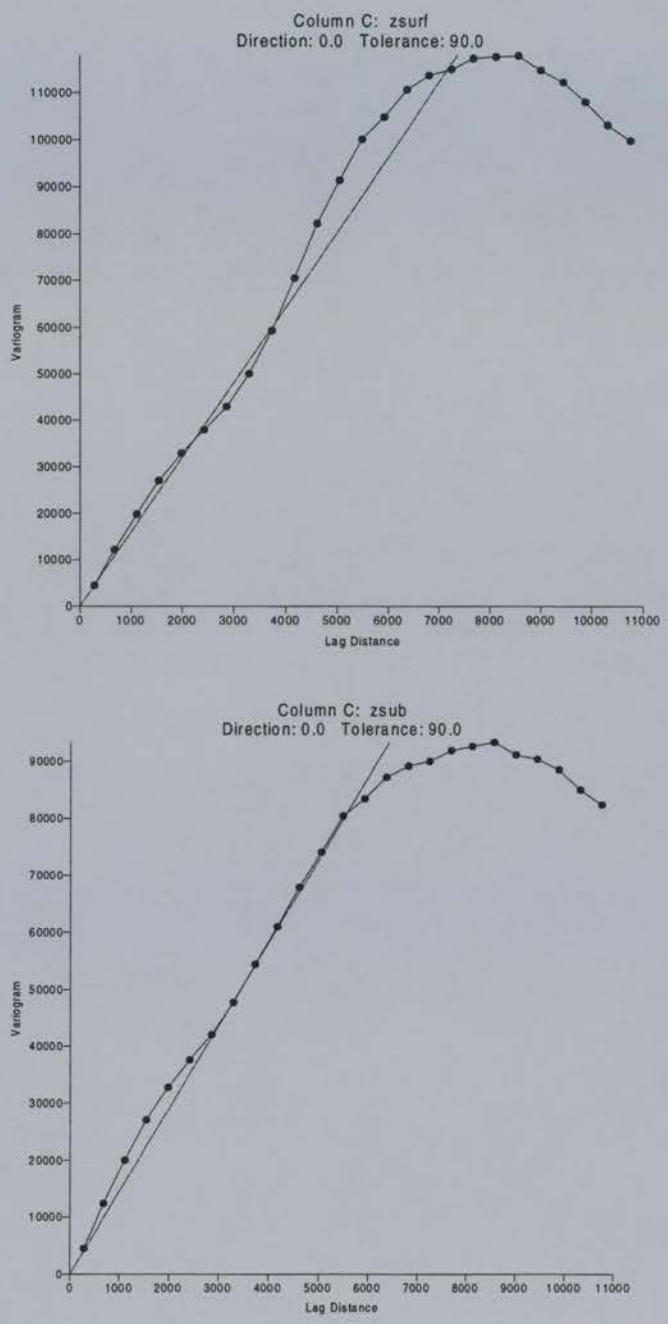

Figure 5.18 Linear variogram models for surface (a) and subsurface (b) datasets. Where model does not fit (beyond 6 km lag distance) the interpolator will not consider data points to be related.

Interpolation method	Mean (m)	Minimum (m)	Maximum (m)	Standard error (m)	Standard deviation (m)	Accept or reject method?
Measured data	**511**	**100**	**1774**	**2**	**282**	
Inverse distance	479	100	1684	5	380	accept
Triangulation	4.53×10^{37}	100	1.70×10^{38}	9.48×10^{35}	7.52×10^{37}	reject
Radial basis function	471	-52	1674	5	396	accept
Natural neighbor	5.35×10^{37}	100	1.70×10^{38}	9.95×10^{35}	7.90×10^{37}	reject
Point kriging	469	-80	1681	5	397	accept
Block kriging	470	-68	1652	5	395	accept

Table 5.1 Descriptive statistics comparing interpolated z values with real z values.

5.5 References

Flowers, G.E., and Clarke, G.K.C., 1999. Surface and bed topography of Trapridge Glacier, Yukon Territory, Canada: digital elevation models and derived hydraulic geometry. Journal of Glaciology, 45(149): 165-174.

Fluke, 1994. FlukeView Software. Fluke Corporation, Almelo, The Netherlands.

Golden, 1999. Surfer Software. Golden Software, Inc., Golden, CO.

Iceland Geodetic Survey, 1990a. Eyjafjallajökull 1:50,000. Defense Mapping Agency Hydrographic/Topographic Center, Washington D.C.

Iceland Geodetic Survey, 1990b. Mýrdalsjökull 1:50,000. Defense Mapping Agency Hydrographic/Topographic Center, Washington D.C.

Isaaks, E.H., and Srivastava, R.M., 1989. *An Introduction to Applied Geostatistics*. Oxford University Press, Oxford, 416 pp.

Knudsen, N.T., and Hasholt, B., 1999. Radio-echo sounding at the Mittivakkat Gletscher, Southeast Greenland. Arctic, Antarctic, and Alpine Research, 31(3): 321-328.

Magellan, 1996a. MCOMM Software. Magellan Systems Corporation, San Dimas, CA.

Magellan, 1996b. MSTAR Software. Magellan Systems Corporation, San Dimas, CA.

Paterson, W.S.B., 1994. *The Physics of Glaciers*. Pergamon, 480 pp.

Swan, A.R.H., and Sandilands, M., 1995. *Introduction to Geological Data Analysis*. Blackwell Science Ltd., Oxford, 446 pp.

Taylor, F.M., 1997. Interpolation of the surface and bed topography of an Iceland glacier: using GIS, GPS, and radio-echo sounding. Unpublished MSc Thesis, University of Edinburgh, Department of Geography.

Chapter 6: Results

6.1 Introduction

This chapter presents the results of the radio echo sounding survey. Salient features of the maps are described.

6.2 Results

The resulting surface and subsurface maps of Eyjafjallajökull are shown in ***Figures 6.1*** and ***6.2***. A cross-section of the ice cap is given in ***Figure 6.3***.

Features produced by the interpolation have been verified observationally (lettered locations in ***Figure 6.4*** (Landmælingar, 1994)). The radial ridge Skerin (A), striking NW from the crater rim is successfully reproduced and Gigjökull's icefall (B) is clearly delineated. However, some smoothing of the topography is unavoidable and the areas where the data are dense show more detail.

The bed of the summit crater descends to 1200 meters and contains a deep trough (C) striking north-south in the western half of the crater. This trough forms the main flowline in the crater, where ice should continue excavating in the future. The bed tilts steeply north towards the rim breach at the top of the Gigjökull icefall. The mounded, elongate feature in the center of the crater (D), slightly visible on the ice surface, is possibly the remnant of a vent from the last eruption. The long axis of this feature strikes SW/NE, it is between 53 and 60 m high, and has a volume of about 0.02 km^3. Radiating out from the summit are ridges, of which Skerin is one, which reflect the magmatic stress regime. Between these are depressions, eroded by ice and meltwater. The west flank of the volcano is steeper, shorter, and rises more continuously from the ice edge to the crater rim than does the east flank. As indicated by the nunatak (E) at 1200 meters, the east flank is characterized by parasitic eruptions, forming cones.

Figure 6.5 is an isopach map of Eyjafjallajökull, with contours of equal ice thickness. The map is calculated as the difference between the surface and subsurface grids of Eyjafjallajökull. The area of greatest detail is where the radar data were collected. The thickest ice is in the crater and on the east and west flanks. There is also an overdeepening at the base of Gigjökull's icefall.

6.3 Summary

The main features revealed by the radio echo sounding survey of Eyjafjallajökull are:

- a deep (>200 m ice thickness) N-S striking trough in the crater which constitutes the main flow line of ice towards the northern rim breach
- an elongate hump in the center of the crater which could be a remnant vent cone
- possible parasitic craters on the east flank
- an overdeepening at the base of Gigjökull's icefall.

These features are analyzed in *Chapter 7*.

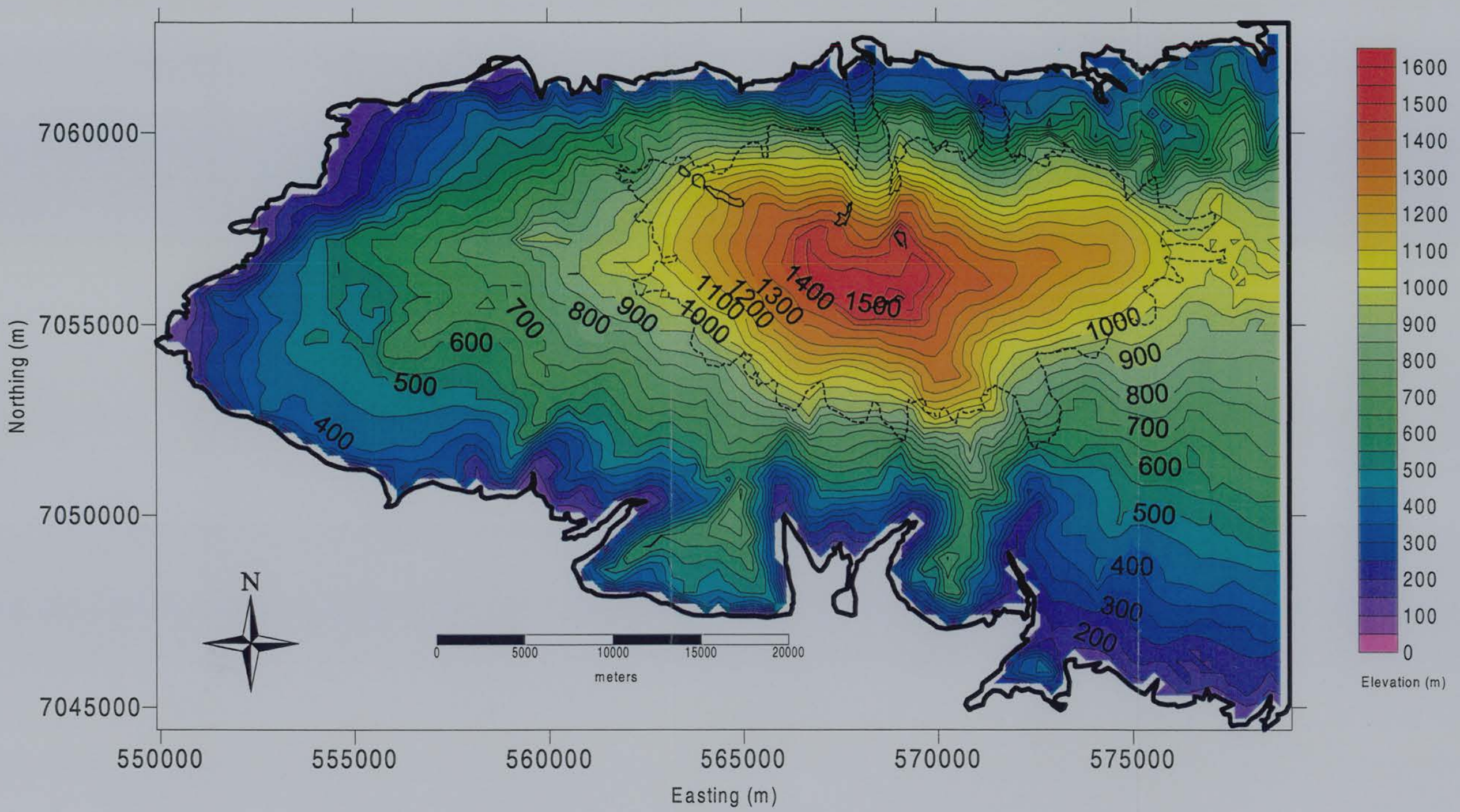

Figure 6.1 Interpolated contour map of the ice surface of Eyjafjallajökull and ice-free flanks of Eyjafjöll. Dashed line is approximate ice edge. Nunataks are outlined in black. Universal Transverse Mercator (UTM) projection, Zone 27.

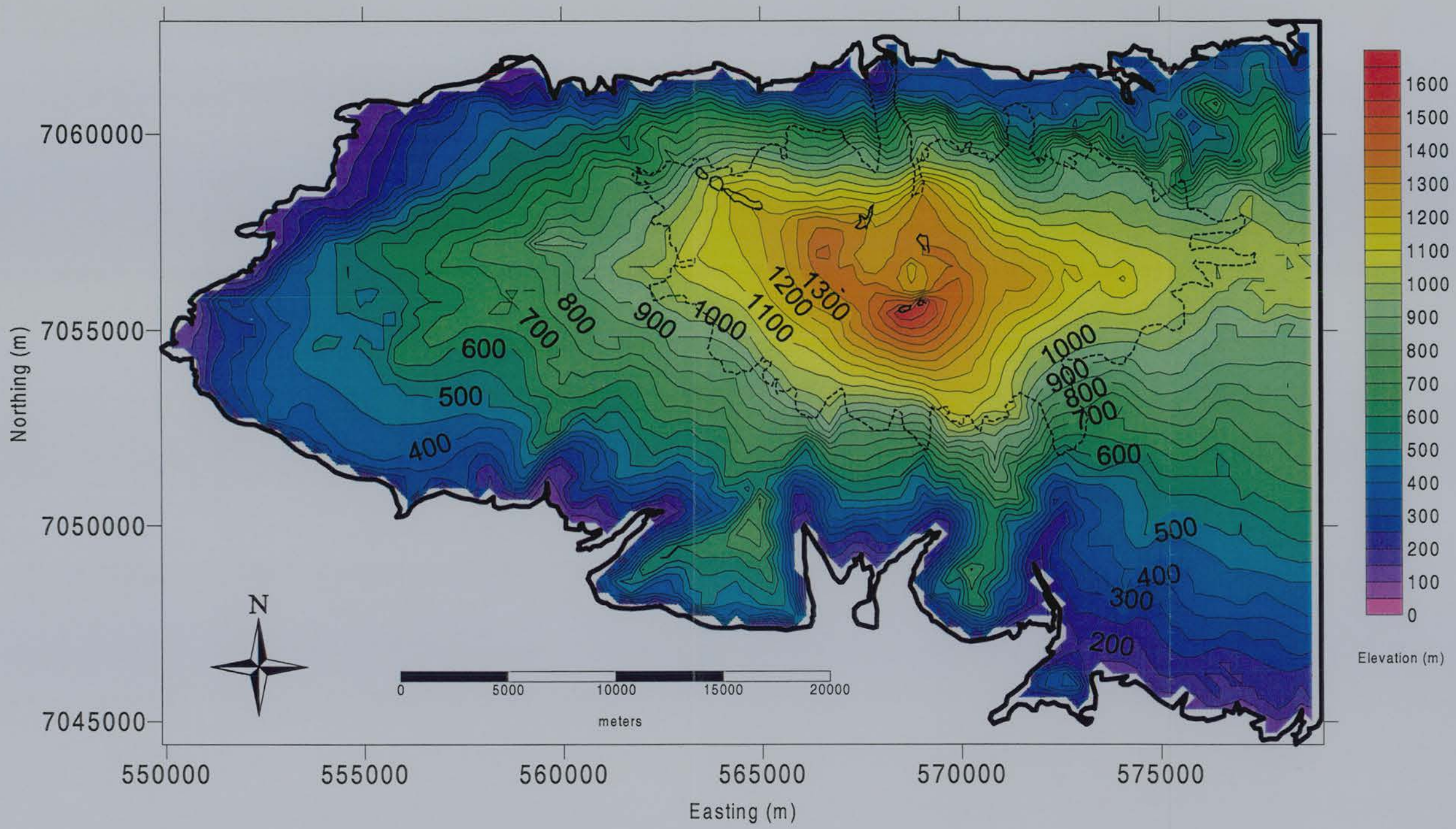

Figure 6.2 Interpolated contour map of the sub-ice surface of Eyjafjallajökull and ice-free flanks of Eyjafjöll. Dashed line is approximate ice edge. Nunataks are outlined in black. Universal Transverse Mercator (UTM) projection, Zone 27.

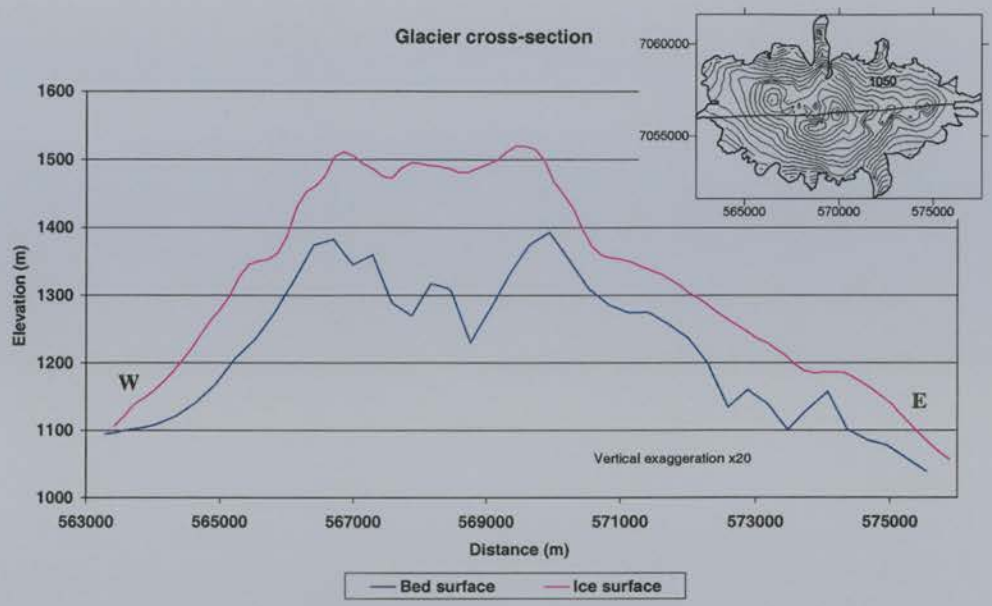

Figure 6.3 E-W cross-section of Eyjafjöll surface topography.

Figure 6.4a Aerial photo of summit crater of Eyjafjallajökull. Letters indicate features evident in surface and subglacial maps. B) Gigjökull icefall, C) deep trough which constitutes main ice flow-line in crater, D) elongate hump which may be remnant of former vent cone.

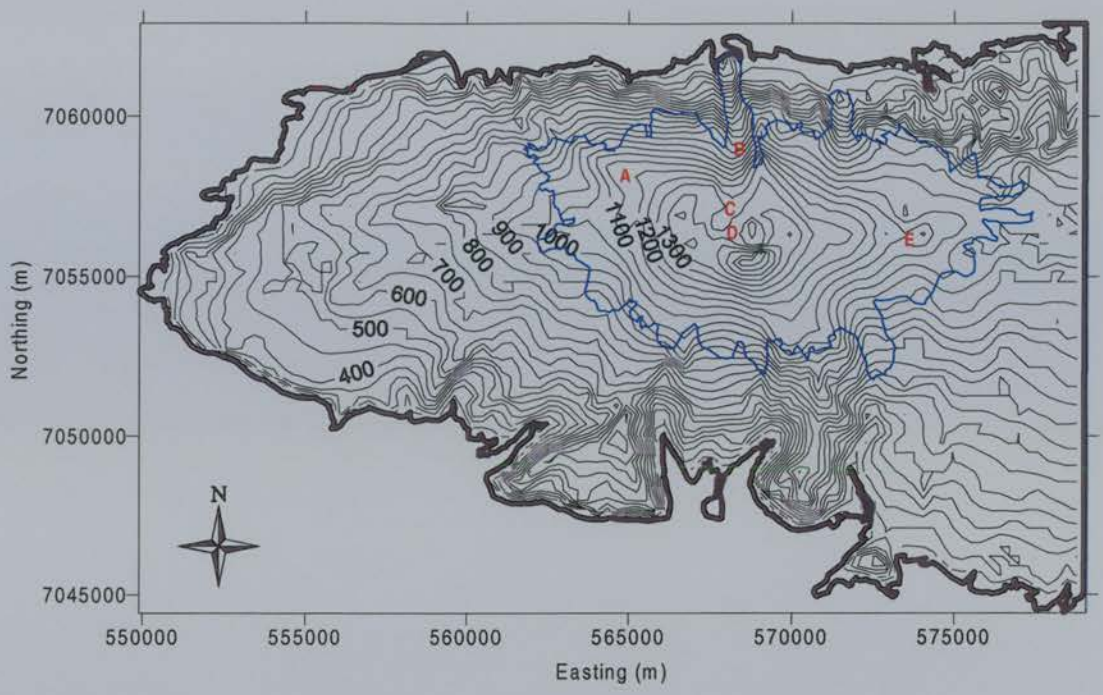

Figure 6.4b Subsurface map of Eyjafjallajökull with letters indicating bed features: a) Skerin, radial ridge, b) Gigjökull icefall, c) deep trough which constitutes main ice flow-line in crater, d) elongate hump which may be remnant of former vent cone, e) parasitic cone on flank.

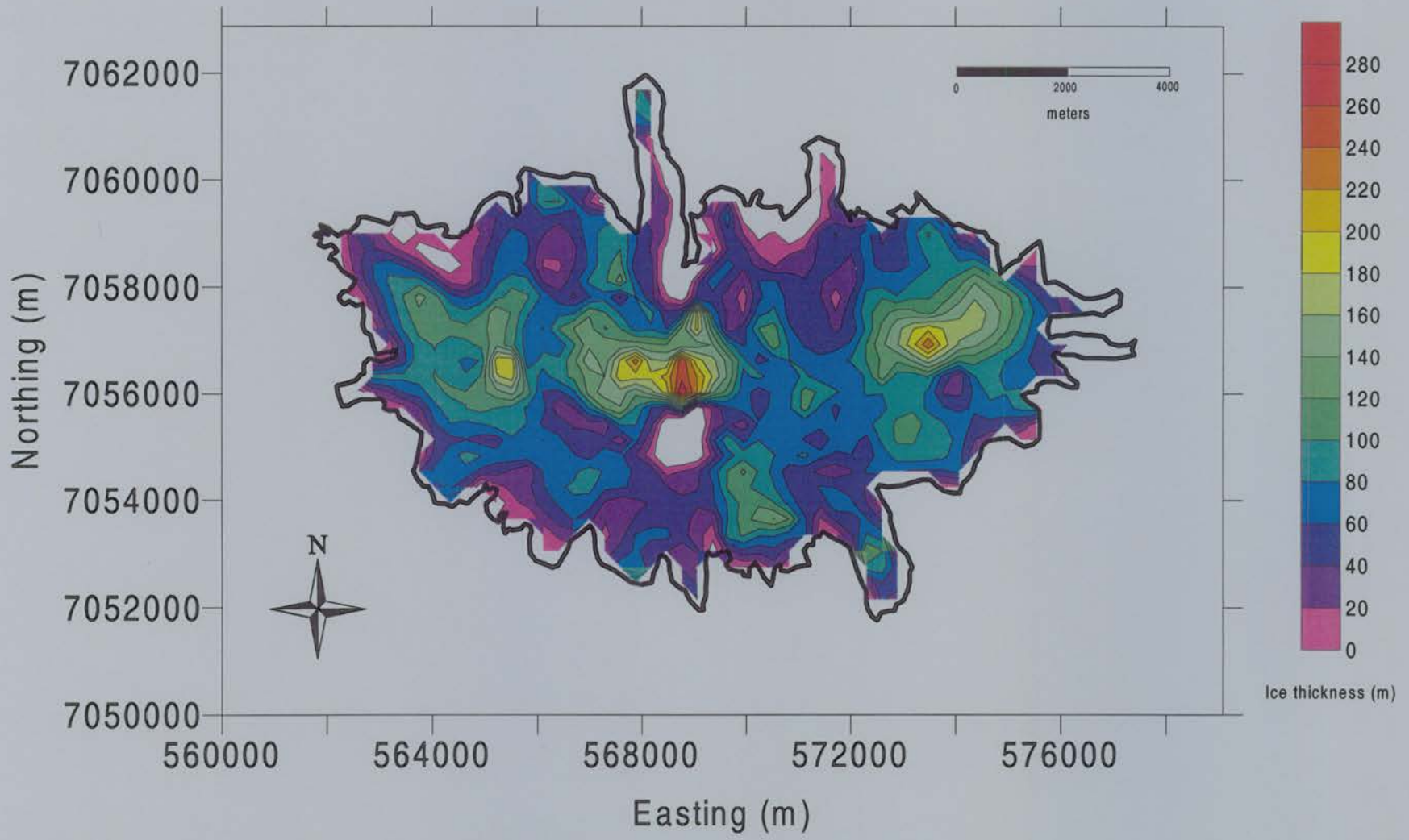

Figure 6.5 Ice thickness isopach map of Eyjafjallajökull.

6.4 References

Landmælingar, 1994. Eyjafjallajökull aerial photo No. 13242 152,82. Landmælingar Íslands, Reykjavík.

Chapter 7: Discussion

7.1 Introduction

In order to reach a greater understanding of the Eyjafjallajökull glaciovolcanic system, it is necessary to become familiar with the processes and landforms associated with subglacial volcanism. These are key to developing insight into the evolutionary dynamics of such a system. This chapter provides the necessary description of the processes and landform products of subglacial volcanism. Volcanic landforms previously identified on the deglaciated sections of Eyjafjöll are described and their morphology interpreted in order to ascertain the conditions in which they were emplaced. The past eruptive environment of Eyjafjallajökull is then assessed.

Many of the properties which constitute subglacial eruptive environments are glacier characteristics measured by the radar survey. The hydrological, thermal, and geometrical structure of the ice cap suggest how future eruptions might proceed. The basal topography indicates meltwater and lava escape routes. Ice structure, thickness, hydraulics, and topography are quantified and combined to characterize the present eruptive environment of Eyjafjallajökull. The implications for the continued evolution of and interaction between volcano and glacier are analyzed. Hazards which could arise from a future subglacial eruption in such an environment are also discussed.

From this foundation, the glaciological implications arising from volcanigenic ice disruption at Eyjafjallajökull are considered. Specifically, the anomalous fluctuations of Gigjökull relative to the rest of the ice cap are explored. Lastly, wider implications of the study are discussed through an examination of the relevance of glaciovolcanic systems as climate change proxies.

7.2 Processes of volcanigenic ice disruption

Glacier ice is disrupted by numerous mechanisms during subglacial eruptions. Disruption interrupts the glaciological state of a glaciovolcanic system and is a significant control on the system dynamics when compared to exogenic influences like climate. The processes explain how ice disruption occurs at a typical site like Eyjafjallajökull. First-hand observations of subglacial eruptions provide evidence.

7.2.1 Ice melt

Most historic observations of subglacial eruptions report that the interaction between ice and lava is dominated by the presence of meltwater. The processes by which meltwater is produced, transported, and lost from a glaciovolcanic system have implications for volcanic landform development and the subsequent interpretation of these landforms.

7.2.1.1 Meltwater production

When magma erupts under ice, the heat causes ***basal melting*** (Major and Newhall, 1989). Meltwater ponds above the vent or drains away, depending on the ice properties. The excavation of ice from a vent by melting causes subsidence of overlying ice. The influx of ice toward the active vent provides a continuous source of ice to be converted into meltwater (Trabant *et al.*, 1994). An investigation of the thermal processes of heat transfer from magma to ice by Allen (1980) concluded that heat from cooling magma is more than sufficient to melt the volume of ice displaced by the extruded magma. As a single pillow of lava cools and solidifies, the released heat can melt approximately four times its own volume of ice (Allen, 1980). Sæmundsson (1979) writes that cooling molten basalt can melt ten times its volume of ice. If this is the case, an average Icelandic fissure eruption is capable of melting up to 1 km^3 of ice within a few days (Sæmundsson, 1979).

Meltwater is also produced when lava extrudes onto a glacier surface. While flowing downslope, some ice melts through heat transfer. ***Lava extrusion*** produces a smaller volume of meltwater than basal melting. Quenched skin forms on the lava at the ice contact, insulating the ice from the lava's heat. The solidifying outer rind on the lava flow slows the rate of heat transfer, causing the lava to advance more quickly than the ice can melt (Lescinsky and Sisson, 1998).

A small volume of ice may also be melted by ***deposition of hot pyroclasts*** ejected from an active vent. Ejecta coarser than about 5mm will melt snow; fine-grained tephra or ash will cause no discernable melting (Trabant *et al.*, 1994).

These three mechanisms of meltwater production (basal melting being the most effective) can remove an enormous quantity of ice during a subglacial eruption. During the 13 day eruption of Gjálp at Vatnajökull in 1996, 3 km^3 of ice was melted and an additional 1.2 km^3 melted in the following three months (Guðmundsson *et al.*, 1997). The 1966 eruption of Redoubt Volcano in Alaska melted approximately 0.13 km^3 of ice from Drift Glacier in three months (Trabant *et al.*, 1994). An estimated 0.07 km^3 of ice over a period of two months was melted during the 1983 eruption of Mount Veniaminof (Yount *et al.*, 1985).

7.2.1.2 Meltwater movement and loss

Much of the meltwater produced at an eruptive vent drains away through subglacial passages. Water typically takes advantage of the pre-existing subglacial drainage system and travels freely down slope under the influence of gravity (if unpressurized) (Lescinsky and Fink, 2000). ***Drainage through subglacial passages*** was described by Yount *et al.* (1985), who observed a subglacial tunnel in the confining ice wall of a meltwater lake above an erupting vent which indicated drainage along the caldera floor. Another tunnel was observed to drain from the lake toward a breach in the caldera wall (Yount *et al.*, 1985).

Meltwater also drains along the margins of valley glaciers and over the glacier surface (Loughlin, 1995). Depending on the subglacial surface, meltwater

may also escape as sheet flow (Smellie and Skilling, 1994) or percolate into porous volcanic strata (Yount *et al.*, 1985).

Draining meltwater may be temporarily dammed. Flow blockage can occur on topographical benches on the bedrock surface and may be caused by collapse of ice blocks into drainage channels. Lava flowing in subglacial tunnels or trenches newly eroded by meltwater may undercut the confining ice walls, causing collapse. Meandering lobes of lava can also block flow. Hydrostatic pressure will eventually cause a blockage to fail, allowing meltwater to burst forth in pulses or surges. Trabant *et al.* (1994) observed meltwater blockage in incised channels by slumping of glacier walls and deposition of ice talus.

Meltwater may also be blocked at the source. If the ice surrounding an active vent is relatively impermeable, the glacier confines the meltwater, causing it to pond *in situ*. Meltwater accumulates until a permeable ice layer is reached, through which water will then drain. Alternatively, water may accumulate in a sufficient volume to float a glacier, wherein ponded meltwater will be quickly released at the base. Catastrophic drainage only occurs if large amounts of water are released quickly.

An additional source of ice and meltwater loss is through evaporation and sublimation, processes which occur close to the active vent. When hot lava comes into direct contact with ice, phreatic (steam) explosions take place. Ice is then lost to the atmosphere by sublimation. This process was observed by both Vinogradov and Murav'ev (1988) and Yount *et al.* (1985). Water may also evaporate from lava-warmed lakes formed above active vents (Yount *et al.*, 1985).

7.2.2 Ice erosion

During subglacial eruptions, disruption of ice can occur by other processes than those associated with melting. Eruption-triggered avalanches, pyroclastic flows, and meltwater itself can directly erode and remove glacier ice.

7.2.2.1 Mechanical

Trabant *et al.* (1994) observed that the largest volume of ice removed from Drift Glacier was not melted in place or released as subglacially or englacially stored meltwater. Instead, most of the ice was mechanically entrained by avalanches caused by pyroclastic flows. They noted that the process was most effective on the rough, highly crevassed surface (an icefall) over which the avalanches advanced. In essence, the ice was quarried. Enormous (house-sized) ice blocks were removed from Vatnajökull during the 1996 Gjálp eruption and deposited on the sandur plain (Guðmundsson *et al.*, 1997).

7.2.2.2 Thermal

Ice can be thermally eroded by meltwater friction (Lescinsky and Fink, 2000) and by hot lahars. Warm meltwater flowing down steep slopes in existing subglacial or englacial passages can rapidly enlarge tunnels as well as incise trenches through ice down to bedrock (Lescinsky and Fink, 2000). Meltwater released by lava extrusion onto ice will flow downslope of advancing lava, incising trenches down to the bed (Lescinsky and Sisson, 1998). Vinogradov and Murav'ev (1988) observed hot lahars cutting channels through ice to bedrock. Flowing pyroclastic debris or blasts of hot gases may also cause scouring and melting (Major and Newhall, 1989).

7.3 Landform products of subglacial volcanism

Many of the subglacial eruption processes described above have taken place at Eyjafjöll. The evidence is found in the volcanic landforms preserved on the volcano. These landforms tell the story of the main eruptive processes which have occurred and in which eruptive environment they took place. The history of Eyjafjallajökull is inferred from this evidence. The following sections describe

typical landforms produced by subglacial eruption processes and interpret their origins. Then, the landforms found at Eyjafjöll in particular are introduced.

7.3.1 Volcanic landforms

The morphology of volcanic features is a product of environment at the time of eruption. Volcanic products emplaced in a subaerial environment are distinguishable from those erupted in a subglacial environment.

The two main eruptive types are fissure and shield eruptions (Einarsson, 1994). Subaerially-erupted fissures form strings of cinder and spatter cones. Subglacially-erupted fissures form tindars: long, steep-sided ridges composed of materials which have interacted with water (Smellie, 2000). Shield, or central vent, eruptions in subaerial environments form dome-shaped features with low-angled slopes. Shield eruptions in subglacial environments form tuyas: flat-topped, steep-sided table mountains (Smellie, 2000).

Tuyas are highly distinctive subglacial volcanic deposits. Classic tuyas in Iceland are monogenetic, but they also occur as recognizable features on polygenetic volcanoes like Eyjafjöll. Tuya formation begins with magma effusion beneath ice. Heat from magma melts ice and pillow lavas extrude into meltwater. The heat melts a vault above the vent and surrounding ice confines the water in an englacial pond. Continued effusion of magma into the lake creates hyaloclastite, a deposit of fine, glassy debris formed by the quenching of magma by meltwater. If an eruption progresses far enough to melt all of the overlying ice, it becomes explosive, depositing hyalotuff, a volcaniclastic sediment, on the hyaloclastite layer. If an eruption then breaks through the water surface, the formation is capped by subaerial lava flows (Jones, 1969; Sigurðsson, 2000; Smellie and Skilling, 1994). The lithologic assemblage of pillow lavas, hyaloclastite, hyalotuff, and capping lavas which composes a tuya is known as the hyaloclastite formation (previously 'palagonite tuff' or the Icelandic 'möberg' (Loughlin, 1995)).

Tuyas indicate the previous height of the ice sheet under which they were formed. The contact between the capping lava and the underlying deposits give a

rough estimate of ice thickness at the time of eruption (Smellie, 2000; Smellie and Skilling, 1994).

Tindars are similar in composition to tuyas, but emanate from a rift, not point, source. Like tuyas, they are composed of hyaloclastite and hyalotuff resulting from interaction between magma and meltwater (Sigurðsson, 2000). Steep sides are formed by confinement of the deposits by surrounding ice. If a subglacial eruption becomes subaerial, a tindar ridge is capped by cinder or spatter cones.

In addition to highly distinctive tuya and tindar landforms, subglacial eruptions produce an array of distinctive deposits that are indicative of their eruptive environment and transport and deposition processes.

7.3.2 Volcanic landforms at Eyjafjöll

Both subglacial and subaerial volcanic deposits are evident at Eyjafjöll, suggesting a varied eruptive environment through time and space. Loughlin (1995) defined a suite of "lithofacies associations" which occur on Eyjafjöll and are indicative of the eruptive environment and lava/ice interaction processes which occurred at the time of emplacement. There are nine associations which can be grouped according to their place of deposition relative to an eruptive vent (***Figure 7.1***). Most consist of materials which were redeposited by meltwater, an indication that they formed during an eruption under thin (<200m) temperate ice (Loughlin, 1995). At least six of the lithofacies associations consist of deposits which indicate that they flowed in subglacial channels opened up by large volumes of turbulent meltwater, pointing to the common occurrence of jökulhlaups during eruptions at Eyjafjöll. Six of the units were formed by mass flow processes (requiring permeable ice) and three were formed by ponding of water (requiring thick ice or damming).

Figure 7.2 shows where the lithofacies associations occur on Eyjafjöll. Proximal units (D, E, G) are deposited close to the eruptive vent. ***Lithofacies association D*** consists of lava tubes frozen in subglacial channels, similar to esker deposits in Rothliesberger tunnels. Lava does not transfer heat efficiently and is easily chilled in ice tunnels, forcing subsequent lava to find different channels.

Lithofacies association E is similar to D, but is more massive lava frozen in valleys, confined by topographic, not ice, channels. E units are formed during small volume subglacial eruptions from radial and E-W fissures. ***Lithofacies association G*** is an unconfined layered deposit. It is a widespread deposit, formed in a shallow, subaqueous/subglacial environment. Containing massive hyaloclastite (indicating large amounts of water), G units comprise three layers. The bottom layer is emplaced by collapse of unstable piles of tephra near the vent and the middle layer by mass flow processes. The upper layer typically consists of subaerially deposited ash.

Medial units are deposited farther away from the active vent and are dominated by ponding processes. ***Lithofacies association C*** is basal sheet lava deposited on a flat or gently sloping base. This unconfined unit consists of lavas intruded and ponded between initial phreatomagmatic deposits and topography. Its formation requires a thick, broad temperate glacier. ***Lithofacies association H*** is thick lava ponded between steep valley sides and a temperate valley-confined glacier. This is an important feature recognized by Lescinsky and Sisson (1998) for its ability to indicate the former presence of valley glaciers. ***Lithofacies association J*** is the equivalent of a tuya or tindar deposit. It is formed by ponding in an englacial lake beneath thick, valley-confined ice sheets (< 400 m). The J features at Eyjafjöll were probably formed in broad, flat-based glacial valleys eroded into the volcano flanks by late-glacial outlet glaciers or by ponding between a larger valley glacier occupying the present sandur plain and the volcano slopes. J units can be as great as 75 m thick and form as a result of large-scale summit or flank eruptions. This is the rarest lithofacies association on Eyjafjöll, because sufficient thicknesses of ice are unlikely to build up (Loughlin, 1995).

Distal units are deposited by meltwater at the margins of the ice sheet or on the outwash plain. ***Lithofacies association A*** are unconfined sheets consisting of volcaniclastics deposited by flood flow and collapsed mass flows of lava. The form of sedimentation indicates pulsing of flow, a result of damming more proximal to the vent. ***Lithofacies association B*** contain the same lithology as A but are channelled

deposits. ***Lithofacies association F*** are topographically-confined deposits formed by collapsing masses of blocky lavas, pillows and hyaloclastites.

7.3.3 Past eruptive environment of Eyjafjöll

The volcanic landforms present on Eyjafjöll tell us a number of things about its past eruptive environment. From this, we may infer the extent and behavior of the past ice cap. To summarize, the central volcano of Eyjafjöll has grown and evolved over the course of about 780,000 years, through six glacial and six interglacial periods (Loughlin, 1995). Large explosive eruptions emanated from the central vent, now evident as a summit crater. Parasitic flank and fissure eruptions also occurred throughout its history. Volcanic eruptions were altered by interaction with a waxing and waning ice cap (Jakobsson, 1979).

For most of its history, Eyjafjallajökull has been a relatively thin, temperate glacier, occupying the summit region of the volcano. During colder glacial periods, ice extended further down the flanks than today, joining the larger Markarfljót valley glacier (Geirsdóttir and Eiríksson, 1994).

The glacier ice has been disrupted numerous times throughout Eyjafjallajökull's history. Each time an eruption took place, ice was removed (Jakobsson, 1979; Simkin and Siebert, 2000). Almost all of the lithofacies associations observed by Loughlin were redeposited by meltwater, confirming the melting of parts of the glacier. The majority of the volcanic landforms observed on Eyjafjöll are such that they required relatively thin, permeable ice to form. A few of the landforms required thicker, more confining ice, but these features are fewer in number and spatially more discrete. Another observation which indicates that the glacier was usually temperate (i.e. thin and permeable) during its history is the presence of many features which appear to have travelled through a well-developed subglacial drainage system. Some, like the frozen lava tubes of lithofacies association D, provide direct evidence of the dimensions of these channels. A well-developed subglacial drainage system is a diagnostic feature of a temperate glacier.

The evidence of the presence of large quantities of meltwater, flooding, and lahar deposits implies that Eyjafjallajökull has undergone repeated catastrophic disruption throughout its history. The glacier's ability to heal itself after the disruption which came with each eruption depended on the magnitude of the disruption and the mass balance of the glacier. If a large volume of ice cycled through the system during the year, the ice probably healed quickly. If disruption occurred during a period of low flux, then the healing process most likely took longer.

7.4 Properties of subglacial eruptive environments

Properties of glaciers exert a fundamental control on the eruptive processes and volcanic landforms described above. The ice thickness, hydraulics, and structure of a glacier constitute the eruptive environment. In combination with basal and ice surface topography, these properties determine how and where lava and meltwater flow.

7.4.1 Structure and thickness

Glacier structure determines whether meltwater and lava flow freely or are channelled and confined. The hydrological structure of a glacier system influences the sequence of events during a subglacial eruption.

Glaciers have a layered structure which dictates the movement of water (the glacier hydraulics). The uppermost layer of ice is composed of permeable snow, firn, and fractured (crevassed) ice, whereas the higher density lower layer is composed of relatively impermeable, unfractured ice (Smellie, 2000; Smellie and Skilling, 1994). The presence of these layers in temperate glaciers is partly a function of thickness. Ice less than 100 m thick is composed mainly of snow, firn, and fractured ice, because the transition from firn to ice typically occurs at 50-70m below the ice surface (Smellie and Skilling, 1994). Thicker glaciers (>100m) have a

larger percentage of this relatively impermeable ice layer. This relationship is linked to glacier type. Unlike polar glaciers, liquid water is present at all times in temperate glaciers and migrates throughout the system, movement which would not be possible without fractured, permeable ice (Menzies, 1995).

The implication of this layered structure is that meltwater produced by a subglacial eruption will be able to escape continuously through permeable ice layers, but will tend to be confined and pond when it encounters impermeable layers. Subglacial eruptions which take place under thick, impermeable ice produce catastrophic outbursts of meltwater when large volumes of ponded meltwater are released. Subglacial eruptions under thin, permeable ice allow meltwater to drain continuously, lessening the possibility of a sudden release. However, damming and ponding at distal sites on a volcano may release smaller pulses of meltwater.

7.4.1.1 Structure and thickness at Eyjafjallajökull

The structure of Eyjafjallajökull is determined by the radar survey. The dielectric properties of the glacier (determined in *Chapter 4*) indicate the structure and thickness.

Electromagnetic waves propagate faster through ice in the crater, indicating that the ice at the base of Gigjökull and on the flanks is denser on average than that in the crater. The ice in the crater contains a firn layer substantial enough to lower the average density. This discrepancy is likely to be a result of the large quantities of liquid water contained in the ice outside the crater. This distal ice is substantially thinner and, especially at Gigjökull and in areas where the slope is steep, more highly fractured. Essentially, the ice in these areas is permeable. The implication of this for the eruptive environment is that, if meltwater from an eruption encounters this ice, it will drain continuously through permeable ice and the subglacial drainage system. These parts of the glacier will have well-developed subglacial drainage systems, especially down valley glaciers like Gigjökull.

The ice in the crater is quite different from the rest of the ice cap. It is thicker (>200 m) and has a lower bulk density. Considering the theoretical structure of thick

ice like this, it seems safe to assume that a layer of dense glacial ice is overlain by a firn layer of less dense, more permeable ice. The implication of this two-layered structure for meltwater produced from an eruption is that ponding will likely occur.

7.4.2 Hydraulics and topography

The direction of englacial meltwater flow is controlled by the hydraulic gradient, which is mainly determined by the ice surface slope (Paterson, 1994). Water flows in a direction perpendicular to the gradient of water pressure potential, which is about eleven times the ice surface slope, and in the opposite direction (Paterson, 1994). If the surface and bed slopes are similar, then the surface slope controls the direction of englacial water flow. For example, the ice surface slope above an active vent will change during an eruption. When heat from an eruption melts ice above a vent, the ice, being less dense than water, subsides, changing the local hydraulic gradient. Meltwater is forced to flow inward toward the vent. Once water has reached the subglacial surface, it tends to follow valley floors. Water preferentially flows in channels determined by the bedrock topography instead of melting out new channels (Paterson, 1994).

Both ice surface topography and subglacial topography are responsible for directing the flow of lava and meltwater which escapes from the vent area. Meltwater and lava follow the subglacial tunnels which trace basal topographical lows. Areas of rapid change in basal slope focus ponding, while areas of decreased ice surface slope are centers of erosion of ice canyons from pyroclastic flows, meltwater, and lava. Vinogradov and Murav'ev (1988) and Trabant *et al.* (1994) observed the major impact of topography in determining the direction of meltwater and lava flow and initiation of erosional processes. Basal topography was responsible for the meandering of lava streams (Vinogradov and Murav'ev, 1988). Locations of incised channels in Drift Glacier were strongly influenced by the ice surface topography. Major ice canyons began at the base of steep icefalls where the slope abruptly decreased (Trabant *et al.*, 1994).

7.4.2.1 Hydraulics and topography at Eyjafjallajökull

The hydraulics and topography of Eyjafjallajökull are determined by the radar survey. Except in the crater, the ice surface slope is similar to the bed slope (well less than 11x), so the ice surface slope controls the flow of englacial water. In the crater, englacial water follows the equipotential slope. In the event of an eruption in the crater, heat from the vent will form a depression in the ice, forcing meltwater and ice towards the vent.

Once the meltwater reaches the subglacial surface, it will either tend to follow the path of least resistance along the basal topography or be driven by the water pressure potential gradient. According to Shreve (1972), the subglacial hydraulic potential (ϕ) is calculated as

$$\phi = \rho_w g B + \rho_i g (H - B)$$

Equation 7.1

where

ϕ = subglacial hydraulic potential

ρ_w, ρ_i = density of water and ice, respectively (g m^{-3})

g = acceleration due to gravity (m s^{-2})

H = ice surface elevation (m)

B = basal surface elevation (m) (Shreve, 1972).

Drainage basins were defined on maps of both basal contours and water pressure potential (***Figures 7.3a,b***). The drainage divides are similar for both, allowing the assumption of atmospheric pressure at the base of the glacier. Therefore, meltwater drainage basins are defined from the basal contour map.

The thin, temperate nature of Eyjafjallajökull indicates the presence of a well-developed subglacial drainage system through which meltwater and lava will preferentially flow. ***Figure 7.3a*** identifies the gullies where meltwater and lava flow are most likely to occur. The steep slopes of the north and south flanks, with their deeply incised valleys, will be the focus of subglacial evacuation of meltwater and lava. Areas of rapid change in basal slope (subglacial benches), glacial confluences,

and sharp bends in drainage channels will focus ponding of lava and meltwater draining through subglacial passages. ***Figure 7.4*** identifies possible areas of ponding. Draining meltwater may be dammed more than once as it travels from the source, down the flanks of the volcano and out onto the sandur plain. This mechanism produces floodwater pulsing. It seems likely that the past meltwater flooding from Gigjökull which has deposited pulses of sediment in the Markarfljót Valley (Maizels, 1989) is a result of ponding both in the crater and at the base of the icefall, in the overdeepening.

Figure 7.4 also indicates the locations where lava will be emplaced in the form of lithofacies association H. Lava does not transfer heat efficiently, so ice is able to resist thermal erosion and consequently is able to direct and confine lava flow. Characteristic features are produced when this process occurs. Evidence of confinement is shown by thick lava flows with steep and glassy margins (Lescinsky and Fink, 2000). Lava flows follow subglacial channels widened by meltwater and are sandwiched between valley walls and valley glaciers (like lateral moraines). These "Lescinsky" features of lava confined between a valley glacier and valley-side topography lead to topographical inversion and subsequent 'wandering' glaciers. The heavily eroded gullies of the steep southern flanks are ideal candidates for this process.

7.4.3 Present eruptive environment of Eyjafjallajökull

The present eruptive environment is a good example of what Eyjafjallajökull is typically like during an interglacial period.

The structure of the ice implies that the present eruptive environment divides into two areas, where separate meltwater flow mechanisms will dominate in the event of an eruption. If an eruption occurs in the crater, there is a greater possibility of a major flood. The impermeable ice contained within the crater is likely to confine meltwater, causing it to accumulate. If ponded meltwater gathers in sufficient quantities, it will probably drain quickly when it encounters fractured or

permeable ice. The sudden release of large quantities of meltwater may cause catastrophic flooding.

If an eruption occurs outside the crater, perhaps on the south flank (the area of most recent volcanic activity), meltwater will drain less catastrophically. The thinner ice here provides smaller volumes of meltwater. On the steep, dissected north and south flanks, major drainage pathways currently exist. The ice is highly fractured (and therefore permeable to meltwater) on these steep slopes. Meltwater drainage is most likely to occur here, in a continuous manner. Damming and ponding may occur at breaks in slope, but the quantity of accumulation is unlikely to be great. Pulses of meltwater issuing from these slopes are possible, but the potential for catastrophic flooding is low. Meltwater drainage on the gentle east and west flanks will probably be steady and continuous.

In the event of an eruption in the crater, ice disruption will likely be greatest at Gigjökull. The northern rim breach through which most of the ice contained in the crater currently flows, will direct lava and meltwater issuing from an erupting vent down this outlet glacier. The steep slope, fractured ice, and subglacial drainage system provide a well-developed meltwater and lava escape route. The flow of lava and meltwater down Gigjökull will enable processes of thermal and mechanical ice erosion.

The steep north and south flanks of the volcano, with their deeply-dissected gorges, will be places where emplacement of lava is likely to occur. On Gigjokull especially, lava may flow and solidify between the valley glacier and bounding ridges. This process will lead to topographic inversion and 'wandering' glaciers.

7.5 Hazards

Subglacial eruptions also cause natural hazards such as floods and lahars, catastrophic events which damage the environment and pose danger to nearby human communities.

There are a number of hazards which result from the interaction of lava, meltwater, and ice during subglacial eruptions. The presence of snow and ice on an

active volcano invariably increases the hazards associated with eruptions (Major and Newhall, 1989). The two main hazards are lahars and flooding. Lahars and floods can be generated by basal melting, surficial lava flows, and pyroclastic flows. Most jökulhlaups or lahars formed by basal melting occur in Iceland (Major and Newhall, 1989).

7.5.1 Lahars

Lahars are flowing masses of volcaniclastic sediments mixed with water (Major and Newhall, 1989). Surficial lava flows form lahars when the leading edge of a lava flow chills and fragments. The debris mixes with ice and avalanches (Major and Newhall, 1989). The destructive potential of an outburst flood increases if debris is entrained along the flow path, transforming the flood into a debris flow (Driedger and Fountain, 1989). Sometimes a number of events occur on the same edifice. At Redoubt Volcano, Trabant *et al.* (1994) observed a mixed avalanche of snow and debris which stopped at the base of Crescent Glacier and formed a deposit. On Drift Glacier, however, hot, dry, volcaniclastic flows swept downslope and transformed into cold, wet, laharic flows which continued down valley into the Drift River (Trabant *et al.*, 1994). Vinogradov and Murav'ev (1988) noticed the intermittent behavior of lahars which flowed down the flanks of Mt. Kluchevskoiy. Masses of loose clastic material and ice blocks collapsed, damming the accumulating meltwater. Periodic breaching of the dams caused the lahars to burst forth in pulses (Vinogradov and Murav'ev, 1988). Lava extrusion onto the ice surface is a major mechanism in lahar and debris avalanche formation. Meltwater streams issuing from the contact between lava and ice entrain glacial and pyroclastic debris and mechanically scour the ice surface. The collapse of this mass leads to laharic avalanching.

7.5.2 Jökulhlaups

Jökulhlaups are glacier outburst floods, occurring when a surge of water which has been englacially or subglacially confined literally "leaps" out of a glacier, sometimes catastrophically flooding lower valleys. Jökulhlaups are the most common hazard associated with subglacial eruptions in Iceland. In 1947 a 1 x 10^6 m^3 flood magnitude occurred when a pyroclastic flow surged onto Hekla's summit glacier (Major and Newhall, 1989). The Oræfajökull floods of 1362 and 1727 were generated by surficial lava flows, according to Major and Newhall (1989) or by basal melting, according to Þórarinsson (1979). Sudden release of ponded or dammed water produced by basal melting is the most common process by which floods are formed (Major and Newhall, 1989; Lescinsky and Fink, 2000). If ice above an active vent is quite thick (>150m), meltwater may pond *in situ*. Eventually it will be released, but the immense accumulation of water needed to resist ice confinement causes greater catastrophic flooding than that caused by surging and pulsing meltwater temporarily blocked during a continuous escape.

7.5.3 Evidence of past hazards

There is evidence in the deposited volcanic landforms on Eyjafjöll of the past occurrence of jökulhlaups and lahars produced by subglacial eruptions. Observers of the one historical eruption of Eyjafjöll in 1822 witnessed a jökulhlaup flooding out of Gigjökull (Dugmore, 1987). There are pulses of flood deposit sediments in the sandur plain surrounding the volcano, pointing to the fact that several jökulhlaups may have occurred during the course of a single eruption (Loughlin, 1995). Evidence of lahars are also present in the deposited volcanic landforms. A thin basal layer of sand-sized material (<15 cm) often occurs at the base of volcanic debris flows at Eyjafjöll (Loughlin, 1995). This is a diagnostic feature of lahars.

7.5.4 Potential hazards

There is the potential for flooding to take place at Eyjafjöll in the event of an eruption. Possible processes are suggested.

If an eruption takes place via an active vent in the crater, ponding over the vent is likely to occur. The subsequent movement of meltwater is likely to follow one of two mechanisms (or a combination) (***Figure 7.5***). If impermeable ice confines meltwater, it will pond and accumulate until the water level reaches the more permeable firn layer, where it will drain. This level is likely to be at the height of the top of the ice fall, where the ice is severely fractured. The ponded water could burst out through the crevasses, flooding down Gigjökull. This is a possible source of previous jökulhlaups which have flowed out Gigjökull. If this scenario occurs, the erosive power of the flooding water may quarry large chunks of ice from the rough, fractured surface of the icefall, carrying them down to the sandur. The break in slope at the bottom of the icefall will focus erosion. Ice canyons may form here, eroding the ice and the overdeepening at the base.

The second proposed mechanism of meltwater movement in the crater is via subglacial drainage through the rim breach towards Gigjökull. This is likely to occur along the main flowline in the crater. The surface depression evident from photos points to a major ice and water drainage route towards the rim breach as do the calculated flow vectors (***Figure 7.6***).

It has been observed that breaches in a caldera rim control the outflow of meltwater, lava, and pyroclastic flows from a caldera. Trabant *et al.* (1994) attributed the "specificity of the attack on Drift Glacier" by pyroclastic flows and meltwater, to the breach in the summit crater rim.

Table 7.1 provides a value of possible flood volume should an eruption occur in the summit crater and direct meltwater and lava down Gigjökull. The volume is calculated as the maximum possible quantity of water that could be released, should all the ice in the catchment be melted. This scenario is, of course, unlikely, but provides a maximum from which to assess the possible danger to the valley below. The quantity is of the same magnitude as those reported for the observed floods on Drift Glacier and Mount Veniaminof (Trabant *et al.*, 1994; Yount *et al.*, 1985).

7.6 Thoughts on the anomalous fluctuations of Gigjökull

The surface area of Eyjafjallajökull is approximately 70 km^2.[1] (***Table 7.1***). This is 30% less than the 101 km^2 estimated by the Danish General Staff Survey of Iceland, who mapped Eyjafjallajökull in 1907 at a 1:50,000 scale (Þórarinsson, 1943). Björnsson (1978) states that the total area of Eyjafjallajökull in 1973 was 78 km^2. Eyjafjallajökull is quickly losing mass. The retreat of Gigjökull, however, is not comparable to the rest of the ice cap (Sigurðsson, 1998) (***Figure 7.7***). Gigjökull retreated more than 500 m between 1930, when it was at its terminal moraines, and today. The glacier rapidly retreated 675 m between 1930 and 1958, but then advanced 163 m between 1958 and 1987. Since 1987, it has again been in retreat. Gigjökull is about 6 km long today, so half a kilometer of retreat constitutes only about 8% of its total length, much less than the 40% of the rest of the ice cap. Obviously, the marginal fluctuations of Gigjökull have been more closely monitored than the rest of the ice cap, mainly because its snout is easily accessible and it is an outlet glacier of the type long considered to be rapidly responsive to climate change. The evidence we have for the marginal fluctuations of the rest of the ice cap are the various mapping surveys, the monitoring of Steinholtsjökull and Seljavellajökull, and numerous local observations of the annual condition of the ice at Fimmvörðuháls. Mýrdalsjökull and Eyjafjallajökull were joined at Fimmvörðuháls until 1950-1960, when the two separated (Rist, 1967). Seljavellajökull has retreated more rapidly since the end of the Little Ice Age than has Gigjökull (Þórarinsson, 1943). The fluctuations of Steinholtsjökull are difficult to decipher since the catastrophic landslide in 1967 disrupted ice at the snout (Kjartansson, 1967). All this evidence supports the notion that the main body of the Eyjafjallajökull ice cap is retreating faster than is Gigjökull.

This observation suggests that two different mechanisms control the fluctuations of Gigjökull and the rest of the ice cap. The most obvious clue is Gigjökull's deep, topographically-confined accumulation area. The crater rim

defines the upper boundary of Gigjökull's catchment. The ice filling the crater is up to 250 m deep. At present, any ice that flows out of the crater does so through a large northern rim breach, providing Gigjökull with a substantial feeder source. It has been suggested (Dugmore, 1989) that the anomalous fluctuations of Gigjökull are the result of being topographically-controlled. The catchment hypsometry supports this theory (***Figure 7.8***).

Gigjökull has a high altitude accumulation area and a narrow, steep middle section (icefall) that widens out at the base into the sandur level ablation area. If climate controls force a lowering of the ELA (down the steep, narrow reaches of the icefall), the area of accumulation will not increase very much, but any increase in lateral extent of the snout will rapidly increase the ablation area. In this situation, the glacier is particularly stable, requiring a massive lowering of the ELA (major climate deterioration, i.e. full glacial conditions) for the accumulation area to increase enough to cause a significant advance of the snout. The same goes for a rising ELA; a great deal of warming would have to occur before the accumulation area is reduced enough to cause significant backwasting of the snout.

The remainder of the ice cap is spread thinly (< 150 m thick) over the sloping flanks. The steeper slopes and wider areas at the ELA level (compared to Gigjökull's narrow ELA zone in the icefall) of the ice cap are more susceptible to drastic retreat if climate warming forces the ELA to rise. Ice will likely remain in the summit crater for a time after most of the ice has melted off the slopes. It seems clear that in the final stages of deglaciation, most of the ice cap will disappear, leaving Gigjökull as a cirque glacier which could remain for some time.

Therefore, it seems prudent to consider Gigjökull and Eyjafjallajökull as separate glaciological systems during periods of deglaciation (i.e. once the ice divide has shifted and the ice level in the crater drops to a point where it only feeds Gigjökull). Considering this, it would seem incautious to use the fluctuations of Gigjökull (exclusively) as representative of the waxings and wanings of the ice cap as a whole and, consequently, to draw conclusions about the past regional climate from these fluctuations. Obviously, Gigjökull is influenced by climate, but in a

[1] Surface area is calculated automatically in Surfer from the digitized ice limits of the Eyjafjallajökull

different way (and at a different pace) than the rest of Eyjafjallajökull. Gigjökull also seems to take the brunt of the eruption-linked floods and lahars, indicating that its climatically-driven fluctuations will be subject to pause while it heals itself from volcanigenic disruption. The disruption of Steinholtsjökull is a recent example of how severely the fluctuations of an outlet glacier can be interrupted by, in this case, a catastrophic landslide (Kjartansson, 1967).

The radar survey shows that a proposed overdeepening (Dugmore, A.., 1997, *pers. comm.*) does exist at the bottom of the icefall (***Figure 7.9***). Excavation of the overdeepening was probably helped by the erosive force of floods and lahars released from the summit crater. If hot lahars and large quantities of meltwater can successfully cut canyons into ice (as observed by Trabant *et al.* (1994)), then their erosive power can surely contribute to the further excavation of the soft till lithology which most likely underlies the ice.

7.7 Endogenic glacial fluctuations caused by glaciovolcanic processes

The disruption to glaciers caused by eruptions has wider implications than just predetermining ice/lava interaction eruption processes or predicting future hazards. The importance of volcanigenic influences on glacier dynamics suggest that glaciers formed on volcanoes are a special case, a 'type', whose use as proxies for inferring climate change should be carefully considered. Instead of using the marginal fluctuations of these systems to determine former ice extent, volcanic landforms (such as tuyas and tindars) can be more usefully interpreted to indicate former ice thicknesses coeval to eruptions, ostensibly giving a more realistic and representative estimate of the state of a glacier than marginal fluctuations, especially since ice levels at the time of eruption are in an undisturbed, pre-disruption state.

Volcanigenic ice disruption can be very significant. If an eruption occurs during a deglaciation phase, the ice may not be replaced. The disturbance may wipe out large parts of the accumulation area of a glacier, thus upsetting the equilibrium and causing more rapid deglaciation than would otherwise occur. Misleading

---

1:50,000 map produced by the Iceland Geodetic Survey in 1990.

conclusions could be drawn from the resulting marginal landforms. Moraines would normally indicate a rapid climate warming needed to cause the severe backwasting. Vinogradov and Murav'ev (1988) observed that the glacier occupying Mt. Kluchevskoiy contained numerous moraine and pyroclastic beds along with various-density intercalations in the ice, suggesting large hiatuses in ice accumulation. On the other hand, volcanigenic ice disruption may only affect one part of the ice mass, like a single outlet glacier, such as Gigjökull. The rest of the icecap may be essentially untouched and therefore may more reasonably reflect the influence of climate.

A common result of volcanigenic glacier fluctuations is the so-called "wandering" glacier (Driedger and Fountain, 1989; Loughlin, 1995; Trabant *et al.*, 1994; Vinogradov and Murav'ev, 1988). Sometimes part of the glacier accumulation area will be cut off from the tongue by a lahar or a lava flow. The subsequently isolated glacier terminus will stagnate, perhaps leaving hummocky moraines. Once the accumulation area has healed, a new glacier front will start moving along a new channel. This process destroys moraine succession. "Wandering" glaciers have been observed a number of times. Drift Glacier was beheaded during the 1966-68 eruption of Redoubt Volcano, losing about 60 x 10^6 m^3 of ice between 1500 m and 2500 m. During the 1989-90 eruption, the same glacier was beheaded, when most of the ice between 750 m and 2500 m was removed (Trabant *et al.*, 1994). Disruption of the accumulation area of a glacier at that scale will certainly affect the behavior of the remaining frontal lobe. Dreidger and Fountain (1989) write that the most obvious feature of South Tahoma Glacier on Mt. Rainier is a 1 km long stretch of stagnating ice that was partially disconnected from the rest of the glacier body by a flood. Vinogradov and Murav'ev (1988) state that the 1966 Piip eruption was responsible for a 900 m *advance* of the Vlodavets Glacier. They add that the eruption stimulated some areas of buried ice into activity. Loughlin (1995) describes a process by which "wandering" glaciers leave incomplete moraine successions at Eyjafjallajökull. She writes that "inverted topography" exists on the flanks and is currently being produced at Eyjafjöll. Lava flows typically follow the bedrock morphology and solidify in former gullies which contained valley glaciers.

Subsequent erosional processes preferentially erode the less resistant sediment on either side of the lava. The valley glaciers then occupy the new gullies, leaving incomplete moraine successions (Loughlin, 1995).

7.7.1 Tephra fall

Another process by which endogenic processes influence the behavior of glaciers is the disruption caused by tephra fall. Ash covering a glacier increases or decreases the rate of ablation, depending on the thickness of the ash layer. Enhanced or retarded melting alters the mass balance of a glacier. A thin layer of tephra causes glacier shrinkage; a thick ash covering causes glacier growth. At Deception Island, post-eruption glaciers shrank quickly when the ash thickness was 3 mm and grew when tephra thickness was greater than 24 mm (Major and Newhall, 1989). This effect on glacier mass balance is taken very seriously indeed, as the UK Guardian newspaper recently reported:

> "After four years of poor rainfall, the drought [in Pakistan] is expected to be one of the worst for decades. In neighboring Afghanistan 500,000 people have been forced to leave their homes in search of food and water.
>
> The Pakistani regime has asked the meteorological office to examine the feasibility of melting the glaciers of the Hindu Kush and the Himalayas.
>
> If charcoal were sprayed on them, the theory goes, the black surface would absorb more sunshine and possibly increase the annual melt by up to 15%.
>
> But this could destabilize the glaciers, block rivers and lead to flooding, according to the director general of the meteorological office, Qamar-uz-Zaman Chaudhry." (McCarthy, 2001)

According to Dugmore (1987), the tephra fall from the 1821-1823 eruption of Eyjafjöll covered the entire ice cap in ash 0.5 cm thick. This probably insulated the glacier, decreasing ablation until new snow covered the tephra. Tephra fallout from nearby volcanoes have affected Eyjafjallajökull as well. The Hekla eruption of 1947 covered northwest Eyjafjöll with 5 cm of tephra, central Eyjafjöll with 1 cm, and eastern Eyjafjöll with 0.1 cm (Dugmore, 1987). This is significant coverage which

probably modified the mass balance of the ice cap for a time. There are many other active volcanoes in the region (e.g. Mýrdalsjökull, Vatnajökull) which may have deposited tephra on Eyjafjallajökull in the past and could in the future as well.

7.8 Summary

Eyjafjöll is a glaciovolcanic system in whose deglaciated volcanic landforms may be found evidence of past eruptive environments. The radar survey provides measured quantities needed to describe the present eruptive environment of the glaciated section of the volcano. Eyjafjallajökull is spatially split into two glaciological systems based on ice thickness and structure. The area containing the summit crater and its outlet glacier, Gigjökull, is less sensitive to the influence of climate in its current topographical confines. In the event of a summit eruption, the thick, impermeable ice in the crater may confine meltwater, then suddenly release it as a jökulhlaup. Thermal and mechanical erosion from flooding meltwater could severely disrupt the ice of Gigjökull. The area outside the summit crater contains thin (<150 m) ice and a probable well-developed subglacial drainage system. This section is more sensitive glaciologically to climate change and, in the event of an eruption, will allow meltwater to drain continuously, lessening the hazard of flooding. On glaciovolcanic systems it is ill-judged to consider marginal landforms of one outlet glacier as evidence of climatic influence on glacier fluctuation. Instead, the entire system should be considered.

Insight into how past fluctuations of the glacier should be interpreted are gained with a greater understanding of the interaction between glacier and volcano, its effect on the evolution of the system, and how it may continue to evolve. The conclusions drawn from this investigation may be applied to other glaciovolcanic systems and inform how this type of system should be assessed in relation to the influence of climate.

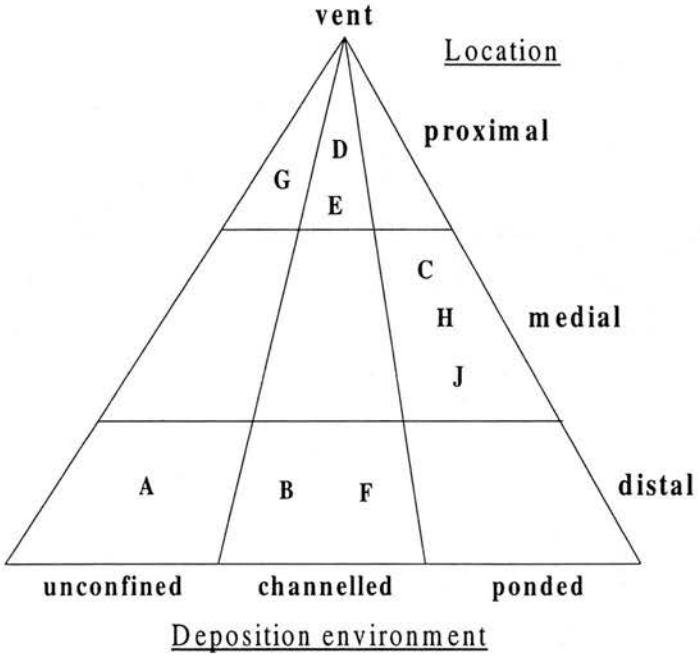

Key to lithofacies associations

A	unconfined distal deposit of volcaniclastics
B	channelled distal deposit of volcaniclastics
C	medial deposit of lava ponded between initial phreatomagmatic deposits and topography
D	channelled proximal deposit of lava in subglacial tunnels
E	channelled proximal deposit of lava in valleys
F	channelled distal deposit of lava and hyaloclastites
G	unconfined proximal deposit of massive lava and volcaniclastics
H	medial deposit of lava ponded between valley side topography and ice
J	medial deposit of lava ponded in englacial lake (tuya/tindar)

Figure 7.1 Lithofacies associations identified on Eyjafjöll classified according to distance from vent and deposition environment.

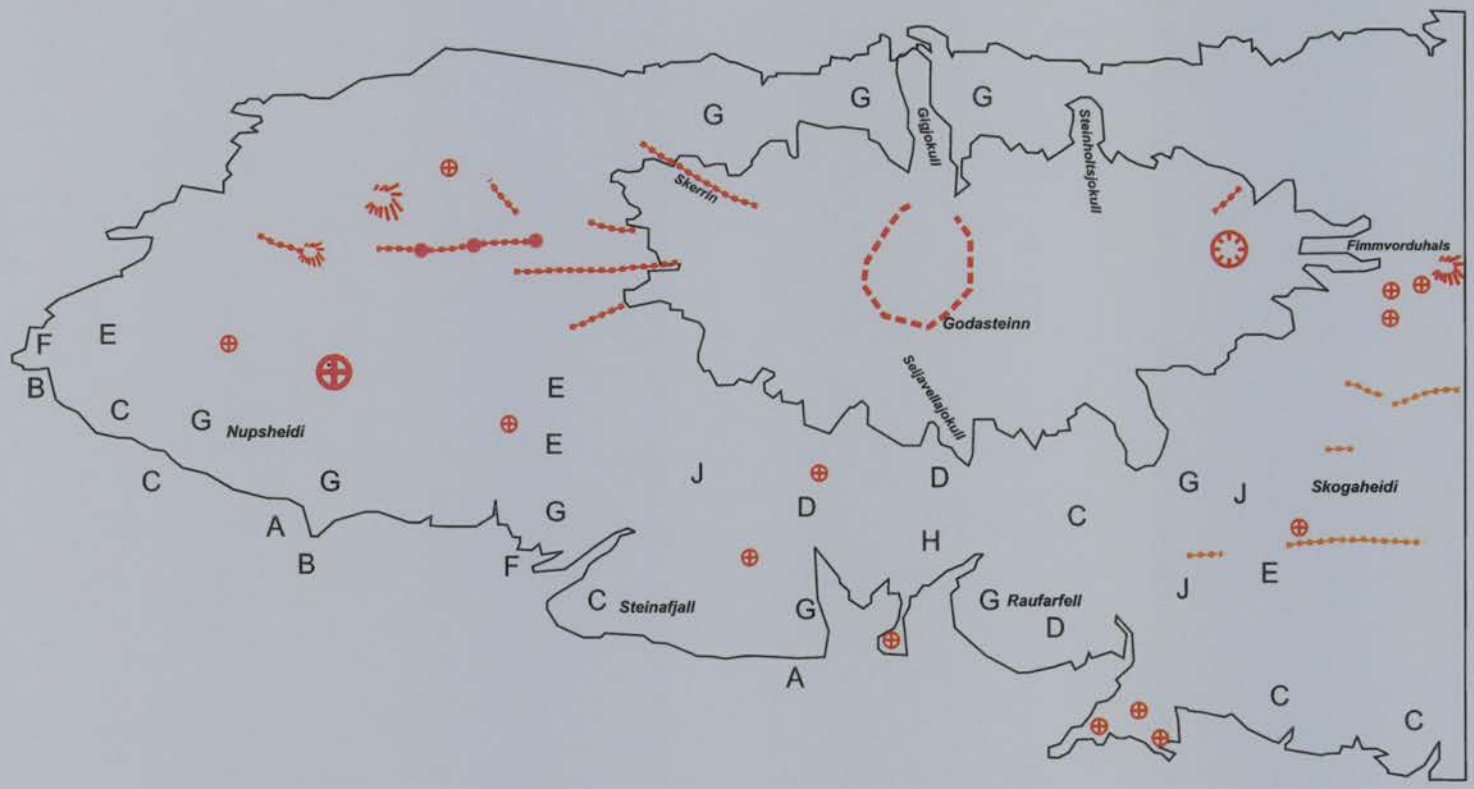

Figure 7.2 Location of lithofacies associations on Eyjafjöll (after Loughlin, 1996).

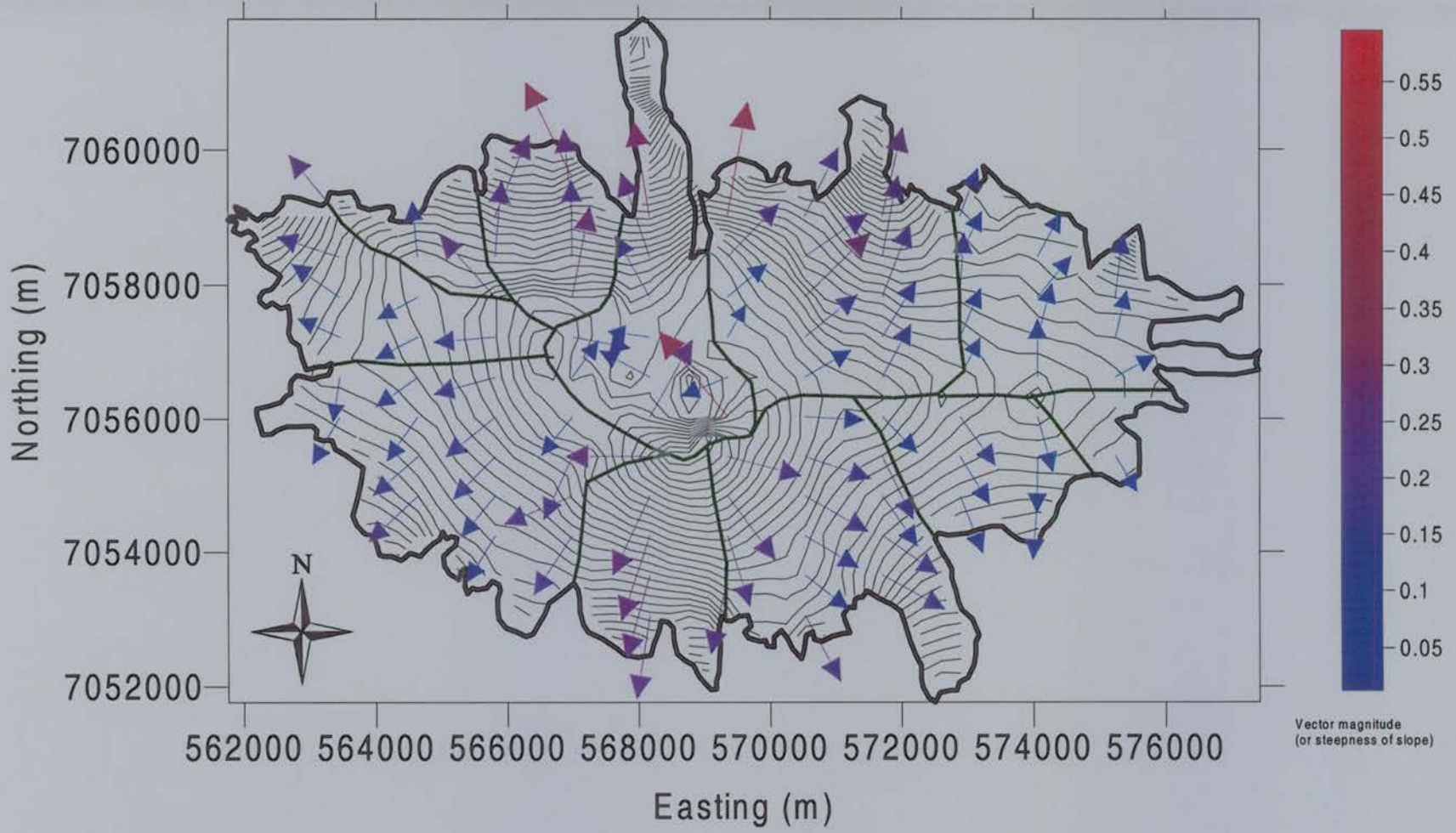

Figure 7.3a Vectors illustrating flow direction and magnitude calculated from basal grid. Green lines identify drainage basins where meltwater and lava flow likely to occur.

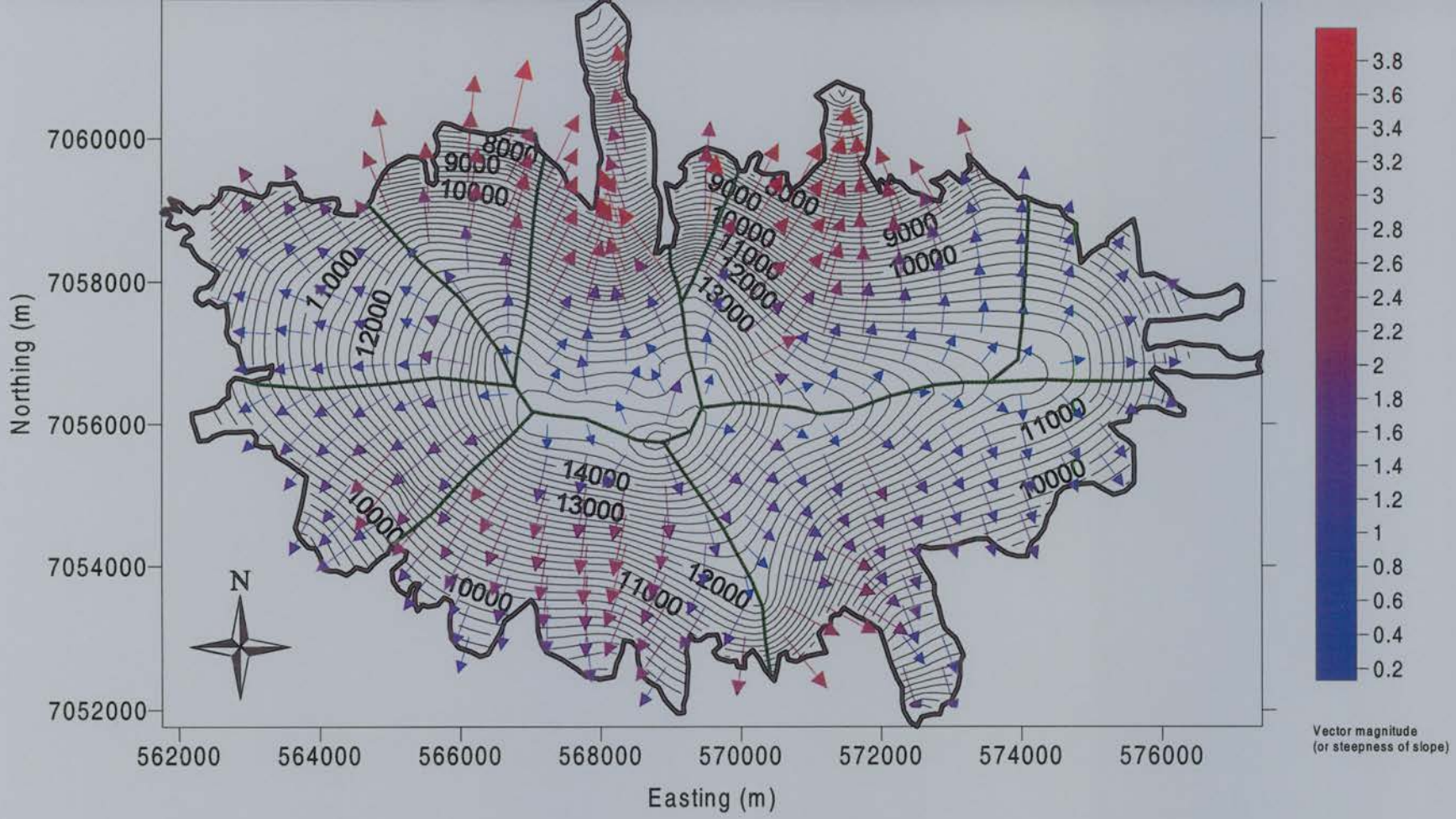

Figure 7.3b Vectors illustrating flow direction and magnitude calculated from subglacial hydraulic potential contours. Green lines identify drainage basins where meltwater and lava flow likely to occur.

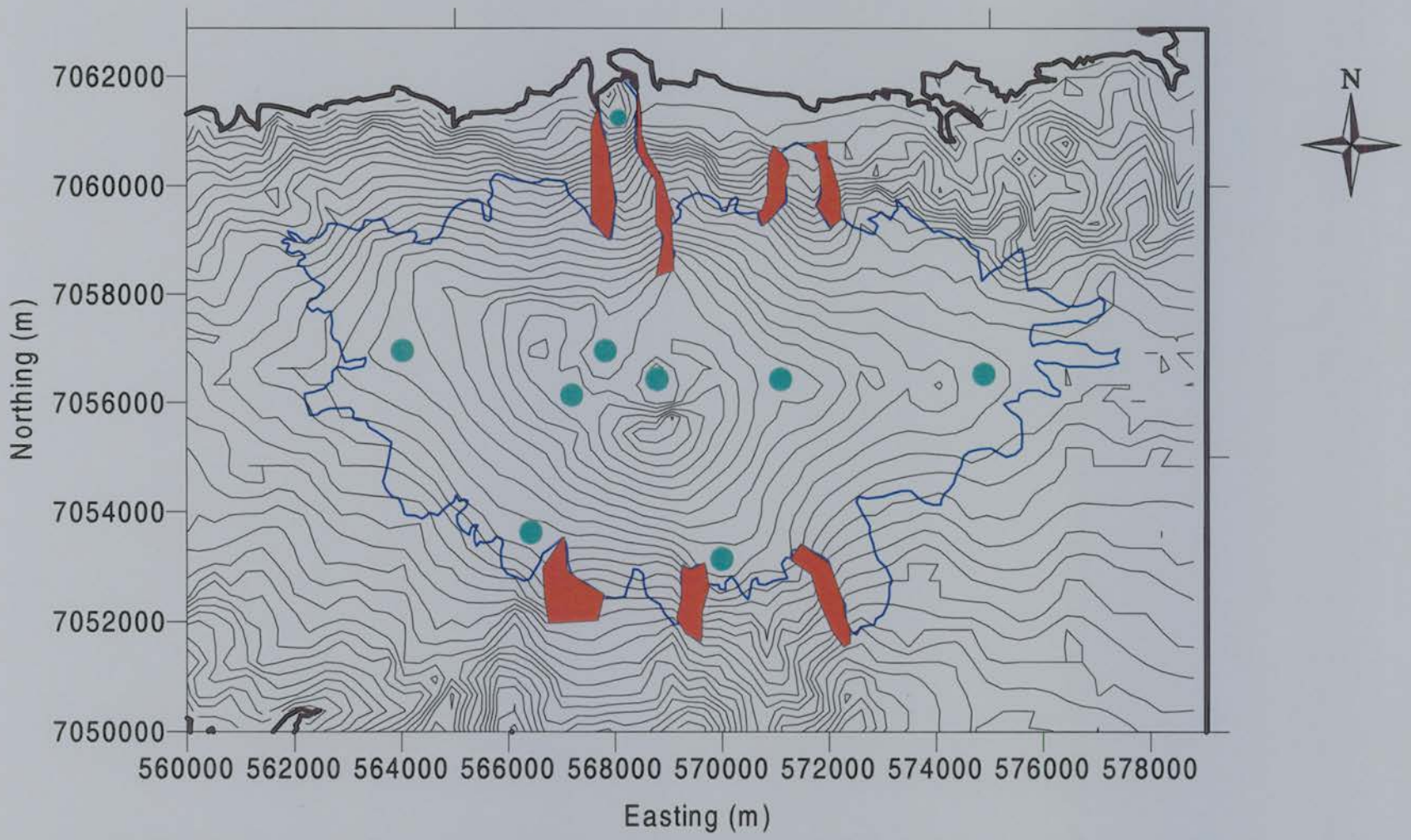

Figure 7.4 Map identifying areas where meltwater and lava are likely to pond (blue dots) and areas where emplacement of 'Lescinsky' features (orange polygons) is possible in the event of a summit eruption.

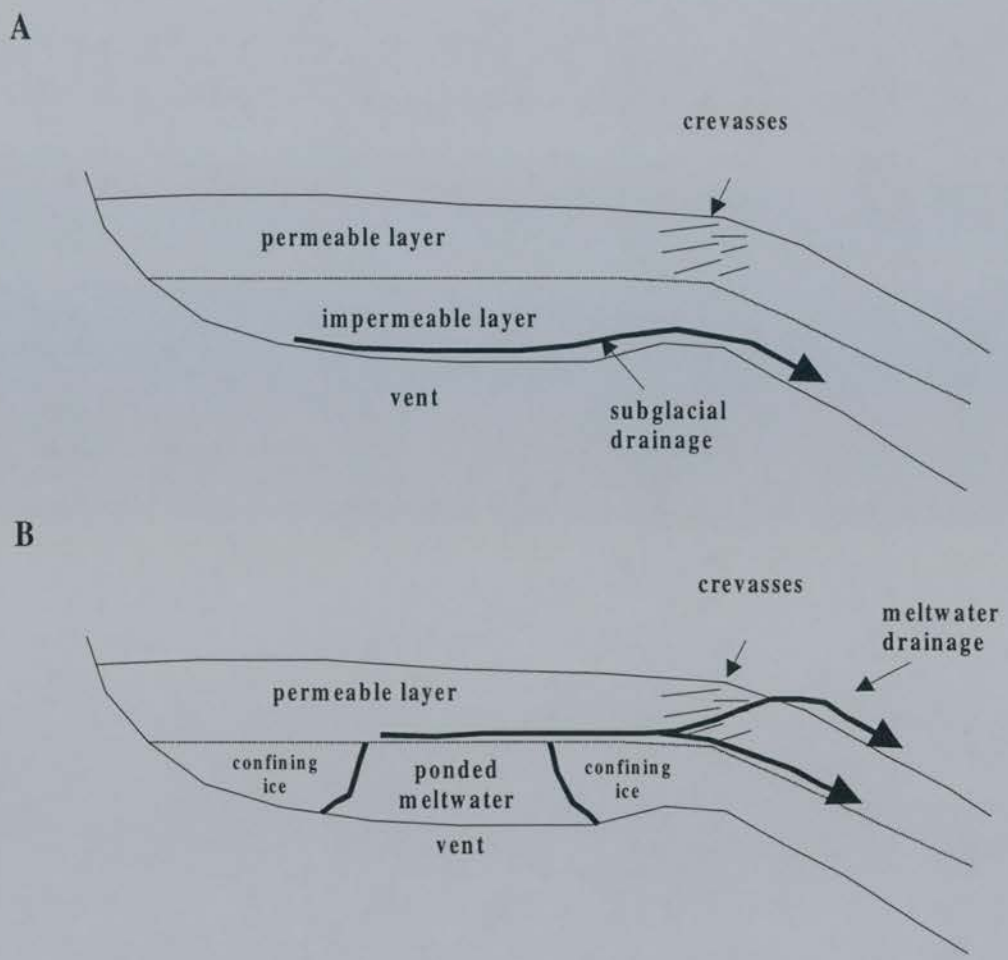

Figure 7.5 Possible meltwater drainage processes in the event of an eruption from a summit vent. a) Meltwater drains continuously from crater down Gigjökull through subglacial channels. Water may pond at the base of the icefall in overdeepening. b) Meltwater is confined above vent by impermeable ice, accumulating until it encounters a permeable ice layer. Meltwater evacuates at this interface, perhaps bursting out through fractured ice (crevasses) at the top of icefall. Meltwater could then flood down the ice surface, quarrying ice blocks by mechanical erosion. When flood reaches the base, erosion will focus at the break in slope, carving ice canyons. Meltwater may pond in the overdeepening and eventually escape in a second flood pulse.

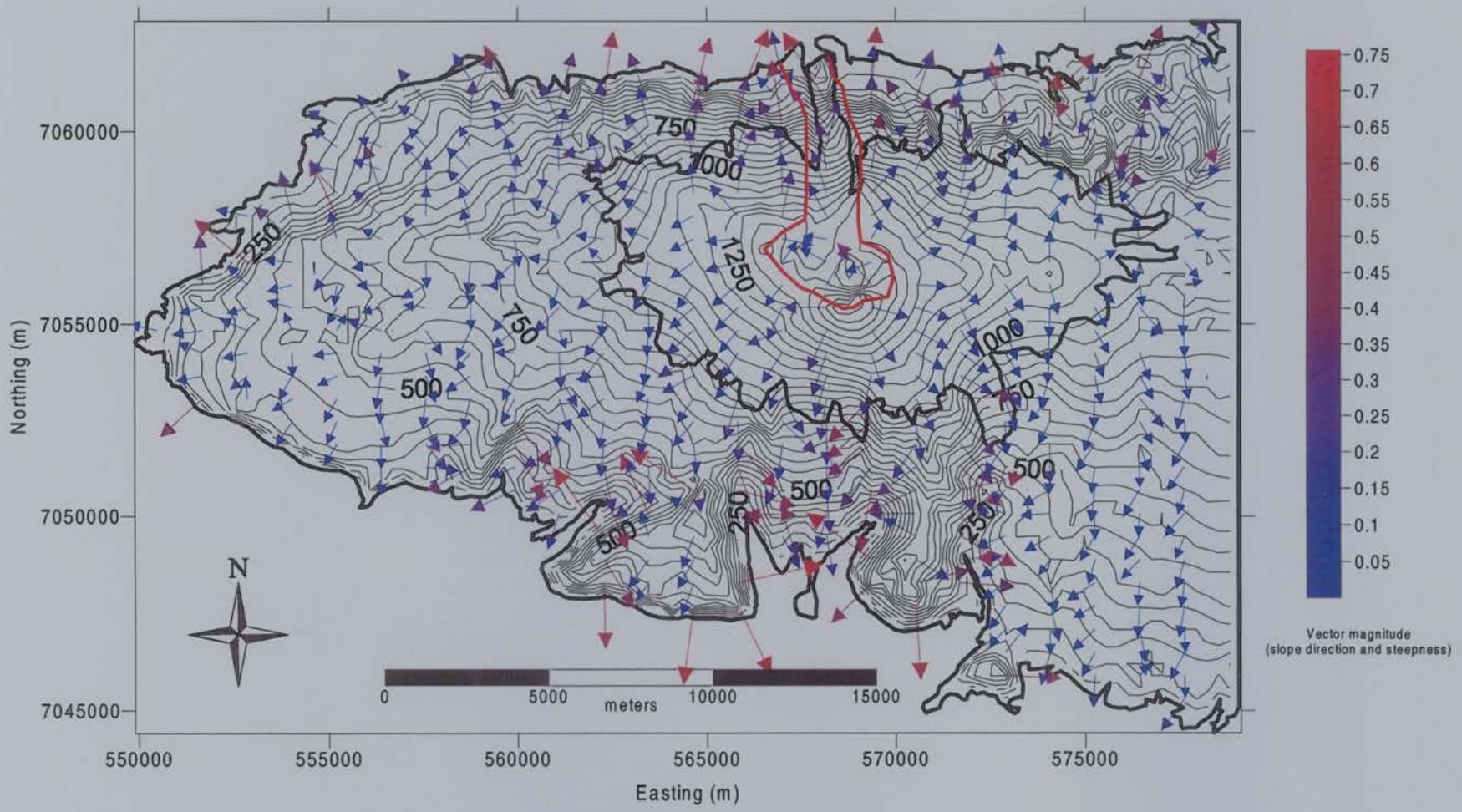

Figure 7.6 Possible significant flood route controlled by rim breach which pose lowland hazards in the event of a major summit eruption.

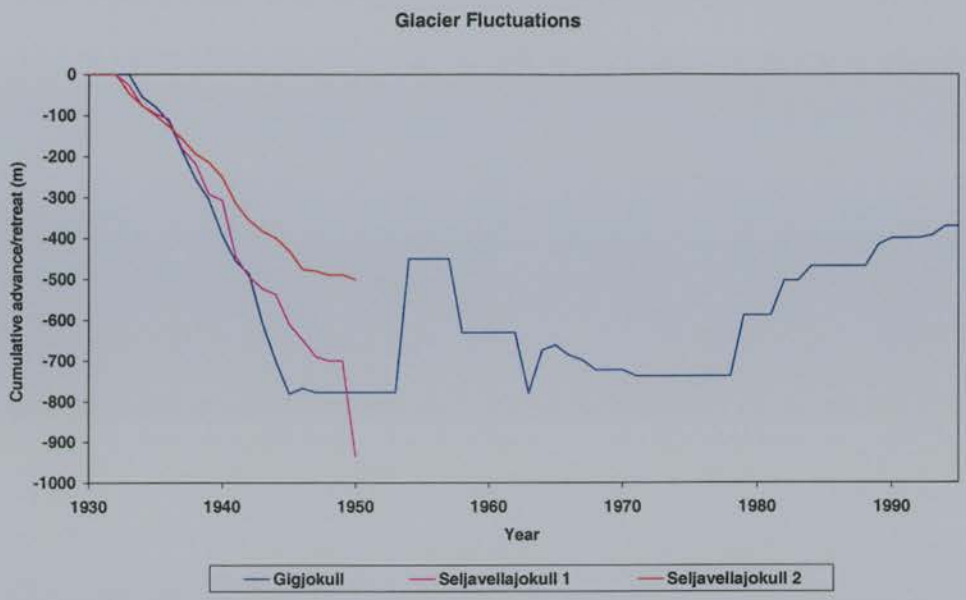

Figure 7.7 Fluctuations of Eyjafjallajökull outlet glaciers during the 20th century according to Sigurðsson (1998).

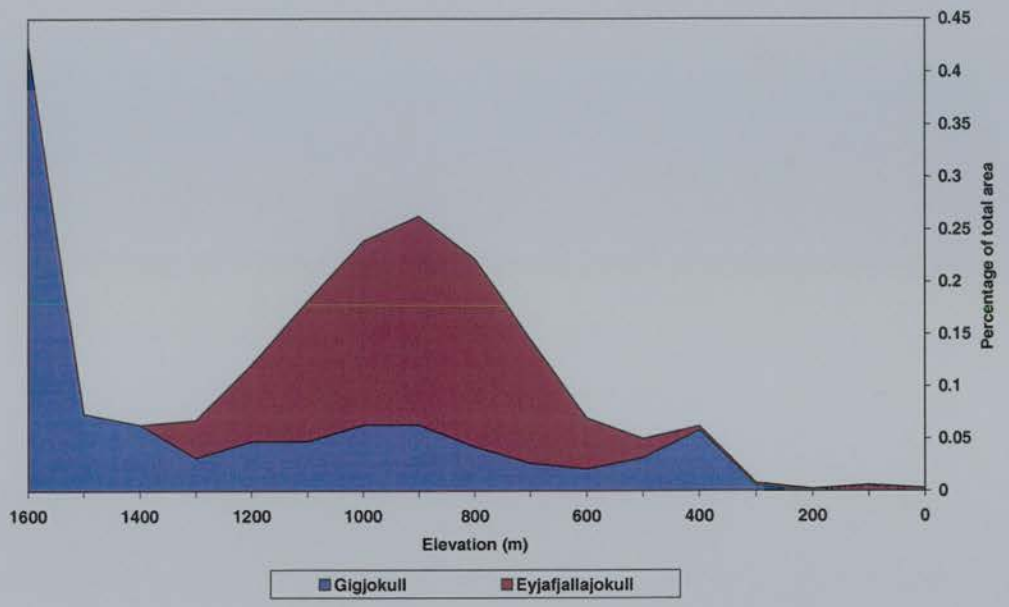

Figure 7.8a Catchment hypsometry of Gigjökull compared to the rest of Eyjafjallajökull.

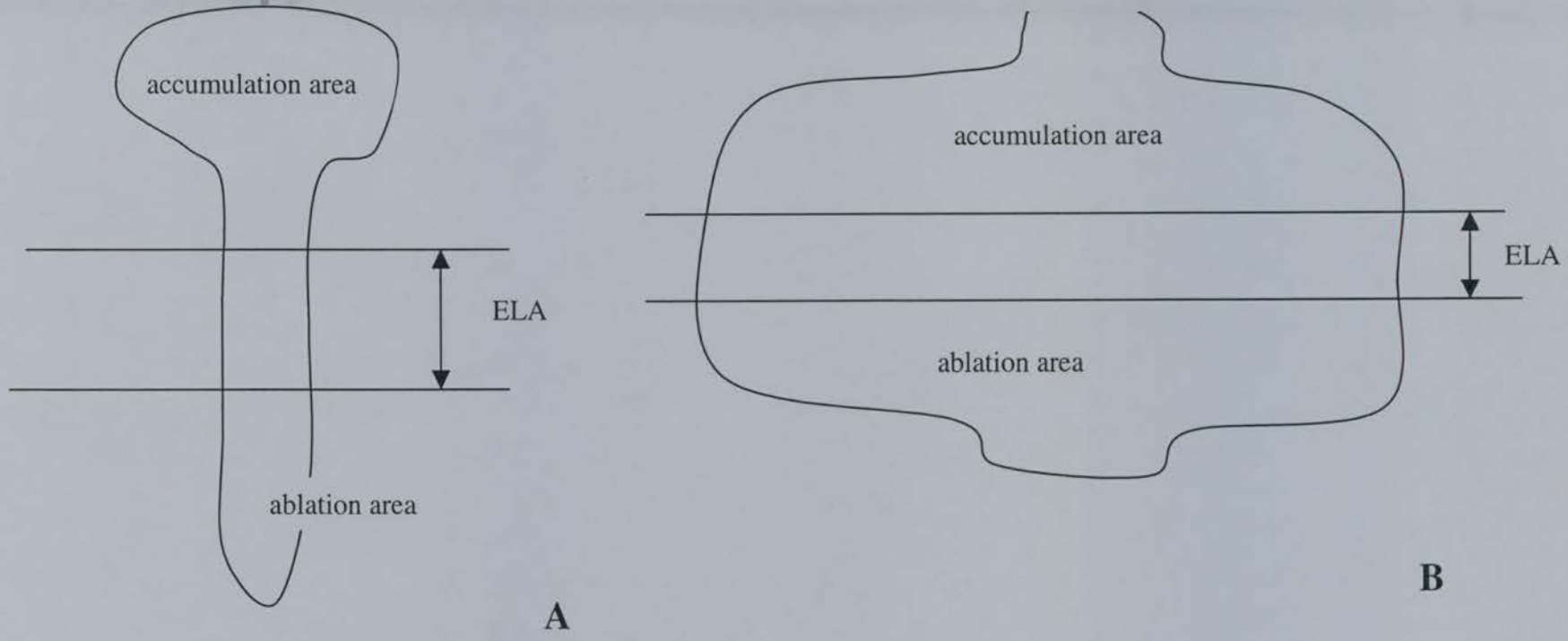

Figure 7.8b Comparison of catchment shape at equilibrium line altitude (ELA): a) Gigjökull, b) Eyjafjallajökull. A change in the altitude of the ELA forced by climate will affect a greater area of the Eyjafjallajökull catchment than Gigjökull. Gigjökull is therefore less sensitive to changes in ELA.

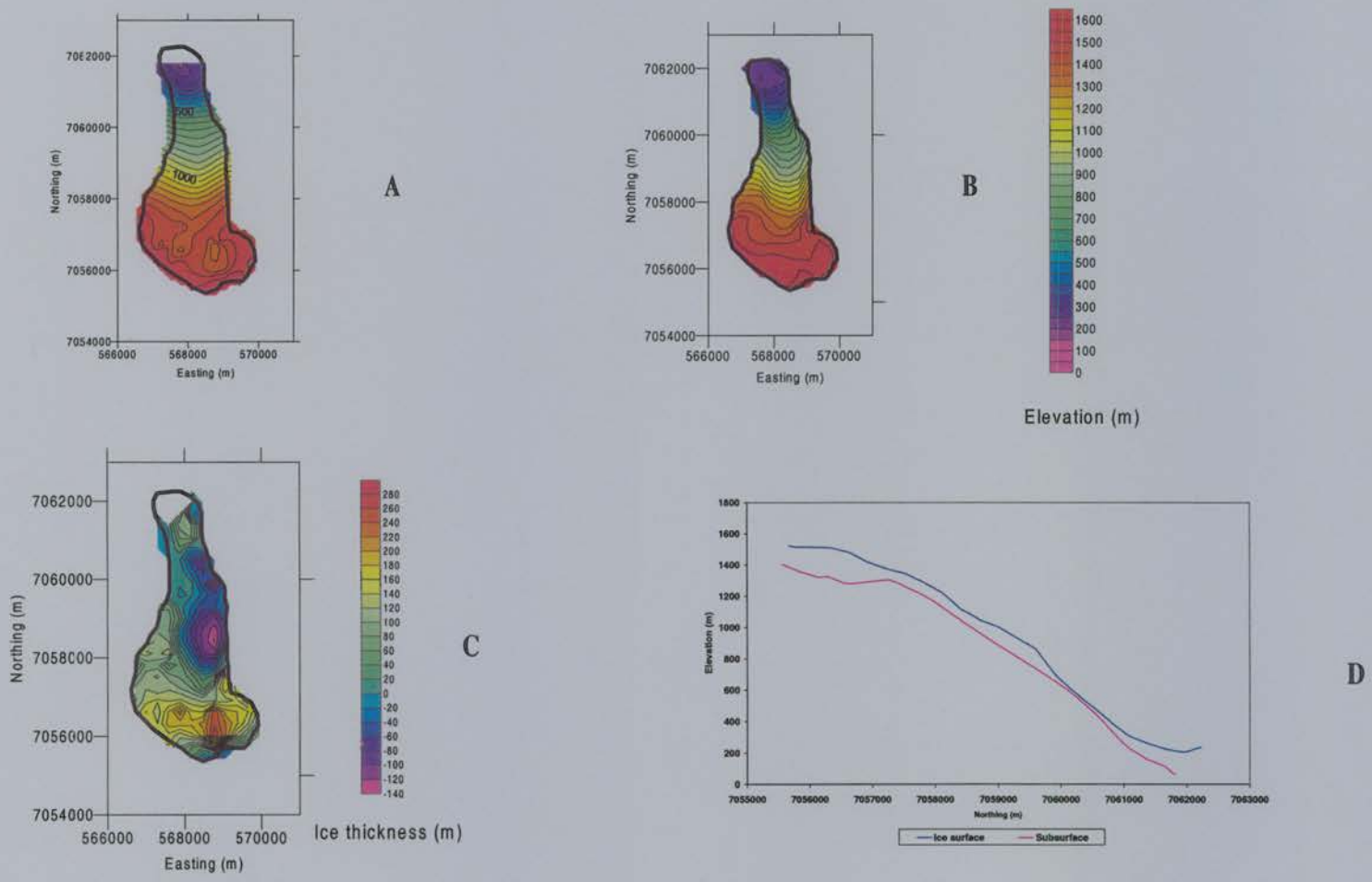

Figure 7.9 Gigjökull: its catchment and thickness. a) subsurface contour map, b) ice surface contour map, c) ice thickness isopach map, d) N-S cross-section.

Site	Area (km^2)	Volume (km^3)	Water Volume (km^3)
Eyjafjallajökull	70	3.5	3.2
Gigjökull catchment	11	0.7	0.63

Table 7.1 Area and volume of Eyjafjallajökull and Gigjökull.

7.9 References

Allen, C.C., 1980. Icelandic subglacial volcanism: thermal and physical studies. Journal of Geology, 88: 108-117.

Björnsson, H., 1978. The surface area of glaciers in Iceland. Jökull, 28: 31.

Driedger, C.L., and Fountain, A.G., 1989. Glacier outburst floods at Mount Rainier, Washington State, USA. Annals of Glaciology, 13: 51-55.

Dugmore, A.J., 1987. Holocene glacier fluctuations around Eyjafjallajökull, South Iceland: A tephrochronological study. Unpublished PhD Thesis, University of Aberdeen.

Dugmore, A.J., 1989. Tephrochronological studies of Holocene glacier fluctuations in South Iceland. In: J.E. Oerlemans (Editor), *Glacier Fluctuations and Climatic Change*. Kluwer Academic Publishers, pp. 37-55.

Einarsson, 1994. *Geology of Iceland: Rocks and Landscape*. Mál og menning, Reykjavík, 309 pp.

Geirsdóttir, Á., and Eiríksson, J., 1994. Growth of an intermittent ice sheet in Iceland during the Late Pliocene and Early Pleistocene. Quaternary Research, 42: 115-130.

Guðmundsson, M.T., Sigmundsson, F., and Björnsson, H., 1997. Ice-volcano interaction of the 1996 Gjálp subglacial eruption, Vatnajökull, Iceland. Nature, 389: 954-957.

Jakobsson, S.P., 1979. Petrology of Recent basalts of the Eastern Volcanic Zone, Iceland. Acta Naturalia Islandica, 2(26): 103.

Jones, J.G., 1969. Intraglacial volcanoes of the Laugarvatn region, south-west Iceland - I. Quaternary Journal of the Geological Society of London, 124: 197-211.

Kjartansson, G., 1967. The Steinholtshlaup, Central-South Iceland on January 15th, 1967. Jökull, 17: 249-262.

Lescinsky, D.T., and Sisson, T.W., 1998. Ridge-forming, ice-bounded lava flows at Mount Rainier, Washington. Geology, 26(4): 351-354.

Lescinsky, D.T., and Fink, J.H., 2000. Lava and ice interaction at stratovolcanoes: use of characteristic features to determine past glacial extents and future volcanic hazards. Journal of Geophysical Research (in press).

Loughlin, S.C., 1995. The evolution of the Eyjafjöll Volcanic System, Southern Iceland. Unpublished PhD Thesis, University of Durham, 319 pp.

Maizels, J.K., 1989. Sedimentology, paleoflow dynamics, and flood history of jökulhlaup deposits: paleohydrology of Holocene sediment sequences in southern Iceland sandur deposits. Journal of Sedimentary Petrology, 59: 204-223.

Major, J.J., and Newhall, C.G., 1989. Snow and ice perturbation during historical volcanic eruptions and the formation of lahars and floods: a global review. Bulletin of Volcanology, 52: 1-27.

McCarthy, R., 2001. Pakistan's drought turns political, The Guardian, London, pp. 15.

Menzies, J., 1995. Glaciers and Ice Sheets. In: J. Menzies (Editor), *Modern Glacial Environments: Processes, Dynamics, and Sediments*. Butterworth-Heinemann, Oxford, pp. 621.

Paterson, W.S.B., 1994. *The Physics of Glaciers*. Pergamon, 480 pp.

Rist, S., 1967. The thickness of the ice cover of Mýrdalsjökull, Southern Iceland. Jökull, 17: 237-242.

Sæmundsson, K., 1979. Outline of the geology of Iceland. Jökull, 29: 7-28.

Shreve, R.L., 1972. Movement of water in glaciers. Journal of Glaciology, 11(62): 205-214.

Sigurðsson, H., 2000. Introduction. In: H. Sigurðsson, Houghton, B.F., McNutt, S.R., Rymer, H., and Stix, J. (Editor), *Encyclopedia of Volcanoes*. Academic Press, New York, pp. 1-13.

Sigurðsson, O., 1998. Glacier variations in Iceland 1930-1995 - From the database of the Iceland Glaciological Society. Jökull, 45: 3-26.

Simkin, T., and Siebert, L., 2000. Appendix 2: Catalog of Historically Active Volcanoes on Earth. In: H. Sigurðsson, Houghton, B.F., McNutt, S.R., Rymer, H., and Stix, J. (Editor), *Encyclopedia of Volcanoes*. Academic Press, New York, pp. 1365-1367.

Smellie, J.L., 2000. Subglacial Eruptions. In: Sigurðsson, H., Houghton, B.F., McNutt, S.R., Rymer, H., and Stix, J. (Editors), *Encyclopedia of Volcanoes*. Academic Press, New York, pp. 403-418.

Smellie, J.P., and Skilling, I.P., 1994. Products of subglacial eruptions under different ice thicknesses: two examples from Antarctica. Sedimentary Geology, 91: 115-129.

Þórarinsson, S., 1943. Oscillations of the Iceland glaciers in the last 250 years. Geografiska Annaler, 25: 1-54.

Trabant, D.C., Waitt, R.B., and Major, J.J., 1994. Disruption of Drift glacier and origin of floods during the 1989-1990 eruptions of Redoubt Volcano, Alaska. Journal of Volcanology and Geothermal Research, 62: 369-385.

Vinogradov, V.N., and Murav'ev, Y.D., 1988. Lava-ice interaction during the 1983 Klyuchevskoiy eruption. Volcanology and Seismology, 7: 39-61.

Yount, M.E., Miller, T.P., Emanuel, R.P., and Wilson, F.H., 1985. Eruption in an ice-filled caldera, Mount Veniaminof, Alaska Peninsula. US Geological Survey Circular, 945: 58-60.

Chapter 8: Conclusions

This chapter summarizes the main findings of the study, reflects on their significance, and points to further work that could be done to improve and extend the results.

The main conclusions of this work are as follows:

- The dielectric properties of the ice at Eyjafjallajökull were determined by deriving the electromagnetic wave propagation velocity in ice at representative sites. The velocity is 138 ± 10 m μs^{-1} at Gigjökull, 140 ± 8 m μs^{-1} on the east flank, and 187 ± 23 m μs^{-1} in the crater.
- The derived velocities indicate that there are two discrete spatial zones of ice at Eyjafjallajökull: thin, dense ice on the volcano flanks and at the foot of Gigjökull, and thicker ice with a lower bulk density contained within the crater.
- Confidence in waveform interpretation was established by taking multiple frequency soundings at each point. Uncertainty in picking equals approximately 3 m in ice depth equivalent.
- Ice depth validation was quantified by conducting experiments whereby it was established that similar depths can be produced from different frequencies. Measurements of the same point at different frequencies and offsets confirmed that depth measurements are repeatable.
- The radio echo sounding survey of Eyjafjallajökull revealed a number of features underlying the ice cap: a deep (>200 m ice thickness) N-S striking trough in the crater which constitutes the main flow line of ice towards the northern rim breach, an elongate hump in the center of the crater which could be a remnant vent cone (striking SW/NE, about 53-60 m high, and with a volume of approximately 0.02 km^3), a possible parasitic crater on the east flank, and an overdeepening at the base of Gigjökull's icefall.
- The volcanic landforms previously identified on the deglaciated sections of Eyjafjöll by Jakobsson (1979), Jónsson (1988), and Loughlin (1995), indicate that, for most of its history, Eyjafjallajökull has been a relatively thin, temperate

glacier, occupying the summit region of the volcano. The glacier has suffered repeated catastrophic disruption.

- The present eruptive environment divides into two discrete areas, based on ice structure and thickness:
    - In the event of a summit eruption, thick, impermeable ice in the crater may confine meltwater, then suddenly release it as a jökulhlaup. Thermal and mechanical erosion from flooding meltwater could severely disrupt the ice of Gigjökull.
    - The area outside the summit crater contains thin (<150 m) ice and a well-developed subglacial drainage system. In the event of an eruption, meltwater will likely drain in a continuous manner through permeable ice.
- There is potential for hazardous flooding to take place at Eyjafjöll in the event of an eruption. If an eruption occurs in the summit crater, meltwater will likely pond above the active vent, accumulate, and catastrophically release. The main potential drainage pathway is through the northern rim breach, at Gigjökull. As much as 0.63 km^3 of water could be produced if the entire catchment of Gigjökull melted.
- Glaciologically, the area containing the summit crater and its outlet glacier, Gigjökull, is less sensitive to the influence of climate than the remainder of the ice cap.

This thesis has achieved a greater understanding of a specific glaciovolcanic system. The findings are significant in that they have wider implications for glaciovolcanic systems in general. These special systems, where volcanic and glacial processes interact to create landforms indicative of the environment in which they were emplaced, should be carefully assessed prior to using their marginal fluctuations as proxies of climate change. As was shown at Eyjafjallajökull, assuming that the oscillations of one outlet glacier are representative of the fluctuations of the entire system, is ill-judged. Volcanigenic ice disruption is a significant factor in the behavioral dynamics of glaciers which overlie volcanoes.

Further work which could be done to enhance the findings of this research should focus particularly on the method of collecting radio echo sounding data from temperate glaciers.

Specifically:

- More work needs to be done in determining what happens with the air wave in the near surface air/ice interface and what implications the supposed interference with the lateral wave has for the estimation of velocity.
- Collecting radio echo sounding data in a continuous manner would improve the horizontal resolution and allow the size and shape of specific landforms to be determined.

References

Jakobsson, S.P., 1979. Petrology of Recent basalts of the Eastern Volcanic Zone, Iceland. Acta Naturalia Islandica, 2(26): 103.

Jónsson, J., 1988. Geological Map of the Eyjafjöll Area. Research Institute Neðri Ás, Hvéragerði.

Loughlin, S.C., 1995. The evolution of the Eyjafjöll Volcanic System, Southern Iceland. Unpublished PhD Thesis, University of Durham, 319 pp.

Appendix A: List of Symbols

Symbol	Definition	Units	Value if constant
A	amplitude of an electromagnetic wave		
c	velocity of electromagnetic waves in free space	m μs^{-1}	300
$2d_1$	antenna separation distance or offset between transmitter and receiver	m	
$2d_2$	travel path of electromagnetic wave through ice from transmmitter to receiver	m	
g	acceleration due to gravity	m s^{-1}	9.8
H_i	ice thickness	m	
$m(x)$	structural, deterministic component of random variable $Z(x)$		
r	radius of first Fresnel zone	m	
T	period		
t	time	s	
t_1	travel time of air wave from transmitter to receiver	μs	
t_2	two-way travel time of ground wave through ice from transmitter to receiver	μs	
t_i	waveform time measurement of difference between arrival of air wave and arrival of ground wave	μs	
u	wave motion; harmonic displacement of an electromagnetic wave from its mean position		
x	displacement of an electromagnetic wave along the x-axis		
$Z(x)$	a random variable at position x in one, two, or three dimensions		
α	angle of ice surface slope		
ε_o	free space permittivity		8.854 x 10^{-12}
ε	permittivity		
ε_r	relative permittivity or dielectric constant		
$\varepsilon'(x)$	random, stochastic component of random variable Z(x)		
$\varepsilon''(x)$	residual, spatially-independent noise component of random variable Z(x)		
ϕ	subglacial hydraulic potential		
$\gamma(h)$	semivariance		

λ	wavelength of electromagnetic wave	m	
v	velocity of electromagnetic wave	m μs^{-1}	
θ_i	angle of incidence		
θ_r	angle of reflection		
ρ	density	g m^{-3}	
τ_b	basal shear stress	kPa	
υ	frequency of an electromagnetic wave	MHz	

Appendix B: Dataset uncertainty and resolution

Uncertainty

Dataset error describes the uncertainty which accompanies scientific measurement (Taylor, 1981). The uncertainty inherent in physical measurement is assessed by estimating the reliability and repeatability of each measurement. The repeatability indicates confidence in the measurement and is given as a range within which the researcher is confident the measured quantity lies.

Dataset error for Eyjafjallajökull is a combination of radar error and Global Positioning System (GPS) error. Quantities measured are horizontal and vertical position of data points, relative to the WGS-84 ellipsoid, and ice thickness. These quantities were measured with two instruments, GPS and radar, requiring an estimate of the measurement uncertainty for each. GPS measures two positions, vertical and horizontal, and radar measures one value, ice thickness, so three estimates of uncertainty are needed.

The uncertainty in ice thickness values measured by radar are derived in *Chapter 4* and defined as the waveform interpretation (or picking) uncertainty.

Ice thickness measurement uncertainty: ± **4-25 m**

The uncertainty in horizontal and vertical position values measured by GPS are dependent on the accuracy and precision of the GPS instrument and the differential post-processing applied. Determining the accuracy of a GPS system can be quite complex and is ideally assessed by performing tests with each individual receiver. These tests were not performed during field work, so positional accuracy can only be estimated by using suggested guidelines (Dana, 1994). Since some positions included in the dataset could not be differentially corrected, the range of uncertainty includes the estimated error for both corrected and uncorrected positions.

Horizontal position uncertainty: ± **10 - 60 m**

Vertical position uncertainty: ± **30 - 100 m** (Dana, 1994).

Resolution

Resolution is a measurement of the ability to separate something into its constituent parts. The horizontal resolution of the Eyjafjallajökull dataset estimates the size of individual components on the bed surface which can be distinguished from one another. The vertical resolution of the Eyjafjallajökull dataset defines the equivalent length in meters between which two signals adjacent to each other in time can be separated.

The vertical resolution is a function of wavelength and is calculated for the specific physical properties of ice at Eyjafjallajökull. These quantities are dependent on antennae length and relative permittivity of ice. The relative permittivity of ice at each of the experimental sites is calculated from the derived wave propagation velocities from the experiments in *Chapter 4* and the relevant equations introduced in *Chapter 2*.

The half-lengths of individual antennas and combinations used in the survey are described in ***Table A1***. The center frequency of transmitted electromagnetic energy is a function of both antenna length and relative permittivity of the media through which it is transmitted (***Equation 2.2***). The relative permittivity of the ice at Eyjafjallajökull, represented by the dielectric constant, is calculated from the propagation velocity of electromagnetic energy in ice (***Equation 2.5***). ***Table A1*** provides the center frequency values calculated from the antenna length and permittivity parameters. Frequencies are calculated for the three experimental sites.

Wavelength is a function of frequency and permittivity (***Equations 2.3, 2.6***). ***Table A1*** gives the wavelengths derived for the three experimental sites. There is a large range in wavelength, from 18-94 m, depending on antenna length. However, most of the data were collected without using the 40 m half-length antennas, so the range is closer to 18-63 m.

Vertical resolution is a function of wavelength; reflectors with vertical dimensions smaller than one-quarter wavelength cannot be resolved (*Chapter 2*). ***Table A1*** shows the range of vertical resolution determined for the data set. Since

almost no data were collected with the 40 m half-length antenna combination, it is safe to conclude that *the vertical resolution of the data set is* **5-16 m**.

The horizontal resolution of the dataset is a function of both the radius of the first Fresnel zone and the spatial sampling. ***Table A2a-d*** presents the first Fresnel zone radius values calculated from ***Equation 2.8*** for the frequencies used at each site. The reflector depths included in the calculation approximate the range of depths encountered at each site. The *range of footprint radius is* **15-76 m**. The *spatial sampling is* **200 m**.

Antenna half-length (m)	υ_c (MHz)			λ_{ice} (m)			Vertical Resolution (m)		
	G	F	C	G	F	C	G	F	C
10	8	8	8	18	18	24	5	5	6
20	4	4	4	35	35	47	9	9	12
30	3	3	3	46	47	63	12	12	16
40	2	2	2	69	70	94	18	18	24

Table A1 Frequency, wavelength, and vertical resolution values calculated for the range of antenna lengths used in the survey. G = Gigjökull experimental site, F = Flank experimental site, C = crater experimental site. Center frequency range (υ_c) = 2-8 MHz. Range of wavelengths in ice (λ_{ice}) = 18-94 m. Range of vertical resolution = 5-24 m.

Site	v (m μs^{-1})	ε_r
Gigjökull	138	5
Flank	140	5
Crater	187	3

Table A2a Electromagnetic wave propagation velocities derived in *Chapter 4* for each experimental site and the relative permittivity of ice at each site calculated from the velocity values.

H_i (m)	Gigjökull: radius of first Fresnel zone (m)			
	2 MHz	3 MHz	4 MHz	8 MHz
50	29	24	21	15
100	42	34	29	21
150	51	42	36	25

Table A2b Size of footprint (r) calculated for Gigjökull experimental site for transmission frequencies of 2-8 MHz and a typical range of ice thicknesses (H_i) encountered at the site. Range of radius of first Fresnel zone = 15 - 51 m.

H_i (m)	Flank: radius of first Fresnel zone (m)			
	2 MHz	3 MHz	4 MHz	8 MHz
50	30	24	21	15
100	42	34	30	21
150	51	42	36	26
200	59	48	42	30

Table A2c Size of footprint (r) calculated for flank experimental site for transmission frequencies of 2-8 MHz and a typical range of ice thicknesses (H_i) encountered at the site. Range of radius of first Fresnel zone = 15 - 59 m.

H_i (m)	Crater: radius of first Fresnel zone (m)			
	2 MHz	3 MHz	4 MHz	8 MHz
50	34	28	24	17
100	48	39	34	24
150	59	48	42	30
200	68	56	48	34
250	76	62	54	38

Table A2d Size of footprint (r) calculated for crater experimental site for transmission frequencies of 2-8 MHz and a typical range of ice thicknesses (H_i) encountered at the site. Range of radius of first Fresnel zone = 17 - 76 m.

References

Dana, P.H., 1994. Global Positioning System Overview. Geography Department, University of Texas, www.utexas.edu/depts/grg/gcraft.

Taylor, J.R., 1981. *An Introduction to Error Analysis: the study of uncertainties in physical measurements*. University Science Books, Sausalito, 327 pp.